

Interacting Atoms in Clocks and Condensates

PROEFSCHRIFT

ter verkrijging van de graad van doctor aan de
Technische Universiteit Eindhoven, op gezag van de
Rector Magnificus, prof.dr. M. Rem, voor een
commissie aangewezen door het College voor
Promoties in het openbaar te verdedigen
op dinsdag 27 juni 2000 om 16.00 uur

door

**Servaas Jan Jozef Margaretha Franciscus
Kokkelmans**

geboren te Heerlen

Dit proefschrift is goedgekeurd door de promotoren:

prof.dr. B.J. Verhaar

en

prof.dr. H.C.W. Beijerinck

Druk: Universiteitsdrukkerij Technische Universiteit Eindhoven

CIP-DATA LIBRARY TECHNISCHE UNIVERSITEIT EINDHOVEN

Kokkelmans, Servaas Jan Jozef Margaretha Franciscus

Interacting Atoms in Clocks and Condensates / by

Servaas Jan Jozef Margaretha Franciscus Kokkelmans. -

Eindhoven : Technische Universiteit Eindhoven, 2000. - Proefschrift. -

ISBN 90-386-1569-8

NUGI 812

Trefw.: atoomklok / fonteinklok / atoombotsingen / Bose-Einstein-condensatie /
atomen; wisselwerkingen / Feshbach resonanties / alkalimetalen

Subject Headings: atomic clock / fountain clock / optical cooling of atoms; trapping /
scattering of atoms, molecules, and ions / Bose-Einstein condensation /
molecular condensates / Raman transition / interatomic potentials and forces

*aan mijn ouders
en aan Esther*

Servaas Kokkelmans
Group for Theoretical and Experimental Atomic Physics and Quantum Electronics
Department of Physics
Eindhoven University of Technology
P.O. Box 513
5600 MB Eindhoven
The Netherlands

Cover Fountain of atoms passing through an electromagnetic field. The dial symbolizes the extremely good clock performance of atomic-fountain frequency standards.

Contents

1	Introduction	3
1.1	Cold atomic gases	3
1.2	Interactions in BEC	4
1.3	Interactions in cold atomic clocks	6
1.4	This thesis	10
2	Interactions and methods	15
2.1	Molecular potentials and other interactions	15
2.2	Boundary conditions: accumulated phase method	20
2.3	Raman photoassociation	24
2.4	Analytic model for photoassociation	28
2.5	A new Feshbach resonance phenomenon	32
3	Predictions for laser-cooled Rb clocks	37
3.1	Introduction	37
3.2	Collisional frequency shift	38
3.3	Rubidium performs better than cesium	40
3.4	Cancellation technique for ^{85}Rb	42
3.5	Contributions for higher energies	43
4	Prospects for Bose-Einstein condensation in cesium	47
4.1	Introduction	47
4.2	Anomalous decay rates	48
4.3	Restrictive potential parameters	49
4.4	Feshbach resonances	50
4.5	Collisional properties of ^{135}Cs	52
4.6	Conclusions	53
5	Direct measurement of scattering phase shifts and discrepancies in cold atom scattering	55
5.1	Introduction	55
5.2	Accurate measurement of scattering phase shifts	56
5.3	Discrepancies in cold atom scattering	56
5.4	Proposed direct phase measurement technique	58
5.5	Effect of p-wave scattering	60

5.6	Prospects	61
6	Formation of ultracold molecules via stimulated Raman scattering	65
6.1	Introduction	65
6.2	Condensate of molecules formed in time-dependent field	66
6.3	Four-state model	67
6.4	Efficient formation of molecules	71
6.5	Determination of spin-dependent interaction for Rb	72
6.6	Subsplitting of rovibrational levels	73
6.7	Raman photoassociation on ^{87}Rb	73
6.8	Determination of interaction strength	75
7	Role of collisions in creation of overlapping Bose condensates	79
7.1	Introduction	79
7.2	Discussion of Na interactions	81
7.3	Collisional decay in overlapping condensates	81
7.4	Equality of singlet and triplet scattering lengths for ^{87}Rb	83
7.5	Conclusions	86
8	Discrepancies in experiments with cold hydrogen atoms	89
8.1	Introduction	89
8.2	Description of frequency shifts and discrepancies	92
8.3	Description of longitudinal relaxation time and discrepancies	95
8.4	Comparison with more rigorous expression for longitudinal relaxation time	96
8.5	Modification of potentials	97
8.6	Influence of magnetic dipole interaction	100
8.7	Conclusions	102
	Summary	104
	Samenvatting	106
	Dankwoord	109
	Curriculum Vitae	110

Introduction

1.1 Cold atomic gases

The phenomenon of Bose-Einstein Condensation (BEC) is one of the most exciting demonstrations of the quantum nature of matter. As was first pointed out by Einstein [1], a system of identical particles obeying Bose-Einstein statistics will under certain circumstances undergo a phase transition to a state with a macroscopic occupation of the lowest single-particle state. The formation of a BEC is a second-order phase transition and starts when the deBroglie wavelength of the particles becomes comparable to the interparticle separation. This requires sufficiently low temperatures and sufficiently high densities. Such circumstances have been realized very close to its ideal form for the first time in cold atomic gases of rubidium [2], sodium [3], lithium [4], and later in hydrogen [5]. The regime of quantum degeneracy in the alkali systems is mostly reached for temperatures between 500 nK and 2 μ K, for densities between 10^{14} and 10^{15} atoms per cubic centimeter. Bose-Einstein condensation is at the basis of several phenomena in physics: superconductivity and superfluidity are believed to be manifestations of BEC. However, the interactions in these solid and liquid systems are too strong to observe the condensate in a pure way. In recent experiments at JILA, MIT and ENS Bose-Einstein condensates have shown indications of superfluidity [6–8]. It has also been shown that the coherence of the atoms remains when they are coupled out of a trap, making a BEC an important source for an atom laser [9]. A condensate may also serve as a playground for other physical phenomena. Since it is possible to reduce the speed of light in an ultra-cold gas to several meters per second [10], it is relatively easy to create a vortex in this medium spinning at comparable velocities, that can make the gas behave as an optical black hole [11].

Atomic frequency standards are pre-eminent because of their very stable and accurate output signals [12]. They are widely used for time-keeping purposes, for world-wide location in the Global Positioning System (GPS), for navigation in long-distance space flights and for high-speed data transmission. They are generally classified into active devices such as the hydrogen maser [13], with stabilities below 10^{-15} for an averaging time of 10^4 s, and passive devices as the cesium fountain clock [14], which should reach accuracies of order 10^{-16} in the near future (equivalent to an uncertainty of one minute over the lifetime of the universe). The high accuracies of atomic clocks led to

a redefinition of the SI second as the duration of 9 192 631 770 periods of the hyperfine transition of the ground-state ^{133}Cs atom. Cold atoms give rise to great advantages in atomic clocks, mainly because the time of free flight between the separated oscillatory fields is highly increased when making use of slowly-moving atoms. This allows an improvement by a factor 100-1000.

The counterpart of BEC is Fermi Degeneracy, that can be realized in a system of particles with half-integer spin obeying Fermi-Dirac statistics. Instead of condensation into the lowest state, the particles fill up the energy levels from below, only one particle per state, until the Fermi surface. Particle interactions are strongly reduced, since by the Pauli principle there are no other states to go to within the Fermi sphere. This is held responsible for the validity of the nuclear shell model, for instance. Fermi degeneracy also plays a role in the stability of neutron stars against collapse. In a cold atomic gas the Fermi degeneracy is expected to take place in the same density and temperature regimes as BEC, and has for the first time been demonstrated in a cold dilute gas of ^{40}K atoms [15].

Another exciting field of physics where cold atoms can play an important role is in quantum information. By addressing a register of two-level atoms with laser light, quantum computations can be performed. The atoms could be trapped in an optical lattice and entangled via cold controlled collisions [16]. Because superpositions of the two states can be stored at the same time in a qubit, an operation on a register of n atoms can be performed on 2^n numbers at the same time, instead of only one in a classical n -bit register. With special algorithms such as the Shor algorithm [17], prime factorization can be carried out in a polynomial time instead of exponential time on a classical computer.

The field of cold atomic physics has largely been stimulated by the possibilities of manipulating atoms with lasers and magnetic fields. With laser cooling, where atoms are slowed down by absorbing and emitting photons [18], it is possible to reach temperatures determined by the recoil limit, i.e., of the order of $1\text{ }\mu\text{K}$ for Cs. To get below this limit, the laser light needs to be switched off and atoms are cooled by evaporative cooling, where the hottest atoms are able to escape from the magnetic or optical trap that holds them. The cold atoms that remain trapped rethermalize via collisions to a lower temperature. This is a good example of the importance of collisions in this field. Interatomic interactions play a crucial role in cold atom experiments, and this thesis contributes to a better understanding of their role.

1.2 Interactions in BEC

An attractive feature of BEC in dilute atomic gases is that it can be theoretically described from first principles. While the deBroglie wavelength should be larger than

the interparticle separation to reach BEC, the interparticle separation in its turn should be much larger than the range of the interatomic interaction, to consider the gas as weakly interacting. Effectively, this range is characterized by the s-wave scattering length a . For ultracold collisions only s-waves ($l = 0$) contribute, and the corresponding scattering phase shift δ can be given as the first term $k \cot \delta = -1/a$ of the effective range series. The elastic scattering wave function is then at large range proportional to $\sin(kr + \delta) = \sin k(r - a)$. This means that we can consider elastic ultracold scattering as equivalent to hard sphere scattering, no matter the complexity of the interatomic interactions. Of course, in the case of a negative scattering length this picture should be extended to 'hard spheres with negative diameter' a .

The condensate is described in a formalism based on quantum field theory [19], where the interactions are taken into account by $\frac{4\pi\hbar^2 a}{m} \delta(\vec{r}_i - \vec{r}_j)$, a zero-range pseudopotential (with atomic mass m), treated in terms of a Hartree-Fock mean field

$$U|\phi|^2 = \frac{4\pi\hbar^2 a}{m} |\phi|^2. \quad (1.1)$$

The dynamics of the condensate field (condensate wave function) $\phi(\vec{r}, t)$ is thus described by the Gross-Pitaevskii equation

$$i\hbar\dot{\phi} = \left(-\frac{\hbar^2}{2m} \nabla^2 + V_{trap}(\vec{r}) + U|\phi|^2 \right) \phi, \quad (1.2)$$

where V_{trap} is the, generally harmonic, trap potential that keeps the atoms together. The condensate wave function is normalized to the total number of particles N . Though the gas is only weakly interacting, the mean field energy can be so large that the condensate wave function differs significantly from the single particle ground state in the trap in the non-interacting case [20]. The stability of a large condensate requires a positive scattering length (effectively repulsive interactions); a negative scattering length (attractive interactions) implies instability for collapse. For a limited number of atoms, however, it is possible to find stable solutions of the Gross-Pitaevskii equation also when a is negative. While for a homogeneous condensate there is no kinetic energy available to prevent a collapse, a trapped condensate can be stable when the energy of the zero-point motion in the trap is larger than the mean field energy. This has experimentally been observed with ^7Li atoms [4], where the scattering length is negative [21]. In case of $a = 0$ there is effectively no interaction (ideal gas case), and the condensate wave function is equal to the ground-state harmonic oscillator solution, apart from normalization.

To reach the point of condensation with evaporative cooling, the collisional cross section should be large enough to far outweigh the inelastic decay. In the $T \rightarrow 0$ limit it is equal to

$$\sigma = 8\pi a^2 \quad (1.3)$$

for a spin-polarized gas. This cross section is two times larger than expected for non-identical particles. We mention further that the nonlinear mean field term results in nonlinear atom optics. One of the first features of this kind observed in a BEC was four-wave mixing, where three wave packets in a condensate formed a fourth packet [22].

1.3 Interactions in cold atomic clocks

Accuracy and stability determine the performance of atomic frequency standards. The accuracy is the degree to which the output frequency corresponds to the ideal free-atom hyperfine transition frequency ν . It is expressed as a fractional uncertainty $\delta\nu/\nu$, with $\delta\nu$ the absolute frequency uncertainty. The frequency stability is the degree to which the frequency is constant during a specific time interval τ , and is indicated by $\sigma(\tau)$, also referred to as the instability. For relatively short time intervals (say up to 1000 s) the instability of passive standards is given by the Allan standard deviation [23] and has a $\tau^{-\frac{1}{2}}$ dependence. For active devices, the instability may even decrease faster ($\sim \tau^{-1}$). For longer time intervals the behavior is different. This is referred to as the long-term stability and depends on the control of environmental conditions and systematic errors. The actual output signal of an atomic clock comes from a slave oscillator, usually a quartz crystal oscillator, that is locked to the atomic transition frequency controlled by a feedback loop. The quartz crystal oscillates at a typical frequency of 5 or 10 MHz and is up-converted to match the atomic reference. This signal serves as input for the microwave cavity in case of a passive standard.

With cold atoms in a fountain it is possible to obtain much better clocks. The atomic fountain clock, schematically shown in Fig. 1.1, makes use of the Ramsey separated oscillatory field method applied to cold atoms. A cold cloud of atoms is prepared in one of the two hyperfine clock states and is launched through a microwave cavity where the atoms experience a $\frac{\pi}{2}$ pulse, that creates a superposition of these two states. During the following parabolic flight determined by gravity, the atomic oscillator is free to evolve until a second cavity passage brings the atoms precisely in the other clock state, provided the cavity frequency has been tuned accurately to the atomic transition frequency. The collisional frequency shift is the limiting factor to accuracy in a fountain since all other systematic shifts are strongly reduced below this level.

The clock transition takes place between two ground-state hyperfine levels. The hyperfine interaction originates from the Fermi-contact term. It is given effectively by

$$V^{hf} = \frac{a^{hf}}{\hbar^2} \vec{s} \cdot \vec{i}, \quad (1.4)$$

where \vec{s} and \vec{i} are the electron and nuclear spin vectors and a^{hf} is the hyperfine constant, that depends on the atomic species. In case of a magnetic field B the Zeeman

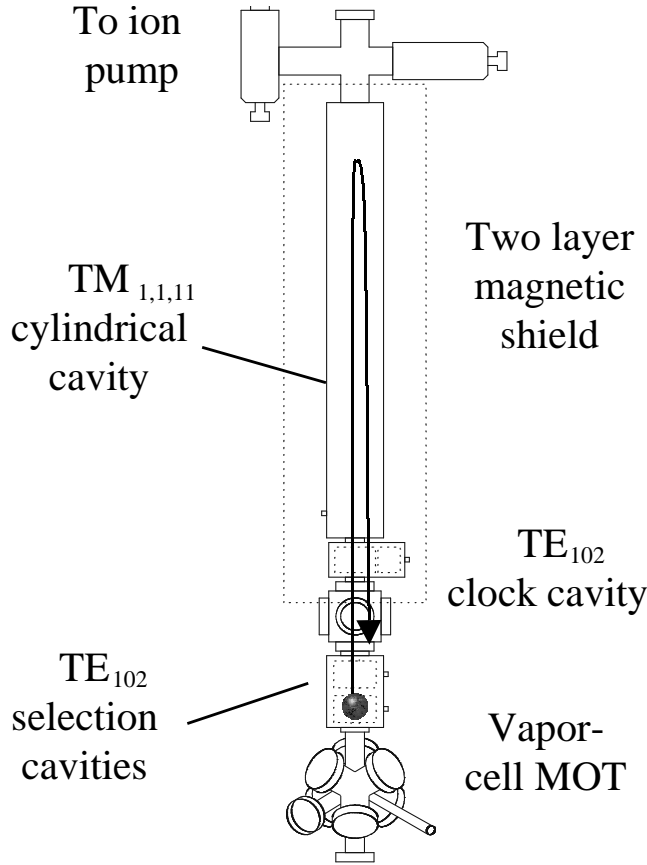


Figure 1.1 Atomic fountain set-up (Gibble group, Yale University). Atoms are first laser-cooled by three pairs of counterpropagating laser beams in the vapor-cell MOT. The laser frequencies are tuned in such a way that a vertically moving reference frame is created, launching the atoms vertically. The lasers are switched off, and the atoms move freely under gravity. After passing the microwave clock-cavity twice, the atoms have made a hyperfine transition, and are detected by a probe laser. With a typical fountain height of 0.5 m, the fountain orbit lasts about half a second.

interaction becomes important:

$$V^Z = (\gamma_e s_z - \gamma_N i_z) B_z. \quad (1.5)$$

The eigenstates of the sum of these interactions are called the hyperfine states $|f, m_f\rangle$, where $\vec{f} = \vec{s} + \vec{i}$. Figure 1.2 shows the hyperfine states as a function of magnetic field for ^{87}Rb as an example. For $B \neq 0$, f is not a good quantumnumber anymore, but it is still used to label the eigenstates. A magnetic field dependence of the clock transition is not desirable. Therefore the field is kept close to zero and the transition

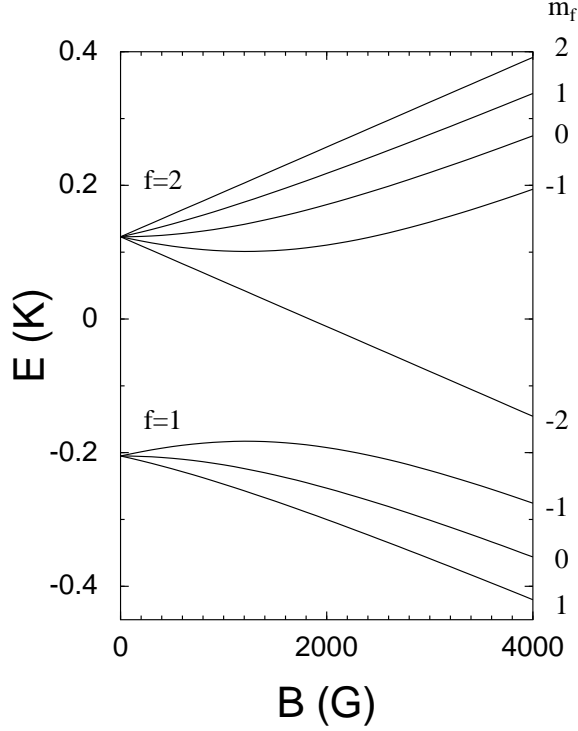


Figure 1.2 Hyperfine diagram for ground-state ^{87}Rb atoms. ^{87}Rb has a nuclear spin quantum number $i = \frac{3}{2}$. Other species with the same nuclear spin have the same diagram, except for a different a^{hf} .

is made between the two $m_f = 0$ levels. Then the transition frequency is in first order independent of B . We denote these states in the following as $|1\rangle$ for the lower and $|2\rangle$ for the upper clock state.

The $\frac{\pi}{2}$ pulse from the cavity field creates a coherent superposition of upper and lower states. A single-atom spin-density matrix describes the atomic ensemble; its evolution equation is given by

$$\frac{d}{dt}\rho_{\kappa\kappa'} + \frac{i}{\hbar}(\varepsilon_{\kappa} - \varepsilon_{\kappa'})\rho_{\kappa\kappa'} = \dot{\rho}_{\kappa\kappa'}^{field} + \dot{\rho}_{\kappa\kappa'}^{coll}. \quad (1.6)$$

The subscripts stand for the hyperfine levels $|f, m_f\rangle$, and ε_{κ} is the corresponding hyperfine energy. The first term on the right hand side comes from the interaction with the cavity field. The second term on the right deals with all two-body interactions and is responsible for relaxation and phase shifts. It obeys an equation that can be derived from the Bogoliubov-Born-Green-Kirkwood-Yvon (BBGKY) hierarchy [24], and

is known as the quantum Boltzmann equation:

$$\dot{\rho}_{\kappa\kappa'}^{coll} = n \sum_{\lambda} \sum_{\sigma\nu\sigma'\nu'} \rho_{\sigma\sigma'} \rho_{\nu\nu'} [(1 + \delta_{\kappa\lambda})(1 + \delta_{\sigma\nu})(1 + \delta_{\kappa'\lambda})(1 + \delta_{\sigma'\nu'})]^{1/2} \times \left\langle \frac{2\pi\hbar}{\mu k} \sum_{lm'l'm'} S_{\{\kappa\lambda\},\{\sigma\nu\}}^{lm,l'm'}(k) S_{\{\kappa'\lambda\},\{\sigma'\nu'\}}^{lm,l'm'*}(k) - \delta_{ll'} \delta_{mm'} \delta_{\{\kappa'\lambda\},\{\sigma'\nu'\}} \right\rangle. \quad (1.7)$$

Here n is the atomic density, $\mu = m/2$ the reduced mass and k the wave number in the entrance channels of the S-matrix elements. The subscripts between brackets are a short-hand notation for normalized (anti)symmetrization of two-body hyperfine states for relative even (odd) orbital angular momentum l with projection m . The $(1 + \delta)$ factors take care of identical particle symmetry, and the $\langle \rangle$ brackets denote a thermal average. Together with this equation comes a subsidiary condition $\varepsilon_{\kappa} - \varepsilon_{\kappa'} + \varepsilon_{\mu'} - \varepsilon_{\mu} + \varepsilon_{\nu'} - \varepsilon_{\nu} = 0$ that should be obeyed while summing over all hyperfine states.

For $\kappa = \kappa'$ the quantum Boltzmann equation leads to the two-body decay rate equation (chapter 8). Here, however, we are interested in the influence of collisions on the coherence between the two clock states. There is only one pair of non-vanishing off-diagonal elements $\rho_{12} = \rho_{21}^*$. The collision terms that contribute to the time evolution of ρ_{12} have the form

$$\dot{\rho}_{12}^{coll} = \rho_{12}(i\delta\omega - \Gamma) = \rho_{12}n \sum_j \rho_{jj} \langle v(i\lambda_j - \sigma_j) \rangle, \quad (1.8)$$

where the complex coefficient $i\delta\omega - \Gamma$ is independent of ρ_{12} , and is explicitly split in an imaginary part with $\delta\omega$ as the collisional frequency shift and a real part with Γ the collisional broadening. This interpretation is clear from the exponential solution of Eq. (1.7), neglecting the field term. Using Eq. (1.8), the quantity $i\delta\omega - \Gamma$ is expressed as a sum over all hyperfine states j that are present in the cloud with partial density $n\rho_{jj}$, times a thermal averaged expression that contains the relative velocity v , as well as frequency shift and broadening cross sections λ_j and σ_j . In this introduction we consider only elastic collisions, since inelastic processes result in loss of atoms from the fountain. We then find

$$i\lambda_j - \sigma_j = (1 + \delta_{1j})(1 + \delta_{2j}) \frac{\pi}{k^2} \sum_l (2l + 1) [S_{\{1j\},\{1j\}}^l S_{\{2j\},\{2j\}}^{l*} - 1]. \quad (1.9)$$

For ultra-cold gases we may restrict ourselves to s-wave collisions (only $l = 0$). In the $T \rightarrow 0$ limit we can express the frequency shift and broadening in terms of scattering lengths:

$$i\delta\omega - \Gamma = -\frac{4\pi\hbar}{m} \sum_j n_j (1 + \delta_{1j})(1 + \delta_{2j}) [a_{1j} - a_{2j}]. \quad (1.10)$$

Very elucidating with respect to the formal quantum Boltzmann equation approach is that this expression can also be understood in terms of mean field energy shifts [25]. The easiest way to see this is from expression (1.1), which we extend to a thermal gas by considering $|\phi|^2$ as the density n of the ensemble. In a gas sample consisting of atoms in a superposition of the clock states interacting with atoms in the $|j\rangle$ state, the upper energy level is shifted by

$$\frac{4\pi\hbar^2}{m}n_j(1+\delta_{1j})(1+\delta_{2j})a_{2j}, \quad (1.11)$$

and the lower level by

$$\frac{4\pi\hbar^2}{m}n_j(1+\delta_{1j})(1+\delta_{2j})a_{1j}. \quad (1.12)$$

Here, a_{ij} is the scattering length for $i+j$ elastic scattering. For a single $|j\rangle$ state the transition frequency shifts by the difference of (1.11) and (1.12). After a summation over all states $|j\rangle$, the shifted frequency between the levels results in expression (1.10). The factors $(1+\delta)$ again take care of identical particle symmetry. We note that the Kronecker deltas disappear in case of a Bose condensate. For the same reason decay rates are reduced in a condensate [26], in general n identical particle effects are reduced by $n!$.

1.4 This thesis

This thesis is based on a series of papers that treat several aspects of cold interacting atoms in systems such as the atomic fountain and Bose-Einstein condensates. The compactness of these papers requires generally prior knowledge to collisional aspects. Therefore, in chapter 2 an overview is given of ground-state and excited-state interatomic interactions. Also, some methods briefly mentioned in these papers are discussed in chapter 2: a description of the accumulated phase method can be found in section 2.2. In section 2.3 we treat Raman photoassociation in more detail, and we give an analytic model for this process in section 2.4. In section 2.5 we explain the concepts of Feshbach resonances.

In chapter 3 we investigate the performance of rubidium atoms in cold atomic clocks. It is shown that a frequency standard based on ^{87}Rb is an order of magnitude more accurate than the best available cesium clocks. We show also that a ^{85}Rb clock has opposite partial collisional frequency shifts that allow to cancel the total shift with a special technique. This paper stimulated several experimental groups to construct a rubidium fountain clock. It is also shown that for ^{85}Rb there is an s -wave Ramsauer-Townsend minimum that obstructs evaporative cooling.

In chapter 4 several ^{133}Cs experiments are analyzed and described in a consistent picture, resulting in very restrictive interaction parameters. We show that the singlet

and triplet potentials are almost resonant and that we need a second-order spin-orbit interaction much stronger than expected to explain the large observed decay rates. We predict Feshbach resonances (see section 2.5), which have later been found experimentally at Stanford University. Due to the potential resonance mentioned in the beginning of the previous section, and the associated large decay rates, ^{133}Cs is not very favorable for BEC. However, we show that the ^{135}Cs isotope should perform much better.

Experiments that have been done after the analysis in chapter 4 was carried out, are not consistent with this analysis, as is shown in chapter 5. Two experiments are even mutually inconsistent. Here we present a method based on atomic clock techniques and a juggling fountain, that allows one to measure differences of scattering phases with unprecedented accuracy. With this method one should be able to study the interactions on a high precision level and solve the discrepancies with the information obtained.

In chapter 6 we analyze the dynamics of a Bose-Einstein condensate coupled to a diatomic molecular Bose gas by coherent Raman transitions. The basic concepts and an analytic model of this Raman photoassociation method are given in sections 2.3 and 2.4. The coupling is enhanced by a time-dependent magnetic field sweep over a Feshbach resonance. We show that this is an efficient way to form a condensate of Na_2 molecules in a low rovibrational state. Also in this chapter we treat a Raman photoassociation experiment on a ^{87}Rb Bose-Einstein condensate, where a peculiar substructure is observed in a single rovibrational line. The splitting is caused by the magnetic dipole and second-order spin-orbit interactions, which cancel partially. From this experiment, we can for the first time extract the strength of V^{so} for rubidium.

In chapter 7 we explain the remarkable stability of two overlapping ^{87}Rb condensates in different spin states by means of the near equality of the singlet and triplet scattering lengths. As a result all scattering lengths are approximately equal, and decay rates are small.

We conclude this thesis with an investigation of the interactions of cold hydrogen atoms in chapter 8. Despite the fact that hydrogen atoms have the most accurately known interaction potentials of all atoms, experiments with cold H gas clouds have pointed at discrepancies with theory. We study changes in the short-range singlet and triplet potentials and find that it is impossible to remove all four discrepancies simultaneously.

References

- [1] A. Einstein, Sitzungsber. Kgl. Preuss. Akad. Wiss., 261 (1924); *ibid.*, 3 (1925).
- [2] M.H. Anderson, J.R. Ensher, M.R. Matthews, C.E. Wieman, and E.A. Cornell, Science **269**, 198 (1995).

- [3] K.B. Davis, M.-O. Mewes, M.R. Andrews, N.J. van Druten, D.S. Durfee, D.M. Kurn, and W. Ketterle, Phys. Rev. Lett. **75**, 3969 (1995).
- [4] C.C. Bradley, C.A. Sackett, J.J. Tollett, and R.G. Hulet, Phys. Rev. Lett. **75**, 1687 (1995); C.C. Bradley, C.A. Sackett, and R.G. Hulet, Phys. Rev. Lett. **78**, 985 (1997).
- [5] D.G. Fried, T.C. Killian, L. Willmann, D. Landhuis, S.C. Moss, D. Kleppner, and T.J. Greytak, Phys. Rev. Lett. **81**, 3811 (1998).
- [6] M.R. Matthews, B.P. Anderson, P.C. Haljan, D.S. Hall, C.E. Wieman, and E.A. Cornell, Phys. Rev. Lett. **83**, 2498 (1999).
- [7] C. Raman, M. Köhl, R. Onofrio, D.S. Durfee, C.E. Kuklewicz, Z. Hadzibabic, and W. Ketterle, Phys. Rev. Lett. **83**, 2502 (1999).
- [8] K.W. Madison, F. Chevy, W. Wohlleben, and J. Dalibard, Phys. Rev. Lett. **84**, 806 (2000).
- [9] M. Holland, K. Burnett, C. Gardiner, C. Cirac, and P. Zoller, Phys. Rev. A **54**, R1757 (1996); M.R. Andrews *et al.*, Science **275**, 637 (1997); D.S. Hall *et al.*, Phys. Rev. Lett. **81**, 1543 (1998); B.P. Anderson, M.A. Kasevich, Science **282**, 1686 (1998); S. Inouye, T. Pfau, S. Gupta, A.P. Chikkatur, A. Görlitz, D.E. Pritchard, and W. Ketterle, Science **402**, 641 (1999).
- [10] L.V. Hau, S.E. Harris, Z. Dutton, and C.H. Behroozi, Nature **397**, 594 (1999).
- [11] U. Leonhardt and P. Piwnicki, Phys. Rev. Lett. **84**, 822 (2000).
- [12] N.F. Ramsey, *Nobel prize lecture*, Rev. Mod. Phys. **62**, 541 (1990).
- [13] R.L. Walsworth, Ph.D. Dissertation, Harvard University, 1991; R.L. Walsworth, I.F. Silvera, E.M. Mattison, and R.C. Vessot, Phys. Rev. A **46**, 2495 (1992).
- [14] K. Gibble and S. Chu, Metrologia **29**, 201 (1992).
- [15] B. deMarco and D. Jin, Science **285**, 1703 (1999).
- [16] D. Jaksch, H.-J. Briegel, J.I. Cirac, C.W. Gardiner, and P. Zoller, Phys. Rev. Lett. **82**, 1975 (1999).
- [17] P.W. Shor, *Proceedings of the 35th Annual Symposium on the Foundations of Computer Science*, edited by S. Goldwasser (IEEE Comp. Soc. Press, Los Alamitos, CA), p. 124 (1994).
- [18] S. Chu, *Nobel prize lecture*, Rev. Mod. Phys. **70** 685 (1998); C.N. Cohen-Tannoudji, *ibid.*, 707 (1998); W.D. Phillips, *ibid.*, 721 (1998).
- [19] A. Fetter and J. Walecka, *Quantum theory of many-particle systems* (McGraw-Hill book company, New York, 1971).
- [20] F. Dalfovo, S. Giorgini, L.P. Pitaevskii, and S. Stringari, Rev. Mod. Phys. **71**, 463 (1999).
- [21] A.J. Moerdijk, W.C. Stwalley, R.G. Hulet, and B.J. Verhaar, Phys. Rev. Lett. **72**, 40 (1994).
- [22] L. Deng, E.W. Hagley, J. Wen, M. Trippenbach, Y. Band, P.S. Julienne, J.E. Simsarian, K. Helmerson, S.L. Rolston, and W.D. Phillips, Nature **398**, 218 (1999).
- [23] D. Allan, Proc. IEEE **54**, 105 (1966).

-
- [24] J.M.V.A. Koelman, S.B. Crampton, H.T.C. Stoof, O.J. Luiten, and B.J. Verhaar, Phys. Rev. A **38**, 3535 (1988).
 - [25] B.J. Verhaar in *Atomic Physics* **14**, AIP, New York, 1995, pp. 211-218.
 - [26] Yu. Kagan, B.V. Svistunov, and G.V. Shlyapnikov, Pis'ma Zh. Eksp. Teor. Fiz. **42**, 169 (1985) [JETP Lett. **42**, 209 (1985)].

Interactions and methods

2.1 Molecular potentials and other interactions

For an accurate calculation of scattering properties we need to have precise interaction potentials. The interactions originate from all the electric and magnetic forces between the nuclei and electrons of the two alkali-atoms. They can be specified as a set of terms in a two-particle effective Hamiltonian

$$H = \frac{p^2}{2\mu} + \sum_{j=1}^2 (V_j^{hf} + V_j^Z) + V^{el} + V^\mu + V^{so}, \quad (2.1)$$

that consists of a kinetic energy term, a summation of the single-atom hyperfine and Zeeman interactions V_j^{hf} and V_j^Z , a term V^{el} that accounts for all Coulomb interactions between nuclei and electrons, a direct spin-spin interaction V^μ containing the atomic magnetic dipole operators, and the spin-orbit interaction V^{so} , that is common for excited alkali atoms, but also occurs as an indirect spin-spin interaction in ground-state systems.

The time scale for electronic processes is very short compared to the time-scale of the collision, therefore the electrons adapt themselves adiabatically to the much slower nuclear motion. This allows us to separate the Schrödinger equation into an electronic and a nuclear equation. This is the famous (adiabatic) Born-Oppenheimer approximation. From the electronic equation we find energy curves $E(r)$ that depend on the internuclear separation r . These curves then serve as input to the nuclear equation.

For ground-state collisions or molecules, the Coulomb interactions result in a central potential V^c , that depends on the total electron spin $\vec{S} = \vec{s}_1 + \vec{s}_2$:

$$V^c = V_S(r)P_S + V_T(r)P_T, \quad (2.2)$$

with V_S and V_T the singlet ($S = 0$) and triplet ($S = 1$) potentials, and P_S and P_T the projection operators on the singlet and triplet subspaces. These potentials and the corresponding states are commonly referred to with their Hund's case (a) labelling $^{2S+1}\Lambda_{\pi_e} = ^1\Sigma_g^+$ or $^3\Sigma_u^+$. The electronic parity π_e is $+1(-1)$ for the $g(u)$ subscript. The symbol Λ is the projection of the total electronic orbital angular momentum \vec{L} on the internuclear axis (see also table 2.1), and its values $\Lambda = 0, 1, 2, \dots$ are usually given in

Table 2.1 Overview of the angular momentum operators related to the molecular states, showing the separate notations for projection on the internuclear and on the space-fixed z -axis.

Angular momentum vector	Projection internuclear axis	Projection space-fixed axis
\vec{L}	Λ	m_L
\vec{S}	Σ	m_S
$\vec{j} = \vec{L} + \vec{S}$	$\Omega = \Lambda + \Sigma$	$m_j = m_S + m_L$
\vec{l}	0	m_l
$\vec{J} = \vec{j} + \vec{l}$	Ω	$m_J = m_j + m_l$

spectroscopic notation $\Sigma, \Pi, \Delta, \dots$. The orbital angular momentum l has projection 0 on this axis. Projections of quantum numbers on the space-fixed z -axis are indicated by the usual notation m , for instance m_S stands for the projection of S . The superscript $\sigma = \pm$ denotes the reflection symmetry relative to a plane through the internuclear axis. At long range the spatial parts of the $^1\Sigma_g^+$ and $^3\Sigma_u^+$ states reduce to their Heitler-London form

$$|^{2S+1}\Lambda_{\pi_e}^\sigma\rangle \rightarrow \frac{1}{\sqrt{2}} [|s(1, A)s(2, B) + (-1)^S s(2, A)s(1, B)\rangle]. \quad (2.3)$$

In this notation $s(1, A)$ stands for electron 1 being in an atomic $s_{1/2}$ state around nucleus A . The electronic parity is assured by the factor $\pi_e = (-1)^S$, also making the total space-spin states antisymmetric under electron exchange. The electronic parity is assured by the factor $\pi_e = (-1)^S$, making the total space-spin states anti-symmetric under electron exchange.

In Figure 2.1 the ground-state potentials are shown for Rb. The singlet potential is much deeper than the triplet potential. The energy difference is caused by the exchange interaction which is a direct consequence of the antisymmetry requirement for electron interchange. These potentials have been calculated by *ab initio* methods [1], but they are generally not accurate enough to reliably predict cold-atom scattering quantities with their extreme sensitivity. This is mainly due to uncertainties in the inner region ($r < r_0 = 19 a_0$). Only in the case of hydrogen atoms (see chapter 8) they are able to describe low-energy scattering accurately. However, it is not necessary to know the complete potentials for an accurate description of the scattering processes. In section 2.2 we describe a method to accomplish this based on the long-range dispersion tail with exchange interaction, in combination with boundary conditions at r_0 that can be extracted from experiments.

The magnetic dipole interaction is a direct spin-spin interaction and is often only included when one is interested in inelastic decay, where the generally much stronger exchange decay is forbidden or strongly reduced. Dipolar decay rates are typically

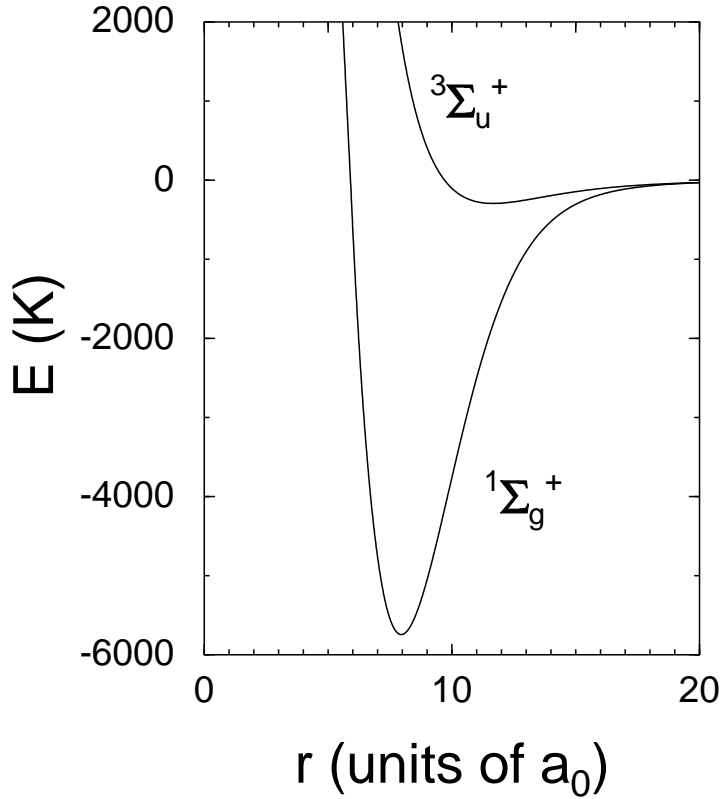


Figure 2.1 Singlet $^1\Sigma_g^+$ and triplet $^3\Sigma_u^+$ ground-state potentials for ^{87}Rb .

three orders of magnitude smaller than exchange decay rates, resulting in a longer lifetime for doubly polarized atoms (fully stretched electronic and nuclear spins) than for instance unpolarized atoms. The interaction is the usual magnetic dipole coupling of intrinsic magnetic moments of electrons and nuclei and can be written in the form

$$V^\mu(\vec{r}) = \mu_0 \frac{\vec{\mu}_1 \cdot \vec{\mu}_2 - 3(\vec{\mu}_1 \cdot \hat{r})(\vec{\mu}_2 \cdot \hat{r})}{4\pi r^3}, \quad (2.4)$$

with $\vec{\mu}_1$ and $\vec{\mu}_2$ the electron or nuclear spin magnetic dipole moments of atom 1 or 2, and $\hat{r} = \vec{r}/r$ the unit vector along the internuclear axis. The electron-electron spin-spin interaction gives the largest contribution, the nuclear-nuclear spin-spin interaction can be safely omitted.

For photoassociation (PA) experiments (described in section 2.3) knowledge of excited state potentials and corresponding spin states is indispensable. A pair of colliding atoms is then excited by a laser photon to an excited molecular bound state. The system can return to the ground-state under spontaneous emission, or it can undergo

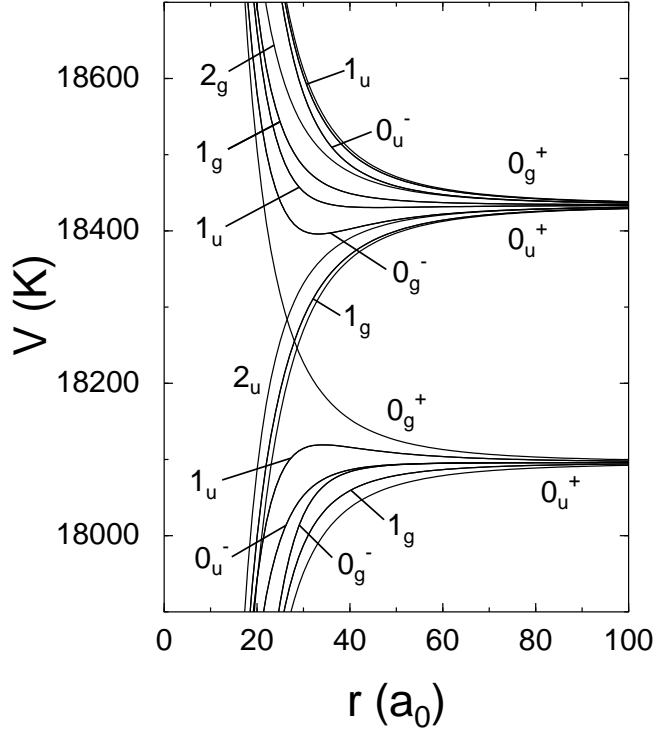


Figure 2.2 Excited state potentials for ^{87}Rb .

stimulated emission by a second resonant laser beam and form a ground-state molecule. This last process is also known as Raman photoassociation.

The excited state potentials are asymptotically connected to the $S_{1/2}P_{1/2}$ or to the $S_{1/2}P_{3/2}$ limit (this is the product of a one-atom electronic S state with a one-atom electronic P state). The main electric interaction between the electrons and nuclei is no longer central, and is given by the electric dipole-dipole interaction

$$V^d(\vec{r}) = \frac{\vec{d}_1 \cdot \vec{d}_2 - 3(\vec{d}_1 \cdot \hat{r})(\vec{d}_2 \cdot \hat{r})}{4\pi\epsilon_0 r^3}, \quad (2.5)$$

where \vec{d}_1 and \vec{d}_2 are the electric dipole operators of atoms 1 and 2 with respect to their own center of mass. Taking only this electric interaction into account, the asymptotic states are given by

$$|^{2S+1}\Lambda, \pi_e\rangle = \frac{1}{2} \left[\{ |s(1, A)p_\Lambda(2, B) + (-1)^S s(2, A)p_\Lambda(1, B)\rangle \} - \pi_e \{ |s(1, B)p_\Lambda(2, A) + (-1)^S s(2, B)p_\Lambda(1, A)\rangle \} \right]. \quad (2.6)$$

Again, for the molecular states having $\Lambda = 0$, we can assign the quantum number $\sigma = \pm$ giving the reflection symmetry of these states relative to an arbitrary plane through the

intermolecular axis. Note that for $\Lambda \neq 0$ this symmetry is no longer a useful quantum number, the reflection parities for different planes through the internuclear axis being incompatible.

Taking only the electric forces into account for the excited state potentials is usually only a good approximation at short internuclear distances ($r < 13 \text{ a}_0$ for Rb): the Hund's case (a) region. At larger separations, the single-atom spin-orbit coupling in the P state, responsible for the fine-structure, becomes comparable to the electronic dipole-dipole interaction, or even dominant (Hund's case (c)). It is given by

$$V^{fs} = \sum_{j=1}^2 \frac{2E^{fs}}{3\hbar^2} \vec{\ell}_j \cdot \vec{s}_j, \quad (2.7)$$

with $\vec{\ell}_j$ the electronic orbital angular momentum of atom j , and E^{fs} the fine-structure splitting. Omitting this interaction is only justified where $V^d \gg V^{so}$, and this is not the case for the internuclear separations we consider in the PA experiments for Rb. Since both interactions together conserve Ω , and not Λ , we use this quantum number to label the adiabatic Born-Oppenheimer potentials. For the Hund's case (c) similar remarks apply with respect to reflection parity for $\Omega = 0$ states as for $\Lambda = 0$ states in the Hund's case (a) above. Due to the large interatomic distance the total set of 16 electronic energy eigenvalues can be found by a rigorous calculation, i.e., by diagonalizing a sum of $V^d + V^{so}$ matrices in a basis of electronic space-spin states [3]. In Figure 2.2 the resulting excited state potentials are shown. A prominent feature of all these potentials is their steepness already at long distance, due to the existence of a diagonal value of V^d in the excited state for a homonuclear system (resonant electric dipole interaction). The hyperfine interaction could also be included, resulting in the so-called 'hyperfine-spaghetti' structure. However, this plays only a role of importance at very large r and is not relevant to the experiments considered here. Further we mention that the magnetic dipole interaction generally plays no role of importance at all for the excited states.

For ground-state alkali atoms there is no diagonal spin-orbit interaction, since a $\Lambda = 0$ state has no preferred direction for the electronic expectation value $\langle \vec{\ell}_1 \rangle$ or $\langle \vec{\ell}_2 \rangle$. However, it appears in second-order when the atomic electron clouds overlap [4]. The electrons then couple via the orbital degrees of freedom with the excited states $|n\rangle = |^2S+1\Lambda_{\pi_e}\rangle$: the excitation occurs by the spin-orbit coupling of one electron spin, the de-excitation by that of the other electron. This generates an Ω -dependent energy shift for the triplet ground-state only:

$$\Delta E_{\Omega}(r) = \sum_n \frac{|\langle n, \Omega | V^{fs} | ^3\Sigma_u^+, \Omega \rangle|^2}{V_T(r) - E_n(r)}. \quad (2.8)$$

Since a common shift of $\Omega = 0$ and 1 states can be included in the effective triplet adiabatic Born-Oppenheimer potential, it is only the (r -dependent) Ω -splitting that plays a role. The magnetic spin-spin interaction splits the $\Omega = 0$ and 1 states in a similar way but with a different r -dependence ($1/r^3$). Therefore, in terms of the total atomic spin vectors and their relative angular position, the two interactions have a similar form:

$$f(r) [\vec{s}_1 \cdot \vec{s}_2 - 3(\vec{s}_1 \cdot \hat{r})(\vec{s}_2 \cdot \hat{r})]. \quad (2.9)$$

Only the radial form factor is different. The similarity in form reflects that their origin is alike: while the direct spin-spin interaction V^μ occurs via the electromagnetic field modes, the indirect interaction V^{so} takes place via the modes of the electronic orbital motion. For the lighter alkali atoms this interaction is negligible, but for the heavier alkalis as Rb and Cs it can be much larger at short range than the direct V^μ . For Cs, it dominates all inelastic scattering processes, and as we have shown (see chapter 4) is even responsible for additional Feshbach resonances. Mies *et al.* [6] showed with an *ab initio* calculation that the interaction has an effective form

$$V_{\Omega=0}^{so}(r) = -2V_{\Omega=1}^{so}(r) = -C^{so}\alpha^2 e^{-\beta(r-r_{so})}, \quad (2.10)$$

with α the fine structure constant and C^{so} , β and r_{so} fit parameters to the *ab initio* results. It was soon realized (see chapter 4) that the strength C^{so} had to be a factor 4 larger than here predicted to account for the observed strong decay [7].

Note that Eq. (2.9) has the structure of an inner product of two second-rank spherical tensors [8]:

$$\begin{aligned} (\vec{s}_1, \vec{s}_2)_2 \cdot (\hat{r}, \hat{r})_2 &= \sum_{\sigma=-2}^2 (-1)^\sigma (\vec{s}_1, \vec{s}_2)_{2\sigma} (\hat{r}, \hat{r})_{2-\sigma} \\ &\sim \sum_{\sigma=-2}^2 (-1)^\sigma (\vec{s}_1, \vec{s}_2)_{2\sigma} Y_{2-\sigma}(\hat{r}). \end{aligned} \quad (2.11)$$

This is of importance for the discussion of the selection rules in the following section.

2.2 Boundary conditions: accumulated phase method

A description of cold collisions between ground-state atoms (and also weakly bound states) requires highly accurate central interaction potentials. In particular the position of the last bound state is very important as expressed by a fractional vibrational quantum number at dissociation, denoted by v_{DS} for the singlet and v_{DT} for the triplet potential. In section 2.1 we mentioned that most *ab initio* potentials do not possess the required accuracy. A way to account for that is by means of a boundary condition at a radius r_0 , defined by an accumulated phase which summarizes the history

of the collision for $r < r_0$ for either the singlet or the triplet channel. The radius is carefully chosen such that two conditions are fulfilled: First, for $r < r_0$ the atomic motion is adiabatic with S as a good quantum number. The singlet and triplet spin states in Figure 2.1 are sufficiently far apart to be negligibly coupled by the sum of the atomic hyperfine interactions in equation (2.1). Second, for $r > r_0$ the potentials can be accurately described by their asymptotic form

$$V_{S/T}(r) = -\frac{C_6}{r^6} - \frac{C_8}{r^8} - \frac{C_{10}}{r^{10}} \mp V^{exch}(r). \quad (2.12)$$

A typical value for rubidium or cesium is $r_0 = 19 \text{ a}_0$. The dispersion coefficients C_6 , C_8 and C_{10} have been calculated with reasonable accuracy [9, 10], but are sometimes improved by experimental results. The exchange interaction V^{exch} has an analytic form derived by Smirnov and Chibisov [11] and contains parameters that have been calculated more recently by Hadinger and Hadinger [12].

The concept of an accumulated phase has originally been introduced in the spirit of the WKB approximation as the local phase at r_0 of a rapidly oscillating radial wave function. Its value $\phi_S(E, l)$ and $\phi_T(E, l)$ at r_0 for the singlet and triplet wave functions is related to the WKB expression

$$\psi_{S/T}(r_0) = A \frac{\sin \left[\int^{r_0} k(r) dr \right]}{\sqrt{k(r_0)}} \equiv A \frac{\sin \phi_{S/T}(E, l)}{\sqrt{k(r_0)}}, \quad (2.13)$$

and its radial derivative. Here $k(r)$ is the local radial wave number:

$$k^2(r) = \frac{2\mu}{\hbar^2} \left[E - V_{S/T}(r) - \frac{\hbar^2 l(l+1)}{2\mu r^2} \right]. \quad (2.14)$$

It is very convenient to define the boundary condition in this way. The validity of the WKB approximation, however, is not necessary since the boundary condition can be reformulated in terms of a logarithmic derivative. Owing to the small E and l ranges involved in ultra-cold collisions and the relevant weakly-bound states below threshold, the phases can be safely expanded up to first-order Taylor terms in E and $l(l+1)$:

$$\phi_{S/T}(E, l) = \phi_{S/T}(0, 0) + \frac{\partial \phi_{S/T}}{\partial E} E + \frac{\partial \phi_{S/T}}{\partial [l(l+1)]} l(l+1). \quad (2.15)$$

The zero-order terms are directly related to the quantum numbers v_{DS} and v_{DT} and are fitted to experimental data. The energy-derivative corresponds to the classical sojourn time $\tau = 2\hbar \partial \phi_{S/T} / \partial E$ of the atoms in the range $r < r_0$. The $l(l+1)$ derivative is connected to the orbital angular motion of the rotating two-atom system. The first-order derivatives are less critical than the zero-order terms and are usually determined from the best available *ab initio* potentials.

For $r > r_0$ there is a coupling region where the exchange interaction is of similar magnitude as the internal hyperfine and Zeeman energies, as indicated in Figure 2.3.

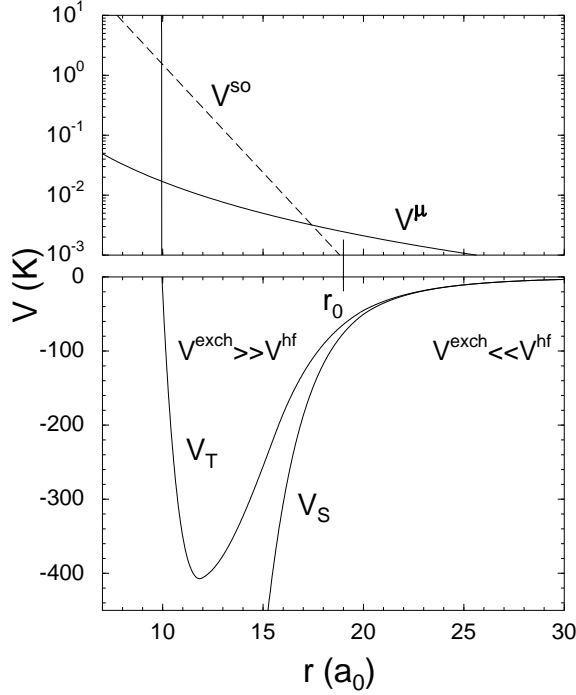


Figure 2.3 Singlet and triplet potentials for ^{133}Cs , together with the radial part of the magnetic dipole interaction V^μ and the second order spin-orbit interaction V^{so} . For $r < r_0$ the hyperfine interaction V^{hf} is dominated by the exchange interaction V^{exch} , but for long range the latter is negligible.

For larger interatomic distances where V^{exch} has become negligibly small, the atomic motion is adiabatic again, and here the two-particle hyperfine states form a good basis.

In the above discussion we have neglected the spin-spin interactions V^μ and V^{so} , which are responsible for corrections on the adiabatic motion and lead to decay. Due to their structure as an inner product of second-rank spatial and spin tensors (see Eq. (2.11)) they can couple states with l values restricted by $|l' - l| = 0, 2$ and $l = 0 \rightarrow l' = 0$ forbidden. As a direct consequence, transitions non-diagonal in l can occur and bound states generally contain a mixture of l values. We come back to that in section 2.5 where we discuss additional Feshbach resonances caused by this effect.

The magnetic dipole interaction V^μ contributes mainly due to its long-range behavior $1/r^3$. We can safely neglect its influence over the relatively short range $r < r_0$. In the same range the indirect interaction V^{so} can be very strong and it exceeds the dipole interaction by several orders of magnitude at short range, but is negligibly small at r_0 and beyond, as can be seen from Fig. 2.3.

The influence of V^{so} can be taken into account in a model-independent way by essentially one additional parameter. This can be seen as follows. In the first place we note that we can account for the mixing by V^{so} between the triplet channels by means of a local S -matrix, that will be part of the boundary condition. The adiabatic solutions without spin-spin interaction are in the vicinity of $r = r_0$ given by

$$F_i(r) = \frac{\sin\left(\int_{r_0}^r k(r) dr + \phi_i\right)}{\sqrt{k_i(r)}}, \quad \phi_i = \phi_{S/T}(E_{tot} - \varepsilon_i, l_i) \quad (2.16)$$

where the channels i differ from each other by their singlet/triplet character, their l value and their internal energy ε_i . To formulate a local S -matrix at r_0 we introduce a complementary solution

$$G_i(r) = -\frac{\cos\left(\int_{r_0}^r k(r) dr + \phi_i\right)}{\sqrt{k_i(r)}}, \quad (2.17)$$

satisfying the Wronskian condition $W[F_i, G_i] \equiv F_i' G_i - F_i G_i' = 1$. We calculate the influence of V^{so} by means of a solution of the Schrödinger equation for $r < r_0$ using the *ab initio* form (2.10) and variations thereof. At r_0 we expand that solution in F and G functions. This defines a local S -matrix, here called the C -matrix, that accounts for the V^{so} interaction. This matrix is independent of the accumulated phases: it depends only on the envelope of the rapidly oscillating F functions. The boundary condition can then, for given v_{DS} and v_{DT} , be specified by

$$\underline{u}(r) = \underline{F}(r) + \underline{G}(r)\underline{C} \quad (r \approx r_0). \quad (2.18)$$

Note that we could have used complex ingoing and outgoing exponentials as basis functions instead of cosine and sine functions. The resulting complex S -matrix has a simple relation with \underline{C} . Choosing the functions (and therefore also \underline{C}) to be real, has the advantage that the computer program can be restricted to real numbers.

It turns out that this C -matrix can to very good approximation be also obtained without solving a coupled channels equation in the range $r < r_0$: a constant times the matrix representation of the spin-spin interaction (2.9), independent of the radial form factor $f(r)$, gives the same result. This can be understood as follows. As calculations show, \underline{C} depends on the spin-spin interaction only in first order. A perturbation argument leads to the conclusion that the elements C_{ij} of \underline{C} have the form of a radial integral of $f(r)$ multiplied by a product $F_i(r)F_j(r)$. Since the latter are almost equal over the range where V^{so} contributes significantly, the matrix representation of the spin-angular part of (2.9) is the only part in which the dependence on i, j survives. We conclude that we can completely discard the detailed form of V^{so} and specify only a single multiplicative constant, the effective strength of V^{so} relative to the *ab initio* result of Mies *et al.* [6].

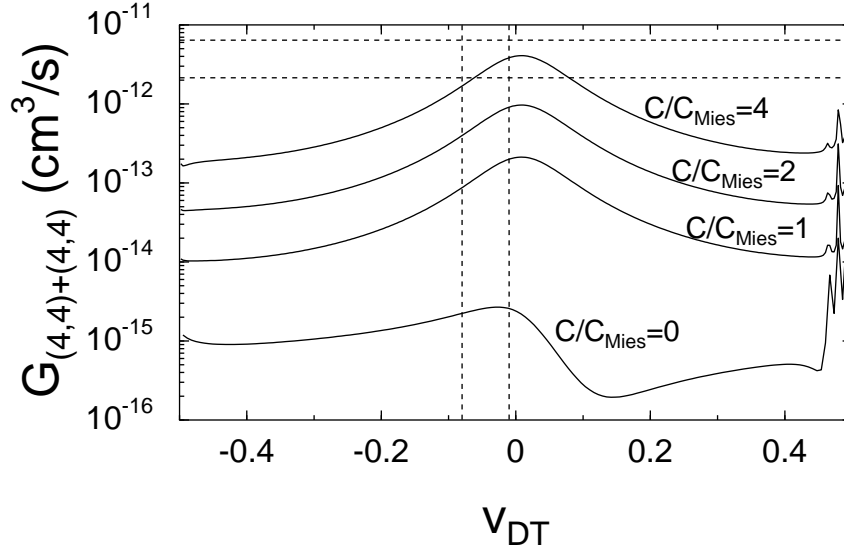


Figure 2.4 Rate coefficient G for the decay of Cs atoms in the $|4, 4\rangle$ hyperfine state, as function of potential parameter v_{DT} and for several strengths of V^{so} . The experimental boundaries for G are given by horizontal dashed lines; the theoretical range for v_{DT} (see chapters 4 and 5) is indicated by two vertical dashed lines.

A result of this method is shown in Figure 2.4, where we calculate the rate coefficient for the decay of the doubly polarized spin state for Cs ($|f, m_f = 4, 4\rangle$) as a function of v_{DT} and for several strengths of V^{so} . It is immediately clear that the magnetic dipole interaction on its own (for $C^{so} = 0$) is too weak to account for the measured decay. In order to get agreement with the experimental rates we even have to increase the *ab initio* strength by a factor four [13].

2.3 Raman photoassociation

Photoassociation (PA) spectroscopy is a powerful tool to probe the interatomic interactions. A colliding pair of cold atoms is excited by a laser beam to an electronically excited bound molecular state (these states were treated in section 2.1). The excitation occurs preferably near the outer turning point of the excited state, where the relative velocity of the atoms is comparable to that in the ground-state (Franck-Condon principle). The excitation probability is approximately proportional to the square of the radial ground-state wave function.

Two different experiments can be distinguished: first, a one-color (one-photon) PA process, where the excitation is followed by spontaneous decay to the ground state; second, a Raman PA process (also called two-color or two-photon PA process), where

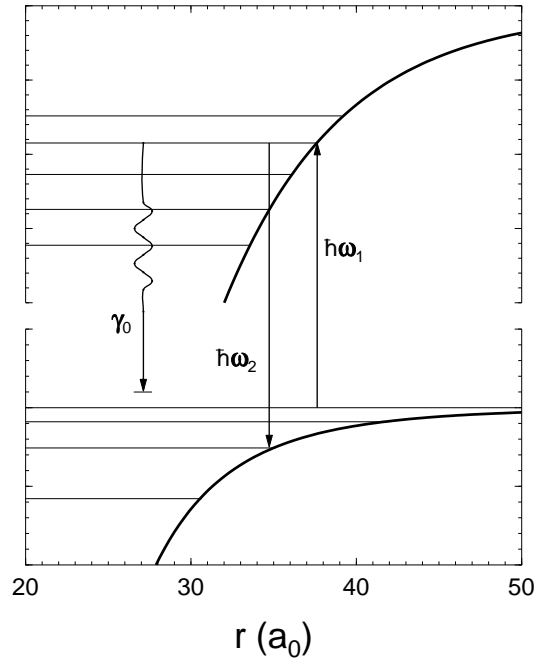


Figure 2.5 One-color and Raman photoassociation for $^{87}\text{Rb}_2$. A colliding atom pair is excited to an excited molecular state by absorption of a laser photon with frequency ω_1 . Spontaneous emission with rate γ_0/\hbar leads to loss of atoms from the trap. When a second laser, with frequency ω_2 , is tuned to a bound-bound transition a resonance is observed by means of a decrease of trap loss.

a second laser, tuned to a ground-state bound level, initiates stimulated emission. In a one-color PA process an increased trap loss is observed when the laser frequency corresponds to an excited rovibrational level. Since the atoms gain considerable radial kinetic energy before decay, they have enough energy to leave the trap. This results in a measurable loss of trapped atoms. With this type of experiment, information is obtained about the structure of the ground-state wave function. The method has been successful in improving the knowledge of interatomic Rb [14], Na [15] and Li [16] interactions. In a Raman PA process, the increase of trap loss is also observed when the first laser is tuned to an excited level. However, the trap loss decreases when the second laser is tuned to a bound-bound transition. This is observed as a dip in the one-color resonance profile. Since the initial collision energy is very small, the frequency difference $\omega_1 - \omega_2$ corresponds to the binding energy of a ground-state bound level. Experiments of this kind have also been done for Rb [17], Na [18] and Li [19]. Both types of experiments are illustrated in Fig. 2.5.

In the following section we describe the Raman photoassociation process in a semi-

analytic way using Feshbach's resonance theory [20]. It has also been described to lowest order in the laser intensities by Bohn and Julienne [21], based on the generalized multichannel quantum defect theory (GMQDT). We are also able to simulate this two-color experiment for all laser intensities with a full coupled channels calculation that contains the three subspaces corresponding to the three stages of the two-atom system in the PA process: the ground-state continuum, the excited-state bound channels and the ground-state bound channels. The interactions within each subspace have already been discussed in section 2.1. Here we derive the expressions for the laser-couplings between the three subspaces. In order to simplify our expressions, we expand the excited molecular states $|\Omega_{\pi_e}^\sigma, Jm_J\rangle$ in the $|\{L\Lambda\Sigma\}, Jm_J, \pi_e\rangle$ molecular basis states. The expansion is carried out numerically following the method indicated in the previous section, which leads by a rigorous diagonalization to r -dependent electronic eigenvalues (equal to potentials in Figure 2.2) as well as eigenvectors. The eigenvectors allow us in the next section to deal with the total bra-state in Eq. (2.29). Also the ground-state two-particle hyperfine states $|\{f_1 m_{f_1} f_2 m_{f_2}\}, lm_l\rangle$ are expanded in the molecular basis $|Sm_S Im_I, lm_l\rangle$. An advantage of these bases is that the coupling matrix-elements are diagonal in the quantum numbers $Sm_S Im_I$ which are unaffected in the excitation and de-excitation processes. The total parity of the excited state should be equal to $\pi_{tot} = -(-1)^l$. This can be easily understood from the fact that the two atomic ground states have parity $+1$, so that the total ground state has parity $(+1)^2(-1)^l = (-1)^l$, while the electric dipole transition changes parity. The excited states $|L\Lambda\Sigma, Jm_J, \pi_e\rangle$ are not automatically equipped with the required total parity. We have to combine these states linearly with opposite $+\Omega$ and $-\Omega$ values to construct states that meet the requirement:

$$|\{L\Lambda\Sigma\}, Jm_J, \pi_e \pi_{tot}\rangle = \frac{|L\Lambda\Sigma, Jm_J, \pi_e\rangle - \pi_{tot}(-1)^{L+S+J}|L - \Lambda\Sigma - \Sigma, Jm_J, \pi_e\rangle}{\sqrt{2(1 + \delta_{\Lambda\Sigma, 00})}}. \quad (2.19)$$

The $\{\}$ brackets indicate that these states have a definite total parity. The linear combination can be found from a transformation of a $|(LS)jl, Jm_J\rangle$ state to a $|(LS)j\Omega, Jm_J\rangle$ state, which are then decoupled to $|L\Lambda\Sigma, Jm_J, \pi_e\rangle$ states. We note that a linear combination is strictly not necessary for $\Lambda = \Sigma = 0$ since then the separate states have already the required parity $\pi_{tot} = -(-1)^{L+S+J}$.

With this definition we calculate the basic laser coupling matrix elements

$$\langle\{L\Lambda\Sigma'\Sigma\}, Jm_J, \pi_e, \pi_{tot}, I'm'_I| - (\vec{d}_1 + \vec{d}_2) \cdot \vec{\epsilon}_L \left(\frac{I_L}{2\varepsilon_0 c}\right)^{\frac{1}{2}} |00Sm_S Im_I, lm_l\rangle, \quad (2.20)$$

in terms of which the required laser coupling amplitude Eq. (2.29) can be expressed. In (2.20) we have made explicit the quantum numbers $L = 0$, $m_L = 0$ for the ground state.

We are then left with the problem of calculating the matrix elements in (2.29) with each of the two terms in (2.19) substituted for the bra-state. Taking the first of these terms as an example, we note that it is the product of a symmetric top eigenfunction [22] and a body-fixed electronic state:

$$|L\Lambda S\Sigma, Jm_J, \pi_e\rangle = \left(\frac{2J+1}{4\pi}\right)^{\frac{1}{2}} D_{m_J, \Lambda+\Sigma}^{(J)*}(\alpha\beta 0) |L\Lambda S\Sigma, \pi_e\rangle, \quad (2.21)$$

with $D_{m'm}^{(j)}(\alpha\beta\gamma)$ a Wigner D -function [8] of the Euler angles α, β , and γ . Furthermore, $|L\Lambda S\Sigma, \pi_e\rangle$ is the product of a space state (2.6) and a spin state:

$$|L\Lambda S\Sigma, \pi_e\rangle = |^{2S+1}\Lambda, \pi_e\rangle \otimes |S\Sigma\rangle \quad (2.22)$$

with body-fixed angular momentum projections Λ and Σ . We now express these states in states with space-fixed projections using Wigner D -functions:

$$|L\Lambda S\Sigma, \pi_e\rangle = \sum_{m_L m_S} D_{m_L \Lambda}^{(L)*}(\alpha\beta 0) D_{m_S \Sigma}^{(S')*}(\alpha\beta 0) |Lm_L Sm_S, \pi_e\rangle, \quad (2.23)$$

use the product relation

$$D_{m_L \Lambda}^{(L)} D_{m_S \Sigma}^{(S')} = \sum_{jm_j \Omega} (Lm_L Sm_S | jm_j) (L\Lambda S\Sigma | j\Omega) D_{m_j \Omega}^{(j)} \quad (2.24)$$

and the values of the resulting matrix-elements with space-fixed projections:

$$\begin{aligned} \langle Jm_J \Omega | D_{m_j \Omega}^{(j)*}(\alpha\beta 0) | lm_l 0 \rangle &= \left(\frac{2J+1}{4\pi}\right)^{\frac{1}{2}} \left(\frac{2l+1}{4\pi}\right)^{\frac{1}{2}} \times \\ &\int_0^{2\pi} d\alpha \int_0^\pi \sin \beta d\beta D_{m_J \Omega}^{(J)}(\alpha\beta 0) D_{m_j \Omega}^{(j)*}(\alpha\beta 0) D_{m_l 0}^{(l')*}(\alpha\beta 0) \\ &= \left(\frac{2l+1}{2J+1}\right)^{\frac{1}{2}} (jm_j lm_l | Jm_J) (j\Omega l 0 | J\Omega) \end{aligned} \quad (2.25)$$

and

$$\begin{aligned} &\frac{1}{2} [\langle s(1A) p_{m_L}(2B) + (-1)^S s(2A) p_{m_L}(1B) | -\pi_e \langle s(1B) p_{m_L}(2A) |] \times \\ &(-1)^{m_L} (\vec{\varepsilon}_L)_{-m_L} (\vec{d}_1 + \vec{d}_2)_{m_L} \frac{1}{\sqrt{2}} [s(1A)s(2B) + (-1)^S s(2A)s(1B)] \\ &= (-1)^{m_L} (\vec{\varepsilon}_L)_{-m_L} \sqrt{2} d. \end{aligned} \quad (2.26)$$

Here we have rewritten the Cartesian inner product of the dipole vector operator with the laser polarization vector in terms of spherical tensor components:

$$\vec{\varepsilon}_L \cdot (\vec{d}_1 + \vec{d}_2) = \sum_{\mu} (-1)^{\mu} (\vec{\varepsilon}_L)_{-\mu} (\vec{d}_1 + \vec{d}_2)_{\mu}. \quad (2.27)$$

Finally we make use of

1. The selection rule $\pi_e = -(-1)^S$ following from the change of electronic parity in the electronic dipole transition (the initial electronic parity is $(-1)^S$).
2. The fact that the electron and nuclear spins are unaffected by the electric dipolar excitation so that the quantum numbers $S m_S I m_I$ are not changed in the transition.
3. The equality

$$\langle p_{m_L} | (\vec{d})_\mu | s \rangle = \delta_{m_L \mu} d \quad (2.28)$$

with d the reduced electric dipole moment determined in the experiments of Ref. [14].

An example of a predicted trap loss function $|S_{PA}|^2$ is shown in Figure 2.6 as a function of the two PA laser frequencies. It is the result of a full coupled-channels calculation. As expected (see the beginning of this section) the trap loss has the profile of a one-color PA peak as a function of ν_1 near a free-bound resonance ($\nu_1 = 0$ MHz), with a superposed suppression when the second laser is tuned in resonance with a bound-bound transition ($\nu_2 - \nu_1 \approx 637$ MHz).

2.4 Analytic model for photoassociation

Raman photoassociation can be described in an analytic way. In this section the resonance theory given by Feshbach [20] is used in combination with a dressed state picture [23] to describe their photoassociation process. The total Hilbert space of ground state and excited state channels is divided in an open-channel subspace \mathcal{P} and a complimentary closed-channel part \mathcal{Q} . In this picture both the bound excited state $|\Phi_1\rangle$ and the bound ground state $|\Phi_2\rangle$ belong to \mathcal{Q} . The \mathcal{P} -space contains the state $|\psi_i^{(+)}\rangle$ corresponding to the initial channel $|\{f_1 m_{f_1} f_2 m_{f_2}\}, l m_l\rangle$ and the state $|\psi_f^{(-)}\rangle$ corresponding to a final decay channel $|\{f'_1 m'_{f_1} f'_2 m'_{f_2}\}, l' m'_l \gamma\rangle$, with an additional spontaneously emitted photon γ . The first laser is responsible for a coupling H_{QP} between the two subspaces giving rise to the transition rate γ_{L_1}/\hbar for formation of the excited state:

$$\begin{aligned} \gamma_{L_1} &= 2\pi \left| \langle \Phi_1 | H_{QP} | \psi_i^{(+)} \rangle \right|^2 \\ &= 2\pi \left| \langle \Phi_1 | (\vec{d}_1 + \vec{d}_2) \cdot \vec{\epsilon}_{L_1} \left(\frac{I_{L_1}}{2\varepsilon_0 c} \right)^{1/2} | \psi_i^{(+)} \rangle \right|^2. \end{aligned} \quad (2.29)$$

For the sake of simplicity we disregard the contributions due to different rotational projections m_J and the $I m_I$ substructure as well as a multiplicity of initial channels

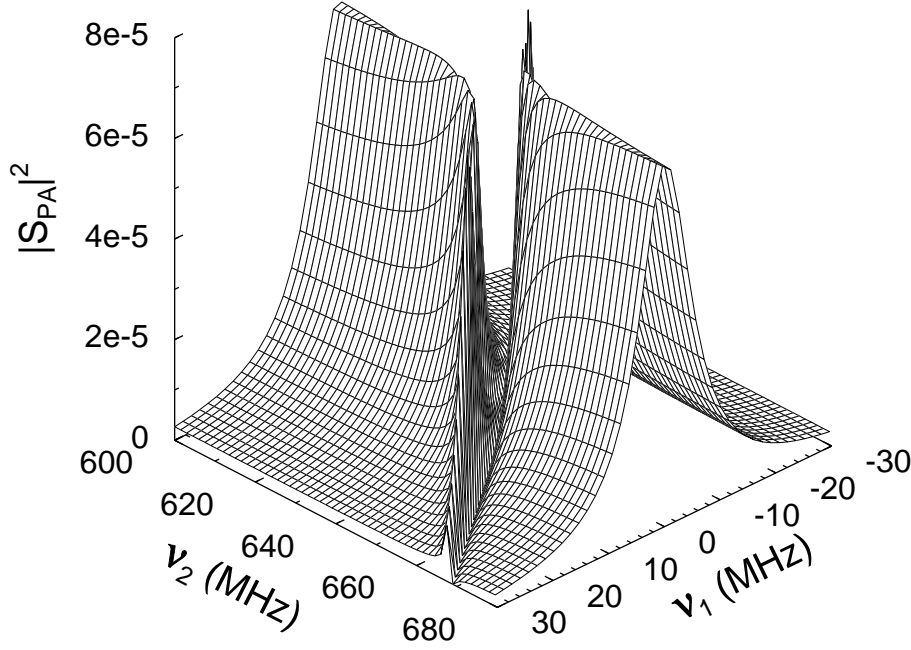


Figure 2.6 Photoassociation trap loss $|S_{PA}|^2$ as a function of the two laser frequencies $\nu_{1,2} = \omega_{1,2}/2\pi$ with the free-bound transition frequency (0.376402×10^{15} Hz) subtracted. Both laser intensities are equal to 10 W/cm^2 . Both lasers are polarized perpendicular to the magnetic field. The probed ground-state level is a ^{87}Rb $l = 0$ level, formed from a ^{87}Rb Bose-Einstein condensate prepared in the $|1, -1\rangle$ state.

and spontaneous decay channels. We note, however, that the derivation can be readily generalized to such situations using Feshbach's theory in the general form of Ref. [20]. In particular, the case of more than two bound states can be treated by increasing the dimension of the Hamiltonian matrix (2.30) below. In the previous section we showed how to calculate γ_{L_1} . For this we need the r -dependent laser coupling matrix elements. In Figure 2.7 all of these elements are shown that exhaust the electric dipole sum rule, starting from the $(1, -1) + (1, -1)$ free channel. The transition between the excited bound state and the final decay channel gives the decay width due to spontaneous decay $\gamma_0 = \left| \langle \psi_f^{(-)} | H_{PQ} | \Phi_1 \rangle \right|^2$. The second laser couples the two bound states within the Q -subspace leading to a Hamiltonian submatrix

$$\underline{\underline{H}} = \begin{pmatrix} E_1 - \frac{i}{2}\gamma & \frac{1}{2}\hbar\Omega_{12} \\ \frac{1}{2}\hbar\Omega_{21} & E_2 \end{pmatrix}. \quad (2.30)$$

Here $\gamma = \gamma_0 + \gamma_{L_1}$ is the total width of the excited state. The Rabi frequency $\Omega_{12} = \Omega_{21}$ represents the coupling between the two levels and is proportional to the square root

of the laser intensity I_{L_2} : $\Omega_{12} = \frac{2}{\hbar} \langle \Phi_1 | (\vec{d}_1 + \vec{d}_2) \cdot \vec{\epsilon}_{L_2} (I_{L_2}/2\epsilon_0 c)^{1/2} | \Phi_2 \rangle$. The energy levels of the bound excited and ground states are indicated by E_1 and E_2 . Note that these energies have to be interpreted in the light of the dressed-state picture. The corresponding bare-state energies are $E_1 + \hbar\omega_1$ and $E_2 + \hbar\omega_1 - \hbar\omega_2$, defined relative to the threshold of the ground state continuum.

The scattering matrix element that describes the transition from the initial free ground-state atoms to the spontaneous decay channel is given by

$$S_{PA} = \frac{\langle \psi_f^{(-)} | H_{PQ} | \omega_+ \rangle \langle \omega_+ | H_{QP} | \psi_i^{(+)} \rangle}{E - \lambda_+} + \frac{\langle \psi_f^{(-)} | H_{PQ} | \omega_- \rangle \langle \omega_- | H_{QP} | \psi_i^{(+)} \rangle}{E - \lambda_-}, \quad (2.31)$$

with $\omega_{\pm} = \sum_i A_i^{\pm} \Phi_i^J$ the eigenfunctions of Hamiltonian (2.30). The corresponding eigenvalues are given by

$$\lambda_{\pm} = \frac{1}{2}(E_1 - \frac{i}{2}\gamma + E_2) \pm \frac{1}{2}\sqrt{(E_1 - \frac{i}{2}\gamma - E_2)^2 + \hbar^2\Omega_{12}^2}. \quad (2.32)$$

We stress that only the Φ_1 component of ω_{\pm} interacts with the states in \mathcal{P} -space. Therefore, the transition amplitude is written as

$$\begin{aligned} S_{PA} &= \frac{\gamma_0^{1/2} A_1^+ A_1^{+*} \gamma_{L_1}^{1/2}}{E - \lambda_+} + \frac{\gamma_0^{1/2} A_1^- A_1^{-*} \gamma_{L_1}^{1/2}}{E - \lambda_-} \\ &= (\gamma_0 \gamma_{L_1})^{1/2} \frac{|A_1^+|^2 (E - \lambda_-) + |A_1^-|^2 (E - \lambda_+)}{(E - \lambda_+)(E - \lambda_-)}. \end{aligned} \quad (2.33)$$

The loss rate due to two-color photoassociation is equal to $\frac{\pi v}{k^2} |S_{PA}|^2$ which has to be averaged over the initial thermal distribution. In first order in the laser intensities, the square of the transition matrix element results in

$$|S_{PA}|^2 = \frac{\gamma_0 \gamma_{L_1} (E - E_2)^2}{[(E - E_+)(E - E_-)]^2 + \frac{\gamma_0^2}{4} (E - E_2)^2}, \quad (2.34)$$

with

$$E_{\pm} = \frac{1}{2}(E_1 + E_2) \pm \frac{1}{2}\sqrt{(E_1 - E_2)^2 + \hbar^2\Omega_{12}^2}, \quad (2.35)$$

i.e.

$$(E - E_+)(E - E_-) = (E - E_1)(E - E_2) - \frac{1}{4}\hbar^2\Omega_{12}^2 + O(\Omega_{12}^4). \quad (2.36)$$

In view of the $(E - E_2)^2$ factor we immediately see that a dip occurs for a two-photon transition resonant with the ground-state bound level. When we set $\Omega_{12} = 0$ we effectively switch off the second laser. This gives the one-color transition probability

$$|S_{PA}|^2 = \frac{\gamma_0 \gamma_{L_1}}{(E - E_1)^2 + \frac{\gamma_0^2}{4}}. \quad (2.37)$$

The above expressions (2.34) and (2.37) in the low intensity limit are equal to those derived by Bohn and Julienne [21].

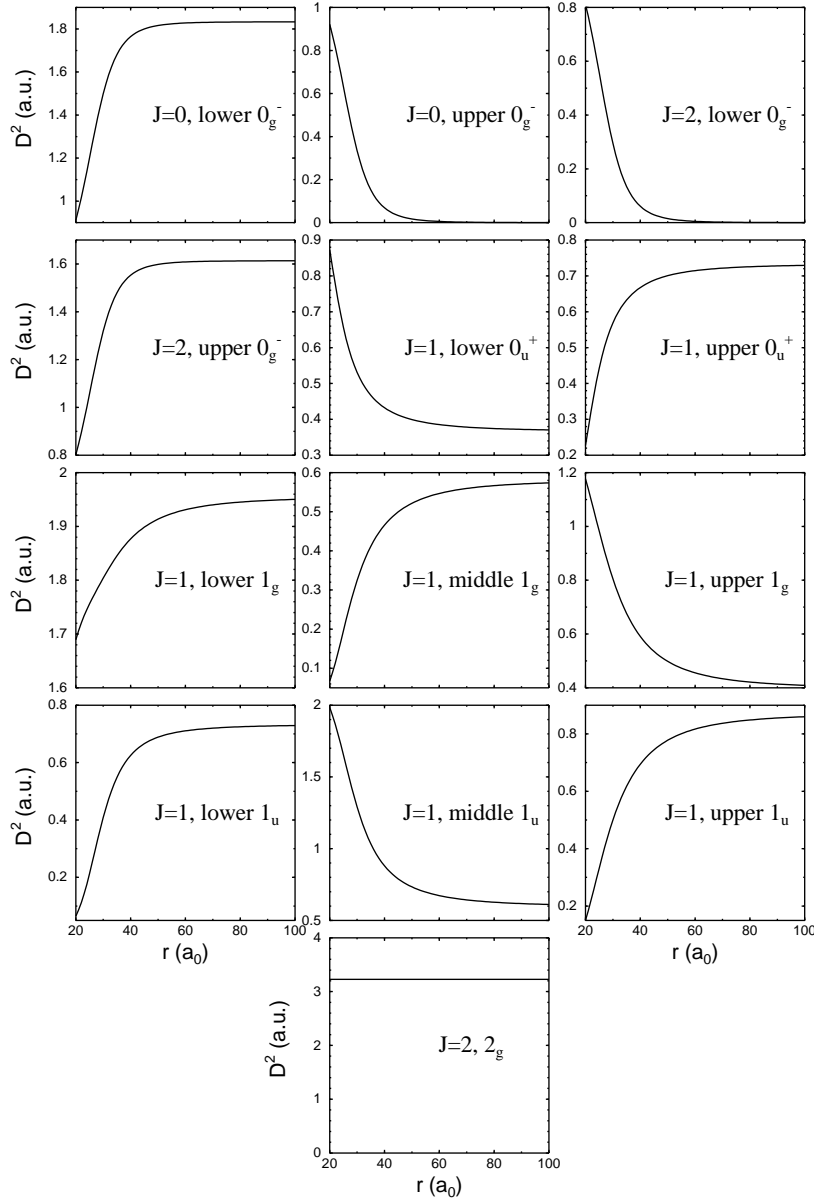


Figure 2.7 Laser coupling matrix elements D^2 divided by $2\pi I_L / (2\epsilon_0 c)$, as function of the internuclear distance r , for several excited states. The polarization is chosen perpendicular to the magnetic field. The initial ground state channel corresponds to two ^{87}Rb atoms in $|f, m_f = 1, -1\rangle$ for an $l = 0$ collision. We included a summation over the m_J and Im_I excited state substructure. The sum over all D^2 values obeys the sum rule $\sum_j D_j^2 = 2d^2$, independent of r .

2.5 A new Feshbach resonance phenomenon

The position of the last bound state in the central interaction potentials is very important for the behavior of the collisional ground-state wave functions, as we mentioned already in section 2.2. For instance, when a bound state in the triplet potential is very close to threshold, i.e. $v_{DT} \approx 0 \pmod{1}$, the potential is resonant and the impact on the scattering process will be large. This special case occurs for Cs (see chapters 4 and 5), resulting in large scattering lengths and enhanced decay rates (section 2.2). In a multi-channel system, however, another type of resonance may occur: a bound state may cross the threshold energy as a function of magnetic field and enter the continuum as a quasi-bound state, resulting in a field-dependent Feshbach scattering resonance. This is illustrated in Figure 2.8, where both the field-dependence of bound states below threshold is shown, and the associated elastic scattering behavior just above threshold characterized by the scattering length. For fields close to resonance the dispersive behavior of the scattering length is given by

$$a(B) = a_{bg} \left(1 - \frac{\Delta}{B - B_0} \right). \quad (2.38)$$

At B_0 the bound state crosses the threshold energy and the scattering length changes sign through infinity. The scattering length differs in sign from its background value a_{bg} (which may weakly depend on the field) over a field width Δ . Feshbach resonances are described in a similar way with Feshbach's resonance theory as the Raman PA process (see section 2.4). Again, the open collision channels correspond to \mathcal{P} -space and are coupled to the closed channels in \mathcal{Q} -space. These resonances have first been studied in nuclear physics [24] and were subsequently studied by Fano in an atomic context [25]. Tiesinga *et al.* pointed out that their occurrence in collisions of ultracold atoms gives rise to a typical resonance behavior of the scattering length as a function of magnetic field, which may be used to tune the interatomic interactions in a condensate [26]. Moerdijk *et al.* [27] derived the resonance formula Eq. (2.38) of the scattering length by applying Feshbach's theory in the low-energy limit. In 1997 we were able to make the first reliable prediction of Feshbach resonances: three resonances in $^{85}\text{Rb} + ^{85}\text{Rb}$ collisions in an easily accessible field range [28]. Later, one of these resonances was observed experimentally [29, 30], just after the first experimental observation of a Feshbach resonance for Na [31].

The coupling between \mathcal{P} - and \mathcal{Q} -spaces for these Rb and Na resonances is restricted to $l = 0$ channels. In Cs, however, a new phenomenon occurs that we found when investigating the prospects for BEC in this alkali species (chapter 4): the phenomenon of Feshbach resonances induced by indirect spin-spin interaction. Unlike Rb and Na, where V^{so} plays a more modest role, three of the four Cs Feshbach resonances that we predict are induced by V^{so} and are a result of coupling between \mathcal{P} -states with $l = 0$

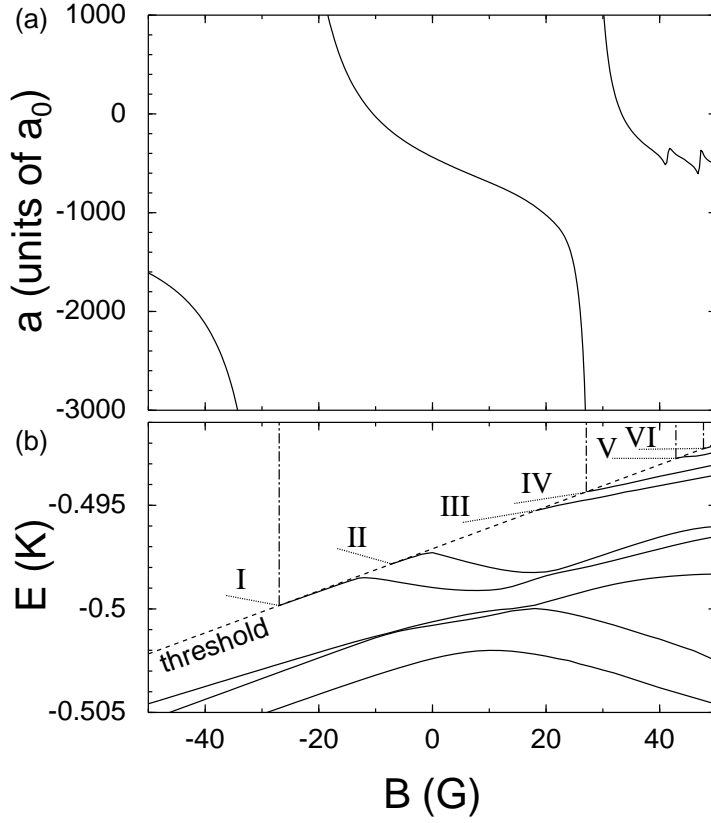


Figure 2.8 (a) Scattering length for Cs atoms colliding in the $|3, -3\rangle$ hyperfine state as a function of magnetic field, showing four Feshbach resonances. A negative field corresponds to a positive field for atoms in the $|3, 3\rangle$ state. The resonances for $B > 0$ are induced by coupling via V^{so} to $l = 2$ channels. (b) Field-dependent threshold energy for the same two-particle $|3, -3\rangle$ hyperfine channel, and field-dependent bound levels which are responsible for the Feshbach resonances in the continuum. Note that the crossing of the levels II and III with threshold are not visible in the scattering length, due to very weak coupling between the corresponding states and the incoming channel.

and Q -states with $l = 2$. These are the three resonances in Fig. 2.8 for positive field values, labeled as IV, V, and VI. In the meantime, the three resonances I, IV, and V have been experimentally observed by Vuletić *et al.* [32]. The widths and strengths, as well as the field positions B_0 , are directly related to the strength parameter C^{so} . On the other hand the resonance for negative field values (i.e. the resonance for the $|3 + 3\rangle$ state) is restricted to $l = 0$ coupling. This resonance has a width of order 10 G, very wide compared to most other Feshbach resonances, and will allow for an excellent field control of the scattering length.

Thus by means of a magnetic field one is able to control the elastic interatomic interactions in a condensate. For Cs, due to the small negative value of v_{DT} , all scattering lengths are negative, making it at first sight impossible to create a stable and large condensate. It should, however, still be possible to create a stable condensate in the $|3+3\rangle$ state by making use of the Feshbach resonance, starting with evaporative cooling at a field value where $a > 0$. Another possible experiment would be the study of the collapse of a condensate by changing the scattering length from a positive value to a negative one.

References

- [1] L. Wolniewicz, J. Chem. Phys. **103**, 1792 (1995) and references therein; W. Weickenmeier, U. Diemer, M. Wahl, M. Raab, W. Demtröder, and W. Müller, J. Chem. Phys. **82**, 5354 (1985); M. Krauss and W.J. Stevens, J. Chem. Phys. **93**, 4236 (1990).
- [2] S.J.J.M.F. Kokkelmans and B.J. Verhaar, Phys. Rev. A **56**, 4038 (1997).
- [3] M. Movre and G. Pichler, J. Phys. B **10**, 2631 (1977).
- [4] R. Schlapp, Phys. Rev. **51**, 342 (1937); For a systematic review of interactions in diatomic systems see: M. Mizushima, *The theory of rotating diatomic molecules* (Wiley, New York, 1975). The indirect spin-spin interaction is treated in this volume, starting at page 233.
- [5] S.J.J.M.F. Kokkelmans, B.J. Verhaar, and K. Gibble, Phys. Rev. Lett. **81**, 951 (1998).
- [6] F.H. Mies, C.J. Williams, P.S. Julienne, and M. Krauss, J. Res. Natl. Inst. Stand. Technol. **101**, 521 (1996).
- [7] J. Söding, D. Guéry-Odelin, P. Desbiolles, G. Ferrari, and J. Dalibard, Phys. Rev. Lett. **80**, 1869 (1998).
- [8] A. Messiah, *Quantum mechanics* (North Holland publishing company, Amsterdam, 1961).
- [9] M. Marinescu, H.R. Sadeghpour, and A. Dalgarno, Phys. Rev. A **49**, 982 (1994).
- [10] A. Derevianko, W.R. Johnson, M.S. Safronova, and J.F. Babb, Phys. Rev. Lett. **82**, 3589 (1999).
- [11] B.M. Smirnov and M.I. Chibisov, Zh. Eksp. Teor. Fiz. **48**, 939 (1965) [JETP **21**, 624 (1965)].
- [12] G. Hadinger and G. Hadinger, J. Mol. Spectr. **175**, 441 (1996).
- [13] Figure 2.4 was originally included in chapter 4. Due to remarks by one of the referees we were forced to leave it out.
- [14] J.R. Gardner, R.A. Cline, J.D. Miller, D.J. Heinzen, H.M.J.M. Boesten, and B.J. Verhaar, Phys. Rev. Lett. **74**, 3764 (1995); H.M.J.M. Boesten, C.C. Tsai, B.J. Verhaar, and D.J. Heinzen, Phys. Rev. Lett. **77**, 5194 (1996); Ph. Courteille, R.S. Freeland, D.J. Heinzen, F.A. v. Abeelen, and B.J. Verhaar, Phys. Rev. Lett. **81**, 69 (1998).
- [15] E. Tiesinga, C.J. Williams, P.S. Julienne, K.M. Jones, P.D. Lett, and W.D. Phillips, J. Res. Nat. Inst. Stand. Technol. **101**, 505 (1996).

- [16] E.R.I. Abraham, W.I. McAlexander, J.M. Gerton, R.G. Hulet, R. Côté, and A. Dalgarno, *Phys. Rev. A* **53**, R3713 (1996).
- [17] C.C. Tsai, R.S. Freeland, J.M. Vogels, H.M.J.M. Boesten, B.J. Verhaar, and D.J. Heinzen, *Phys. Rev. Lett.* **78**, 1245 (1997).
- [18] K.M. Jones, S. Maleki, L.P. Ratliff, and P.D. Lett, *J. Phys. B* **30**, 289 (1997).
- [19] E.R.I. Abraham, W.I. McAlexander, C.A. Sackett, R.G. Hulet, *Phys. Rev. Lett.* **74**, 1315 (1995).
- [20] H. Feshbach, *Ann. Phys.* **19**, 287 (1962).
- [21] J.L. Bohn and P.S. Julienne, *Phys. Rev. A* **54**, 4637 (1996).
- [22] J.M. Eisenberg and W. Greiner, *Nuclear theory* (North Holland publishing company, Amsterdam, 1987), Vol. 1.
- [23] C. Cohen-Tannoudji, J. Dupond-Roc, and G. Grynberg, *Atom-photon interactions* (John Wiley & Sons, New York, 1992).
- [24] H. Feshbach, *Ann. Phys.* **5**, 357 (1958).
- [25] U. Fano, *Phys. Rev.* **124**, 1866 (1961).
- [26] E. Tiesinga, B.J. Verhaar, and H.T.C. Stoof, *Phys. Rev. A* **47**, 4114 (1993).
- [27] A.J. Moerdijk, B.J. Verhaar, and A. Axelson, *Phys. Rev. A* **51**, 4852 (1995).
- [28] J.M. Vogels, C.C. Tsai, R.S. Freeland, S.J.J.M.F. Kokkelmans, B.J. Verhaar, and D.J. Heinzen, *Phys. Rev. A* **56**, 2 (1997).
- [29] P. Courteille, R.S. Freeland, D.J. Heinzen, F.A. van Abeelen, and B.J. Verhaar, *Phys. Rev. Lett.* **81**, 69 (1998).
- [30] J.L. Roberts, N.R. Claussen, J.P. Burke, C.H. Greene, E.A. Cornell, and C.E. Wieman, *Phys. Rev. Lett.* **81**, 5109 (1998).
- [31] S. Inouye, M.R. Andrews, J. Stenger, H.-J. Miesner, D.M. Stamper-Kurn, and W. Ketterle, *Nature* **392**, 151 (1998).
- [32] V. Vuletić, C. Chin, A.J. Kerman, and S. Chu, *Phys. Rev. Lett.* **83**, 943 (1999).

Predictions for laser-cooled Rb clocks

S.J.J.M.F. Kokkelmans, B.J. Verhaar, K. Gibble, and D.J. Heinzen

Published in Phys. Rev. A **56**, R4389 (1997)

Using information from a recent ^{85}Rb two-color photoassociation experiment, we evaluate the merits of fountain clocks based on ^{87}Rb and ^{85}Rb isotopes as alternatives to ^{133}Cs and find that they offer significant advantages. In the case of ^{87}Rb the collisionally induced fractional frequency shift is 15 times smaller than for ^{133}Cs . This small shift is associated with a small difference in the triplet and singlet scattering lengths for ^{87}Rb . For ^{85}Rb , the shift produced by the two $m_f = 0$ clock states may have opposite signs allowing the shift to be eliminated by controlling the relative populations of these states. We also present collision quantities relevant to atomic fountain clocks containing multiply launched groups of atoms, and for evaporative cooling of ^{85}Rb atoms.

3.1 Introduction

Techniques developed in recent years to produce and manipulate cold atoms are expected to lead to rapid improvements in atomic clocks. The development of an atomic fountain based on laser-cooled atoms [1, 2] has created prospects for a considerably improved accuracy and stability of the cesium frequency standard. In a fountain clock, a cloud of atoms is cooled to μK temperatures and launched upwards through a microwave cavity. The cloud is slowed by gravity and then returns through the cavity. The combination of slow atoms and a long interrogation time between the two cavity traversals can potentially lead to a 100- to 1000-fold improvement of accuracy and stability [3]. Soon after the first demonstration of a Cs fountain clock [2] it was suggested that elastic collisions between the atoms during their ballistic flight between the two cavity passages shift the phase of the atomic coherence and produce an apparent frequency shift [4]. A subsequent experiment by Gibble and Chu observed this effect, measuring a large shift $\delta\nu = -16$ mHz for a cold Cs density $n = 10^9$ cm $^{-3}$ and a temperature $T = 1$ μK [3]. As a consequence of the fundamentally quantum character of the collisions, the collisional shift has a nonzero $T \rightarrow 0$ limit [4], and, at 1 μK , the shift is nearly the $T \rightarrow 0$ value. While the real world performance of an atomic clock

certainly depends on a complicated balance of many factors, the cold collision shift is one of the largest and most difficult systematic errors to accurately measure.

Reviewing possibilities to eliminate the cold collision shift, Gibble and Verhaar [5] noted that clocks based on other atomic species may give a better performance and pointed out that cold collision shifts could, in favorable circumstances, even be eliminated. Two of the alternative species, ^{87}Rb and ^{85}Rb , are considered in this Rapid Communication. As we will show, ^{87}Rb is a very promising isotope for cold-clock applications because its collisional shift is small. ^{85}Rb turns out to be promising because the cold collision shift can probably be eliminated by adjusting the atomic populations in the fountain [5].

To assess the merits of these isotopes as clock species, we need reliable information on the cold-atom interaction properties. The last few months have seen a breakthrough in the knowledge of such interactions, mainly because of the importance of these to Bose-Einstein condensation. Three one-color photoassociation (PA) experiments [6–8] led to a determination of parameters in the triplet sector. A first indication for the singlet sector came from the observation of two overlapping Bose condensates [9], pointing to nearly equal node structures of the singlet and triplet radial wave functions at long range (i.e., nearly equal singlet and triplet scattering lengths, see chapter 7 [10]). The determination of the energies of 12 close-to-dissociation vibrational levels of $^{85}\text{Rb}_2$ in a recent two-color PA experiment, has led to the most systematic and accurate knowledge of cold rubidium atom-atom interactions so far, including the singlet sector [11].

A prediction made possible by this development consisted of a number of magnetic field values where field-induced resonances in $^{87}\text{Rb}+^{87}\text{Rb}$ and $^{85}\text{Rb}+^{85}\text{Rb}$ scattering should occur [12]. As another prediction, here we calculate the collisional frequency shifts for cold rubidium atomic clocks.

3.2 Collisional frequency shift

For both isotopes we consider an atomic clock operating on the transition at frequency ω between the lower and upper $m_f = 0$ states at a field of order 1 mG. We indicate the possible Zeeman and hyperfine f, m_f substates of the Rb ground state by the index j , singling out the lower and upper clock states as $j = 1$ and 2, respectively. A derivation on the basis of the quantum Boltzmann equation [13] shows the collisional shift $\delta\omega$ and line broadening Γ of the clock transition to have the form of a sum over all atomic states j :

$$i\delta\omega - \Gamma \equiv \sum_j n_j \langle v(i\lambda_j - \sigma_j) \rangle, \quad (3.1)$$

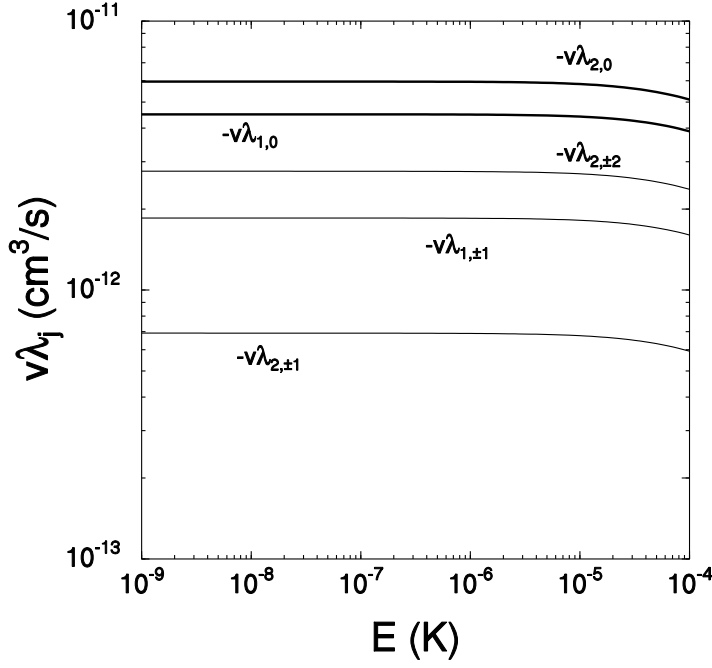


Figure 3.1 Predicted s-wave frequency shift rate constants $v\lambda_j$ for ^{87}Rb as a function of collision energy.

with $\langle \rangle$ a thermal average, n_j the density of atoms in state j , v the relative velocity, and λ_j and σ_j the so-called shift and width cross sections. The sum over j includes all populated substates, including the two clock states $j = 1$ and 2 . The shift due to states other than $j = 1$ and 2 is absent if the fountain contains only the two clock states. The shift and width cross sections are obtained from S -matrix elements for the elastic scattering processes $1 + j \rightarrow 1 + j$ and $2 + j \rightarrow 2 + j$, in which the two clock states participate:

$$i\lambda_j - \sigma_j = (1 + \delta_{1j})(1 + \delta_{2j}) \frac{\pi}{k^2} \sum_l (2l + 1) \left[S_{\{1j\},\{1j\}}^l S_{\{2j\},\{2j\}}^{l*} - 1 \right], \quad (3.2)$$

with m the atomic mass, l the partial wave index, and $\hbar k = \sqrt{mE} = \frac{1}{2}mv$. In our case temperatures are low enough to restrict ourselves to s-wave ($l = 0$) collisions. For $T \rightarrow 0$ we can apply the effective-range approximation and express the low-energy S -matrix elements in (complex) scattering lengths: $S_{\{nj\},\{nj\}} \approx 1 - 2ika_{nj}$. We then obtain

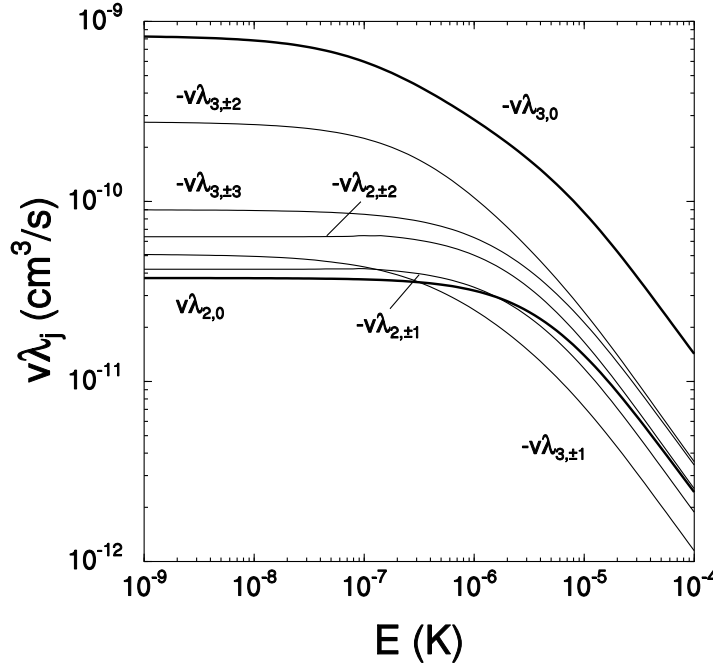


Figure 3.2 Same as Fig. 3.1 for ^{85}Rb .

$$\delta\omega = -\frac{4\pi\hbar}{m} \sum_j n_j (1 + \delta_{1j})(1 + \delta_{2j}) \text{Re}(a_{1j} - a_{2j}), \quad (3.3)$$

$$\Gamma = -\frac{4\pi\hbar}{m} \sum_j n_j (1 + \delta_{1j})(1 + \delta_{2j}) \text{Im}(a_{1j} + a_{2j}). \quad (3.4)$$

The above expressions for $\delta\omega$ and Γ can be interpreted in terms of a Hartree-Fock mean field [14], leading to shifts and imaginary parts of the energies of the individual clock states 1 and 2.

3.3 Rubidium performs better than cesium

On the basis of the above-mentioned explanation for the reduced intercondensate decay rate, one would also expect a near coincidence of all other scattering lengths, and this implies, by Eq. (3.3), a small collisional shift. This is indeed borne out by coupled-channels calculations. In Figs. 3.1 and 3.2 we present the predicted partial collisional shift rate constants $v\lambda_j$ for ^{87}Rb and ^{85}Rb , respectively. Besides the important results for the clock states $j = 1$ and 2 , we also present results for the other m_f states. (Values for opposite m_f are equal for $B \approx 0$ [4, 13].)

Table 3.1 Predicted collision shifts $(nv\lambda)_j/2\pi$ and broadening rates $(nv\sigma)_j$ for ^{87}Rb at $E/k_B = 1\mu\text{K}$ and $n_j = 10^9\text{ cm}^{-3}$. For a total density 10^9 cm^{-3} , an ^{87}Rb clock has a cold-collision shift $\delta\nu/\nu = -1.2 \times 10^{-13}$ vs -17×10^{-13} for ^{133}Cs . ^{87}Rb has a hyperfine frequency $\nu = \omega/(2\pi) = 6.835\text{ GHz}$.

f, m_f	$(nv\lambda)_{f,m_f}/2\pi$ in mHz	$(nv\sigma)_{f,m_f}$ in s^{-1}
1, 0	$-0.7^{+0.2}_{-0.2}$	$(1.7^{+1}_{-0.9}) \times 10^{-5}$
2, 0	$-0.9^{+0.2}_{-0.2}$	$(1.3^{+2}_{-0.7}) \times 10^{-4}$
1, ± 1	$-0.29^{+0.02}_{-0.02}$	$(3^{+3}_{-2}) \times 10^{-5}$
2, ± 1	$-0.110^{+0.007}_{-0.009}$	$(3^{+2}_{-1}) \times 10^{-5}$
2, ± 2	$-0.44^{+0.03}_{-0.04}$	$(1.2^{+0.9}_{-0.3}) \times 10^{-4}$

In Tables 3.1 and 3.2 we give the partial collision shifts $(nv\lambda)_j/2\pi$ and partial broadenings $(nv\sigma)_j$ for the Rb isotopes for a partial density of 10^9 cm^{-3} . For atomic clocks, we expect that the broadening rates are sufficiently small to not limit the accuracy or stability, although they may play an important role in other experiments [15]. The error limits are intended to provide a conservative estimate of the range of possible values.

In a laser-cooled ^{133}Cs clock, the cold-collision shift can be reduced by reducing the atomic density. This, however, lowers the shot-noise-limited signal-to-noise ratio (S/N) and hence increases the short-term instability of the clock. Therefore, to appropriately compare the potential performance of two clocks, we compare the fractional collision shift $nv\lambda_j/(2\pi\nu)$ at the same fractional short-term instability. The latter is given by $\delta\nu/\nu = \Delta\nu/(\pi\nu S/N)$ for a single launch in a fountain, where $\Delta\nu$ is the transition line width. Since Rb and Cs fountains are expected to have the same fountain height, $\Delta\nu$ will be the same for both. Therefore, the instability will be generally independent of the transition frequency because the shot-noise-limited S/N scales as ν^{-1} . This occurs because, given the same atomic density and temperature in the two clocks, a lower transition frequency allows for a larger hole in the microwave cavity implying that the number of detected atoms scales as ν^{-2} , so that $S/N = N^{\frac{1}{2}} \propto \nu^{-1}$. Of course, this is only true if there are no technical obstacles to achieving the shot-noise limit. This may be particularly important for ^{85}Rb fountains where the S/N ratio must be three times higher than that for ^{133}Cs to achieve the same stability, due to its lower transition frequency. Therefore, the appropriate comparison is the fractional collision shift at the same density, since the fractional instability only depends on the density (and not on the transition frequency), if the shot-noise limit is realized.

The cold-collision fractional frequency shift for ^{87}Rb is $\delta\nu/\nu = -1.2 \times 10^{-13}$ at $E = 1\mu\text{K}$ and a density of 10^9 cm^{-3} ; this is 15 times smaller than that for ^{133}Cs .

Table 3.2 Same as Table 3.1 for ^{85}Rb . For a population ratio $n_{3,0}/n_{2,0} = -\lambda_{2,0}/\lambda_{3,0} \approx \frac{1}{9}$ the collision shifts produced by the populations in the two clock states cancel. For ^{85}Rb , $\nu = 3.0357$ GHz.

f, m_f	$(nv\lambda)_{f,m_f}/2\pi$ in mHz	$(nv\sigma)_{f,m_f}$ in s^{-1}
2, 0	5^{+10}_{-8}	$(1^{+9}_{-1}) \times 10^{-3}$
3, 0	-45^{+11}_{-3}	$(2.2^{+2}_{-0.9}) \times 10^{-1}$
2, ± 1	-5^{+2}_{-3}	$(6^{+10}_{-4}) \times 10^{-3}$
3, ± 1	-4^{+1}_{-1}	$(2^{+3}_{-1}) \times 10^{-2}$
2, ± 2	-8^{+3}_{-4}	$(1.1^{+2}_{-0.6}) \times 10^{-2}$
3, ± 2	-17^{+5}_{-3}	$(9^{+11}_{-5}) \times 10^{-2}$
3, ± 3	-10^{+3}_{-5}	$(3^{+4}_{-2}) \times 10^{-2}$

Besides this factor of 15 improvement, ^{87}Rb and ^{133}Cs are remarkably similar as both clock states produce negative collision shifts of similar size and therefore we anticipate that the systematic errors associated with the cold-collision shift in both clocks will scale accordingly.

3.4 Cancellation technique for ^{85}Rb

The cold-collision shifts for ^{85}Rb in Table 3.2 are also interesting for future atomic clocks. Near the central values of the predicted $(nv\lambda)_j$ intervals, the two clock-state populations produce opposite collision shifts so that the cold collision shift can be canceled by adjusting the population ratio of these two states in the fountain [5]. By driving a $\frac{\pi}{5}$ pulse on the first pass through the microwave cavity, there will be 10% of the atoms in the $|f = 3, m_f = 0\rangle$ state and 90% in $|f = 2, m_f = 0\rangle$. In this way, an ^{85}Rb clock has no cold collision shift. The principal advantage of eliminating the shift is that an extrapolation to zero density no longer requires accurate density measurements [5]. This may allow the clock to operate at much higher densities and therefore obtain higher stabilities. Driving a $\frac{\pi}{5}$ pulse reduces the Ramsey fringe contrast by 40% [5]. Therefore, to achieve the same stability, an ^{85}Rb clock will have to operate at a density 2.75 times higher than a ^{133}Cs or ^{87}Rb clock. Thus, for $n = 2.75 \times 10^9 \text{ cm}^{-3}$, the collision shifts produced by the individual clock states are $\pm 4 \times 10^{-12}$. These are twice as large as the shift of a ^{133}Cs clock and 30 times larger than the shift of an ^{87}Rb clock. In addition, because the transition frequency for ^{85}Rb is half that of ^{87}Rb , this will require a potentially technically challenging S/N . For these reasons, a clock based on ^{85}Rb may be best suited for microgravity applications where the long interrogation times require a smaller S/N to achieve the same stability. Investigation of the cancellation technique and its systematic errors is needed to show whether the

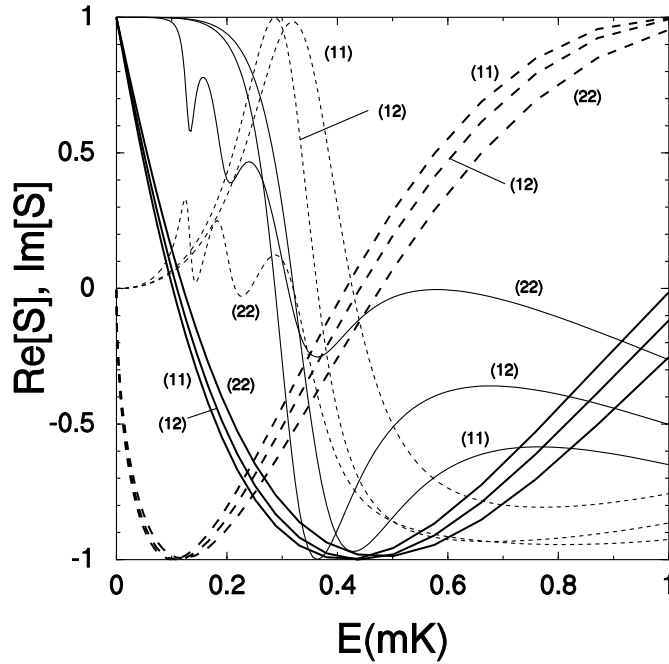


Figure 3.3 Real (solid) and imaginary (dashed) part of the $l = 0$ (bold) and $l = 2$ (normal) S -matrix elements for elastic collisions between the clock states of ^{87}Rb , indicated by 1 and 2.

advantages in the density extrapolation offset the larger cross section and 40% smaller S/N . Note that the error bar for $(nv\lambda)_{2,0}$ does not guarantee the opposite sign for the $(2,0)$ and $(3,0)$ collision shifts that is needed for the above cancellation method. With the current interaction uncertainties, we find that the collision shifts can be canceled in about 75% of the multiparameter volume.

Figure 3.2 shows that the partial collision shifts are nearly energy independent below $1 \mu\text{K}$ for ^{85}Rb . For ^{87}Rb (see Fig. 3.1), the partial collision shifts are almost constant to much higher energies $E \sim 100 \mu\text{K}$. At nK energies, the rates will be important for experiments, including clocks, using Bose condensed samples [16].

3.5 Contributions for higher energies

The s-wave results mentioned previously are sufficient to describe the effects of low-energy collisions ($E < 10 \mu\text{K}$). Future fountain clocks may juggle atoms to achieve higher short-term stabilities [17]. For the scattering between two successively launched balls of atoms in a juggling fountain [18], d-wave effects are potentially important. In the case of ^{87}Rb we expect a sizable effect from the d-wave triplet shape resonance [7],

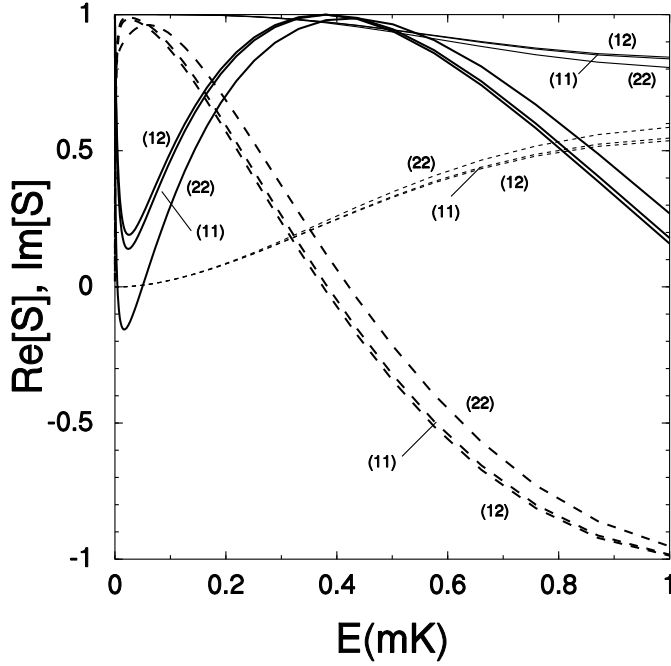


Figure 3.4 Same as Fig. 3.3 for ^{85}Rb .

which will also influence mixed singlet-triplet channels. For ^{85}Rb we expect to see effects associated with a Ramsauer-Townsend s-wave minimum in the elastic cross section σ_{2-2} , which appears to obstruct evaporative cooling in a cloud of $|2-2\rangle$ atoms at energies of a few hundred μK [19]. In that connection it is of interest to know whether the d-wave elastic amplitude, with its rapid increase with collision energy, might fill the s-wave minimum of σ_{2-2} and also dominate the s-wave collision shifts.

In Figs. 3.3 and 3.4 we present a selection of elastic d-wave S-matrix elements, of importance for the clock collision shifts at higher collision energies, and compare them with the corresponding s-wave S-matrix elements for the same range of energies. Clearly for ^{85}Rb , close to 400 μK the latter elements have their unscattered value 1, while the d-wave values are still small. Calculating the elastic s- and d-wave elements for the $(2-2) + (2-2)$ channel, we find a similar result (solid lines in Fig. 3.5): a pronounced Ramsauer-Townsend minimum in $\sigma_{2-2}^{l=0} \sim |S_{\{(2-2)(2-2)\}, \{(2-2)(2-2)\}}^{l=0} - 1|^2$, only partially filled by the d-wave cross section (this holds to fields of at least 750 G).

Figure 3.4 for ^{85}Rb shows some remarkable differences with Fig. 3.3 for ^{87}Rb . A first point is the rapid energy dependence of the s-wave curves close to $E = 0$, similar to that in Fig. 3.2. It is probably related to the close proximity of a pole in the complex energy plane, corresponding to a virtual triplet state and a large negative

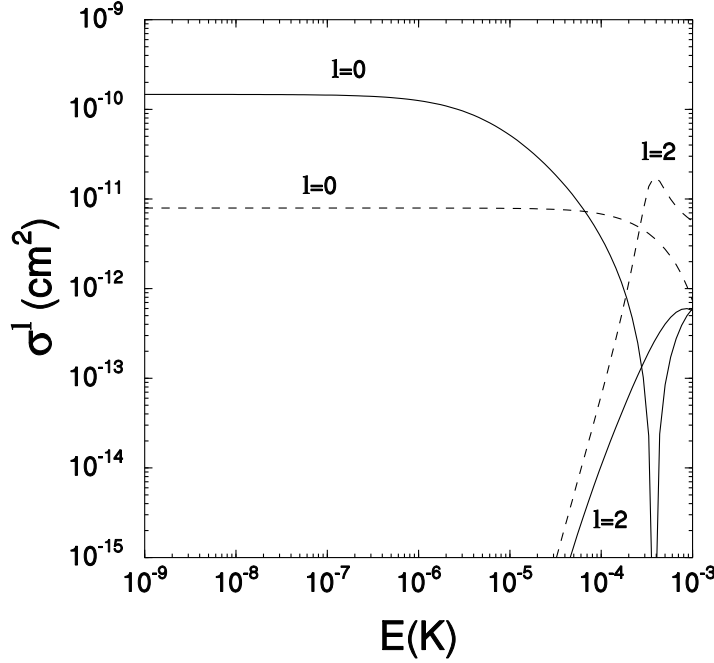


Figure 3.5 S-wave ($l = 0$) and d-wave ($l = 2$) contributions to the elastic cross section of the $m_f = -f$ state of the lower hyperfine manifold, as a function of collision energy, i.e. $\sigma_{f=2, m_f=-2}$ for ^{85}Rb (solid) and $\sigma_{f=1, m_f=-1}$ for ^{87}Rb (dashed).

scattering length. A second point of difference is the complexity of the d-wave curves for ^{87}Rb . Apparently the (1,2) channel, which is pure triplet, displays the above-mentioned d-wave shape resonance behavior. A similar behavior arises also in the two remaining mixed- S channels, due to the same approximate equality of singlet and triplet node structures that gave rise to the small collisional frequency shifts in the foregoing. This and other similarities between channels are easily understood using a simple three-parameter long-range collision model proposed in Ref. [20]. The d-wave shape resonance also shows up in the σ_{1-1} elastic cross section of ^{87}Rb (dashed curves in Fig. 3.5).

Acknowledgement

K.G. acknowledges support from the National Science Foundation, a NIST Precision Measurement Grant, the NASA Microgravity Research Division, and Yale University. D.J.H. acknowledges support from the R.A. Welch Foundation, the National Science Foundation, and the NASA Microgravity Research Division.

References

- [1] M. Kasevich *et al.*, Phys. Rev. Lett. **63**, 612 (1989).
- [2] A. Clairon *et al.*, Europhys. Lett. **16**, 165 (1991).
- [3] K. Gibble and S. Chu, Metrologia **29**, 201 (1992).
- [4] E. Tiesinga *et al.*, Phys. Rev. A **45**, 2671 (1992).
- [5] K. Gibble and B.J. Verhaar, Phys. Rev. A **52**, 3370 (1995).
- [6] J.R. Gardner *et al.*, Phys. Rev. Lett. **74**, 3764 (1995).
- [7] H.M.J.M. Boesten *et al.*, Phys. Rev. A **55**, 636 (1997).
- [8] H.M.J.M. Boesten *et al.*, Phys. Rev. Lett. **77**, 5194 (1996).
- [9] C.J. Myatt *et al.*, Phys. Rev. Lett. **78**, 586 (1997).
- [10] S.J.J.M.F. Kokkelmans *et al.*, Phys. Rev. A **55**, R1589 (1997); P.S. Julienne *et al.*, Phys. Rev. Lett. **78**, 1880 (1997); J.P. Burke *et al.*, Phys. Rev. A **55**, R2519 (1997).
- [11] C.C. Tsai *et al.*, Phys. Rev. Lett. **79**, 1245 (1997).
- [12] J.M. Vogels *et al.*, Phys. Rev. A **56**, R1067 (1997).
- [13] B.J. Verhaar *et al.*, Phys. Rev. A **35**, 3825 (1987); J.M.V.A. Koelman *et al.*, *ibid.* **38**, 3535 (1988).
- [14] B.J. Verhaar in *Atomic Physics 14*, AIP, New York, 1995, pp. 211-218.
- [15] M. Bijlsma *et al.*, Phys. Rev. A **49**, 4285 (1994).
- [16] P. Bouyer *et al.*, Phys. Rev. A **56**, 1083 (1997).
- [17] K. Gibble in *Proceedings of the Fifth Symposium on Frequency Standards and Metrology*, edited by J.C. Bergquist Ed. (World Scientific, Singapore, 1996), p. 66.
- [18] R. Legere and K. Gibble, (private communication).
- [19] C. Wieman and E. Cornell, (private communication).
- [20] B.J. Verhaar *et al.*, Phys. Rev. A **48**, R3429 (1993).

Prospects for Bose-Einstein condensation in cesium

S.J.J.M.F. Kokkelmans, B.J. Verhaar, and K. Gibble

Published in Phys. Rev. Lett. **81**, 951 (1998)

We analyze all of the cold-collision data for Cs, consisting of atomic fountain frequency shifts and elastic scattering rates, to determine phase parameters that completely characterize cold collisions between two ground-state cesium atoms. We show that the fast decays of spin-polarized gas samples in two recent attempts to reach Bose-Einstein condensation in cesium are due to potential and Feshbach resonances which enhance the depolarizing atom-atom collisions. We discuss the prospects for realizing Bose-Einstein condensation in ^{133}Cs and in ^{135}Cs .

4.1 Introduction

The observation of Bose-Einstein condensation (BEC) in a dilute ultracold gas of alkali atoms [1–3] in 1995 is generally considered to be one of the most fascinating applications of atomic cooling techniques. Since these pioneering experiments, the field of BEC continues to lead to surprising results. A year ago, Myatt *et al.* observed an unexpected slow decay of overlapping ^{87}Rb condensates in two different spin states [4], due to a near coincidence in two scattering lengths, as explained in chapter 7 [5, 6]. In contrast, a recent experiment by Söding *et al.* [7] shows such a surprisingly large decay rate of trapped ultracold Cs in the $f, m_f = 4, 4$ state that the realization of BEC appears to be impossible. The other potentially viable hyperfine state, $f, m_f = 3, -3$, does not offer a solution since recent observations show it also decays anomalously quickly [8]. The fast decay occurs even at very weak magnetic fields where it is normally highly suppressed. In this Letter, we theoretically explain these observations and point to ways to circumvent the fast decays. Interatomic collisions, responsible for the decays, are therefore crucial to understand.

The interactions between cold cesium atoms were previously studied in 1993 [9], using the limited experimental information available [10]. New data and progress in theory have led us to reinvestigate this problem. Here, we use a larger set of cold-

Table 4.1 Experimental data included in analysis. Subscript m indicates an even distribution over magnetic substates.

	Quantity	Group, Ref.
1.	$\sigma_{(4,4)+(4,4)}$	Arndt <i>et al.</i> [15]
2.	$\sigma_{(3,-3)+(3,-3)}$	Monroe <i>et al.</i> [4]
3.	$\frac{1}{2}(\delta\nu_{3,0} + \delta\nu_{4,0})$	Gibble and Chu [10]
4.	"	Ghezali <i>et al.</i> [23]
5.	$(\delta\nu_{3,0} - \delta\nu_{4,0})/\frac{1}{2}(\delta\nu_{3,0} + \delta\nu_{4,0})$	Verhaar <i>et al.</i> [9]
6.	$\delta\nu_{3,m}$	Gibble and Chu [10]
7.	"	Ghezali <i>et al.</i> [23]
8.	$\delta\nu_{4,m}$	Ghezali <i>et al.</i> [23]
9.	$\sigma_{(3,0)+(4,m)}$	Gibble <i>et al.</i> [24]
10.	$G_{(4,4)+(4,4)}$	Söding <i>et al.</i> [7]
11.	$G_{(3,-3)+(3,-3)}$	Söding <i>et al.</i> [8]

collision data that consists of atomic fountain frequency shifts and elastic scattering rates. The phase parameters from this analysis completely characterize cold collisions between two ground-state cesium atoms. We show that the total set of experimental data can be described in a consistent picture, a fascinating aspect of which is that a Feshbach resonance happens to be in very close proximity to the conditions of some of the experiments. It arises due to a transition of the colliding atoms to a quasibound state with a different spin structure.

4.2 Anomalous decay rates

The anomalous Cs decay rates are an especially important new result. For atoms lighter than Rb, the magnetic dipole-dipole interaction V^{dip} between the valence electron spins, the so-called direct spin-spin term, adequately describes the decay of totally polarized alkali gases. For Cs, it is insufficient to explain the large decay rate. An indirect spin-spin interaction V^{ind} is known to occur [11] however. It increases very strongly with Z and is expected to dominate V^{dip} for cesium. It is an interaction of the spins via modes of the electronic orbital degrees of freedom, instead of via modes of the electromagnetic field as in the case of V^{dip} . Its strength and radial form factor, comparable to the factor $1/r^3$ in V^{dip} , have been predicted by an *ab initio* calculation [12].

Table 4.1 summarizes the experimental data for our analysis. This analysis includes the atomic hyperfine interaction of each atom, the relative motion of the two nuclei, the

above V^{dip} and V^{ind} terms, and the $S = 0$ and 1 interaction potentials at long range $r > 20 a_0$. The less well-known $r < 20 a_0$ parts are treated by means of boundary conditions at $r_0 = 20 a_0$ for the rapidly oscillating $S = 0$ and 1 radial wave functions. The boundary conditions consist of the local phases ϕ_S^0, ϕ_T^0 of these oscillating wave functions at r_0 and their first derivatives $\phi_S^E, \phi_T^E, \phi_S^l, \phi_T^l$ with respect to E and $l(l+1)$, which summarize the "history" of the collision in the part of space $r < r_0$ [9]. The dependence on the derivative parameters is weak, owing to the small E and l ranges involved in cold collisions. We calculate these using the best available singlet [13] and triplet [14] potentials. The generally fractional s-wave vibrational quantum numbers at dissociation, v_{DS} and v_{DT} (modulo 1), for the singlet and triplet potentials are essentially equivalent to the first two phase parameters. They however provide for more direct physical insight being a measure of how far the last bound or the first unbound Cs + Cs state is from the dissociation threshold.

4.3 Restrictive potential parameters

We begin by considering the first three experimental observations in Table 4.1. These impose very restrictive conditions in the v_{DS}, v_{DT} parameter plane. The observation of a near-zero energy potential resonance [15] in the totally polarized, pure triplet $(4, 4) + (4, 4)$ elastic collision selects a narrow strip $-0.08 < v_{DT} < +0.17$ (bold solid lines in Fig. 4.1). In contrast, the extremely small elastic cross section in the $(3, -3) + (3, -3)$ collision observed at about 30 μK [16], imposes a restriction in both v_{DS} and v_{DT} , due to the mixed singlet-triplet character of the initial spin state. Interestingly, it corresponds to a Ramsauer-Townsend minimum associated with a Feshbach resonance, which is nearby. Together, these conditions already localize the parameters rather strictly to about 1.5% of the area of the parameter plane. Another highly constraining quantity is the large $\delta\nu_{30} + \delta\nu_{40}$ total fountain collisional frequency shift [10]. Beyond the dotted lines the calculated shift goes rapidly to 0 and changes sign, in strong disagreement with experiment. Next we apply a least-squares analysis to all entries 1 - 9 in Table 4.1. We find a very narrow χ^2 minimum of 4.2 for essentially 7 degrees of freedom, indicated by the shaded area:

$$v_{DS} = -0.096 \pm 0.005, \quad v_{DT} = -0.065 \pm 0.005. \quad (4.1)$$

Our calculations show that the regions selected in the v_{DS}, v_{DT} plane depend only weakly on the strength of the indirect spin-spin interaction.

The result (4.1) allows us to calculate the singlet and triplet scattering lengths:

$$a_T \equiv a_{4,4} = -350_{-35}^{+30} a_0, \quad a_S = -208 \pm 17 a_0. \quad (4.2)$$

The excellent localization in the v_{DS}, v_{DT} plane defined by the above experimental observations is also a good starting point to predict the decay rates. It is expected that

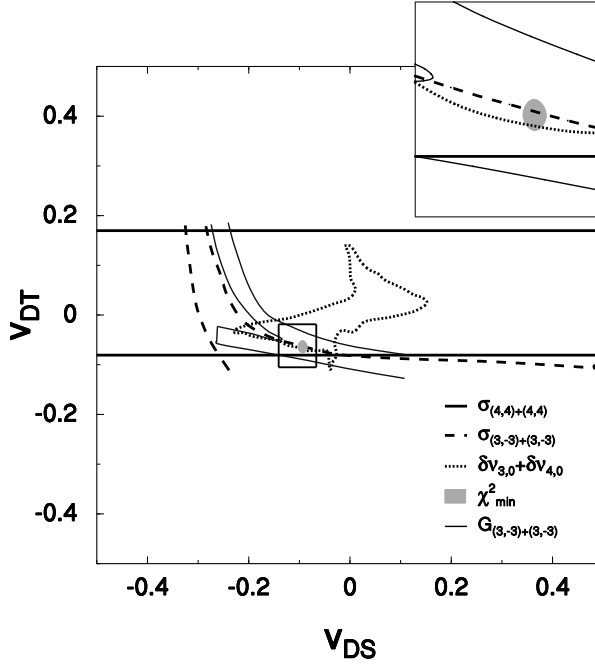


Figure 4.1 Minimum of χ^2 in v_{DS}, v_{DT} plane and enlargement of the region near the χ^2 minimum. The parameters v_{DS}, v_{DT} correspond to the fractional numbers of bound states for the singlet and triplet potentials.

the inelastic decay rates are strongly enhanced by the proximity of potential resonances or Feshbach resonances, since both facilitate the penetration of the colliding atoms to short distances, where the inelastic transitions take place through V_{dip} and V_{ind} . For the $|4, 4\rangle$ state, we find the decay to be dominated by V^{ind} . It is enhanced by the proximity of the same pure triplet potential resonance that enhances the above-mentioned elastic scattering cross section $\sigma_{(4,4)+(4,4)}$. We indeed find the largest $G_{(4,4)+(4,4)}$ values concentrated in the same horizontal strip in Fig. 4.1 [17]. To a good approximation, they are independent of v_{DS} . Item 11, the decay rate constant $G_{(3,-3)+(3,-3)}$, is even more restrictive. It has a pronounced Feshbach resonance dependence on v_{DS}, v_{DT} , leading to an excessively strong decay. The largest rates are concentrated in the region bounded by the thin solid lines in Fig. 4.1, which supports the previous conclusion.

4.4 Feshbach resonances

An important aspect of future work aspiring to achieve BEC in Cs is avoiding the fast decay rates. With that in mind, we present in Fig. 4.2 the calculated B dependence of the decay rate constant $G_{(3,-3)+(3,-3)}$ at 1 μ K for the strength of V^{ind} consistent

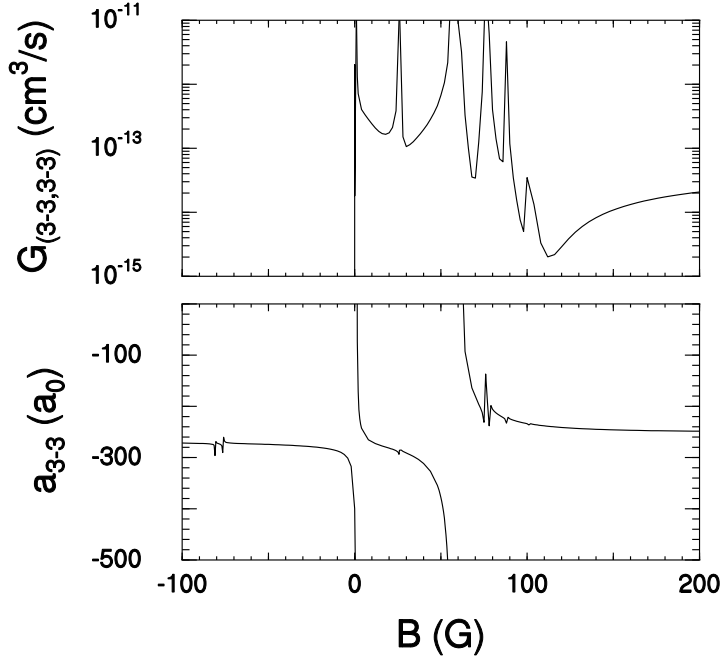


Figure 4.2 Predicted decay rate of $(3,-3)$ level at $1 \mu\text{K}$ due to spin-spin interactions, and scattering length $a_{3,-3}$, versus field strength.

with the measured $G_{(4,4)+(4,4)}$. In addition we calculate the scattering length $a_{3,-3}$ for atoms in the $|3, -3\rangle$ state. In contrast to the $|4, 4\rangle$ decay, we find a number of Feshbach resonances for fields up to 200 G, with a clear correspondence between the resonance features in $G_{(3,-3)+(3,-3)}$ and $a_{3,-3}$. The resonance closest to $B = 0$ is responsible for the enhancements of the (in)elastic rates and frequency shifts occurring prominently in the data of Fig. 4.1. For fields between 110 and 200 G the rate constant has dropped two orders of magnitude relative to the value $1 \times 10^{-12} \text{ cm}^3\text{s}^{-1}$ observed in the Paris experiment, in full agreement with the measured large stability of atoms in this state at fields $B \approx 170$ G [16, 19]. The realization of BEC for large gas samples, however, would require such a reduced decay in combination with a positive scattering length, an effectively repulsive interatomic interaction, while the calculated $a_{3,-3}$ is equal to about $-240 a_0$. BEC does appear to be possible, however, for a small enough condensate: the relevant ratio $a_{3,-3}/a_{HO}$ of the scattering length to the length scale of the harmonic oscillator ground state in the Paris experiment is not very different from that of the Rice trap [2], for which both experiment and theory have shown that a condensate is stable for fewer than 1000 atoms.

4.5 Collisional properties of ^{135}Cs

Another possibility, previously considered for laser-cooled clocks [20], is to use a different isotope of cesium. The most attractive possibility for BEC would be ^{135}Cs . For different isotopes the radial phases ϕ_S^0 , ϕ_T^0 , scale very accurately proportional to the square root of the atom mass [9], as expected in the WKB approximation. Applying the \sqrt{m} scaling rule to the ^{133}Cs singlet and triplet phases at r_0 , we find

$$v_{DS}(^{135}\text{Cs}) = 0.074 \pm 0.015, \quad v_{DT}(^{135}\text{Cs}) = 0.371 \pm 0.015. \quad (4.3)$$

Here, we use the above-mentioned potentials to determine the number of triplet radial nodes for ^{133}Cs within r_0 to be 40 ± 1 and the number of singlet nodes 138 ± 1 . Using (4.3), we can calculate all desirable quantities for ^{135}Cs ground-state collisions, in particular:

$$a_T \equiv a_{4,4} = +138 \pm 5 a_0, \quad a_S = +500_{-70}^{+100} a_0. \quad (4.4)$$

We conclude from the positive value of a_T that a stable totally polarized Bose condensate is possible in a ^{135}Cs vapor. Also, the ratio of the rates of elastic collisions to inelastic, depolarizing collisions is favorable: using the calculated values [21] for these quantities, we find the "practical" limit [22] attainable by forced evaporative cooling is 120 nK, a factor 8 lower than for the $|4, 4\rangle$ state of ^{133}Cs .

For the $|3, -3\rangle$ state the conditions are even more favorable because there is no adjacent Feshbach resonance. Over the field range from 0 to 1000 Gauss, we find the scattering length to be nearly constant and positive:

$$a_{3,-3}(B) = +163_{-8}^{+15} a_0. \quad (4.5)$$

In the same range the rate constant is always less than $10^{-14} \text{ cm}^3\text{s}^{-1}$ and, for field values below five Gauss, less than $10^{-15} \text{ cm}^3\text{s}^{-1}$. A ^{135}Cs Bose condensate in the $|3, -3\rangle$ state is thus expected to be stable. Also, this isotope allows for evaporative cooling to very low temperatures: the practical cooling limit is 0.1 nK and, for field values below five Gauss, even lower by a factor 100.

The precision of the present analysis also leads to much more accurate $\delta\nu_{3,0}$ and $\delta\nu_{4,0}$ frequency shifts for ^{135}Cs :

$$\delta\nu_{3,0} = -15 \pm 4 \text{ mHz}, \quad (4.6)$$

$$\delta\nu_{4,0} = 1.3_{-0.04}^{+0.02} \text{ mHz}, \quad (4.7)$$

for an energy of $1\mu\text{K}$, where they have nearly reached their zero energy limit. The opposite sign of these shifts will allow the cold collision frequency shift to be cancelled as proposed in Ref. [20].

4.6 Conclusions

Summarizing, we have developed a consistent picture for collisions of ultracold cesium atoms by analyzing a set of data, consisting of atomic fountain frequency shifts and elastic scattering rates. We have shown that the fast decays observed recently are due to the influence of potential and Feshbach resonances, in combination with an indirect spin-spin interaction. We have discussed the prospects for the realization of Bose-Einstein condensation in ultracold gas samples of both ^{133}Cs and ^{135}Cs . The prospects are particularly favorable for ^{135}Cs in the $|3, -3\rangle$ state.

References

- [1] M.H. Anderson *et al.*, Science **269**, 198 (1995).
- [2] C.C. Bradley *et al.*, Phys. Rev. Lett. **75**, 1687 (1995).
- [3] K.B. Davis *et al.*, Phys. Rev. Lett. **75**, 3969 (1995).
- [4] C.J. Myatt *et al.*, Phys. Rev. Lett. **78**, 586 (1997).
- [5] S.J.J.M.F. Kokkelmans *et al.*, Phys. Rev. A **55**, R1589 (1997); P.S. Julienne *et al.*, Phys. Rev. Lett. **78**, 1880 (1997); J.P. Burke *et al.*, Phys. Rev. A **55**, R2511 (1997).
- [6] C.C. Tsai *et al.*, Phys. Rev. Lett. **78**, 1245 (1997).
- [7] J. Söding *et al.*, Phys. Rev. Lett. **80**, 1869 (1998).
- [8] J. Söding *et al.*, (private communication).
- [9] B.J. Verhaar, K. Gibble, and S. Chu, Phys. Rev. A **48**, R3429 (1993).
- [10] K. Gibble and S. Chu, Metrologia **29**, 201 (1992).
- [11] This interaction was first studied by R. Schlapp, Phys. Rev. **51**, 342 (1937). A detailed treatment can be found in M. Mizushima, *The theory of rotating diatomic molecules* (Wiley, New York, 1975) p. 233. P.S. Julienne *et al.* (Priv. Commun.) first pointed out its possible role in the decay of spin-polarized alkali systems.
- [12] F.H. Mies *et al.*, J. Res. Natl. Inst. Stand. Technol. **101**, 521 (1996).
- [13] W. Weickenmeier *et al.*, J. Chem. Phys. **82**, 5354 (1985).
- [14] M. Krauss and W.J. Stevens, J. Chem. Phys. **93**, 4236 (1990).
- [15] M. Arndt *et al.*, Phys. Rev. Lett. **79**, 625 (1997).
- [16] C.R. Monroe *et al.*, Phys. Rev. Lett. **70**, 414 (1993).
- [17] The absolute magnitude of the measured rate constant $G_{(4,4)+(4,4)}$ points to a strength of V^{ind} four times larger than predicted by Mies *et al.* [12]. An indication for a similar discrepancy was found for Rb [18].
- [18] H. Boesten *et al.*, Phys. Rev. Lett. **77**, 5194 (1996).
- [19] E. Cornell, (private communication).
- [20] K. Gibble and B.J. Verhaar, Phys. Rev. A **52**, 3370 (1995).

- [21] We find $\sigma_{(4,4)+(4,4)} = 13.4 \times 10^{-12} \text{ cm}^2$ and $G_{(4,4)+(4,4)} = 0.263 \times 10^{-12} \text{ cm}^3 \text{ s}^{-1}$.
- [22] W. Ketterle and N.J. van Druten, Adv. At. Mol. Opt. Phys. **37**, 181 (1996).
- [23] S. Ghezali *et al.*, Europhys. Lett. **36**, 25 (1996).
- [24] K. Gibble *et al.*, Phys. Rev. Lett. **75**, 2666 (1995).

Direct measurement of scattering phase shifts and discrepancies in cold atom scattering

S.J.J.M.F. Kokkelmans, R.J. Legere, K. Gibble, and B.J. Verhaar

Submitted to Phys. Rev. Lett.

We propose a new type of scattering experiment that uses atomic clock techniques and a juggling atomic fountain to precisely measure scattering phase shifts. We also describe inconsistencies between recent ultracold Cs-Cs scattering experiments and previous measurements. The proposed technique can resolve these discrepancies by accurately probing atomic interactions.

5.1 Introduction

Atomic scattering experiments and spectroscopy have produced a detailed understanding of interatomic interactions. Given the vast and seemingly complete knowledge, it is therefore very surprising that a series of measurements on H-H scattering at low temperatures are inconsistent with state-of-the-art theory. During the past year, it has become clear that a similar discrepancy exists for ultracold Cs-Cs scattering. Here, we analyze recent Cs measurements and propose a new type of scattering experiment that can directly measure scattering phase shifts. Such an experiment will clarify the current discrepancies in Cs and very precisely test our theoretical understanding of low energy atomic interactions.

It is difficult to accurately measure scattering cross sections. In atom-atom scattering experiments, the atomic density has to be accurately measured. For cold atom scattering, cross sections are often only measured within a factor of 2. In other areas of physics, such as nuclear or high-energy accelerator experiments, it is the target thickness or the beam profile and density that has to be accurately determined. Therefore, scattering experiments with accuracies better than 1% are generally extremely difficult and these uncertainties often encumber the connection between experiments and the underlying interactions.

5.2 Accurate measurement of scattering phase shifts

It is straightforward to relate scattering phase shifts to the underlying interatomic interactions. Here we propose a new type of scattering experiment that uses atomic clock techniques and a juggling atomic fountain to accurately measure atomic scattering phase shifts. In an atomic fountain clock [1], a laser-cooled ball of atoms is launched through a microwave cavity that excites a coherence between two ground states. This coherence freely precesses while the atoms are slowed by gravity and then return through the microwave cavity. On this second passage, the microwaves in the cavity convert the phase of the coherence to a population difference between the two clock states. The population difference is then measured producing a Ramsey fringe. In a juggling atomic fountain, two balls of laser-cooled atoms are launched vertically in rapid succession [2]. To measure scattering phase shifts, the first ball will be prepared in one of the clock states and the microwaves excite and probe the atoms during successive passages through the cavity. The second ball is prepared in an internal energy eigenstate. When the two balls collide, the atoms in the first ball are in a coherent superposition of the two clock states and each of these states scatters off of the second ball experiencing an s-wave phase shift. In a clock, the unscattered as well as the scattered components of each atom are detected, resulting in a density dependent frequency shift [3]. Here, however, we exclude the unscattered part of each (clock) atom in the first ball and detect only the scattered fraction after it returns through the microwave cavity. Because the scattering differentially shifts the deBroglie phases of the two internal states of the clock atoms, the microwaves convert this phase difference into a population difference on the return passage. By detecting the populations, the difference in the s-wave scattering phase shifts can be directly measured as a phase shift of a Ramsey fringe pattern. This phase shift does not depend on the atomic density (in the single collision limit); the number of scattered atoms, the amplitude of the Ramsey fringe, is linearly proportional to the density. This technique will enable precise measurements of the differences of scattering phase shifts for a variety of spin states in a range of well-defined collision energies. A comparison with calculated phase shifts will more definitely point at where theory succeeds or fails to describe the measurements, and will help to resolve the existing discrepancies.

5.3 Discrepancies in cold atom scattering

Low temperature atomic scattering is important in a number of research areas, including Bose-Einstein condensation and superfluidity [4,5] of dilute gases, Fermi degenerate gases [6], and atomic clocks [3]. An appealing aspect of these dilute ultracold systems is that they should allow a theoretical description from first principles [7]. Connecting the macroscopic properties of the gas with the microscopic two-body interactions has

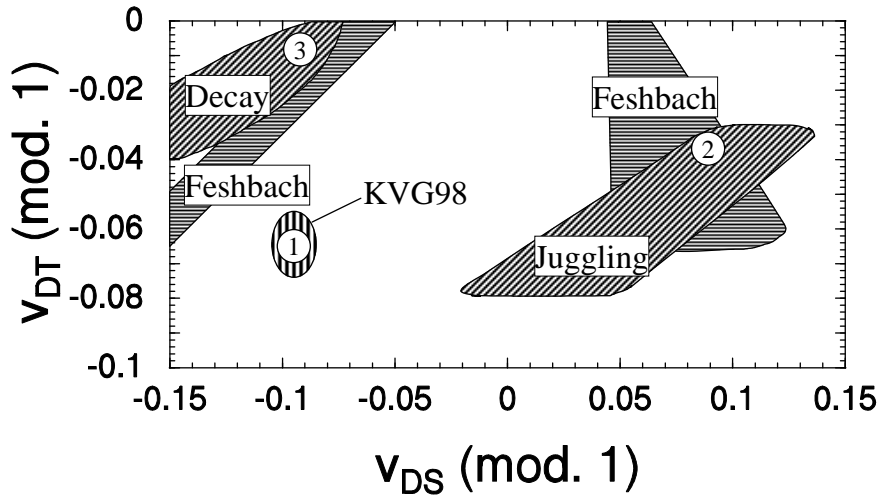


Figure 5.1 The v_{DS}, v_{DT} plane for ^{133}Cs , near singlet and triplet potential resonances. The parameter region from our analysis [12] is indicated 'KVG98', as well as the regions from our analysis of 'Decay' [16], 'Juggling' [2], and 'Feshbach' [17]. These define three parameter regions (1) - (3).

produced a number of beautiful and consistent successes [8,9]. Despite these successes, unsettling problems remain. They may be due either to fundamental errors in the formalism connecting the atom-atom interactions to the observed macroscopic properties, or to interaction terms not included or incorrectly included in the existing analysis, or to both.

The scattering of cold H atoms is on a different footing than other species since calculated *ab initio* potentials have sufficient accuracy to describe the low energy scattering. Several years ago, however, it became clear that discrepancies exist between theory and experiment for cold hydrogen collisions [10]. Even if we allow small changes in the short-range singlet and triplet potentials, it is not possible to remove all discrepancies simultaneously, as explained in chapter 8 [11].

For cold Cs-Cs scattering, a theoretical analysis of experiment determines the atomic interactions. Different experiments lead to inconsistent information about these interactions. In Fig. 5.1, we show several preferred regions in the v_{DS}, v_{DT} plane. Here, v_{DS} and v_{DT} are the non-integral vibrational quantum numbers at dissociation for the singlet and triplet potentials; $v_D = 0$ corresponds to an infinite scattering length. Our previous ^{133}Cs analysis in chapter 4 included all of the available cold collision data (KVG98) [12]. During that work, it was realized [12,13] that the second-order spin-orbit interaction V^{so} should be about 4 times stronger than originally thought [14] to

account for the rapid decay of a doubly spin polarized $|f, m_f\rangle = |4, 4\rangle$ Cs gas [15]. This analysis of eleven different experiments resulted in a remarkably consistent and highly constrained picture of low energy Cs-Cs interactions and led to a prediction for Feshbach resonances in the $|3, -3\rangle$ state.

Three new experiments have been completed in the past two years that challenge the previous consistency: 1) the observation of the energy and field dependent decay rate of a Cs gas in the $|f, m_f\rangle = |3, -3\rangle$ state [16], 2) scattering in a juggling Cs fountain [2], and 3) the observation of the predicted ^{133}Cs Feshbach resonances but at slightly shifted field strengths [17]. The v_{DS} and v_{DT} regions in Fig. 5.1 corresponding to these experiments show clear discrepancies. The dependencies on C_6 and the strength of V^{so} (and to a lesser extent ϕ_S^E and ϕ_T^E [12]) are not shown, but these are optimized as a function of v_{DS} and v_{DT} to get the best agreement with the data [18]. Agreement with the Feshbach field positions and widths is obtained in each of two parameter regions indicated by 'Feshbach' [19]. The measured resonance decay strengths, however, exceed the theoretical predictions by at least a factor 3. It's conceivable that V^{so} could account for some of the discrepancies in Fig. 5.1. If the strength [12, 13] as well as further properties of V^{so} predicted by the existing *ab initio* calculation [14] are in doubt, then the 'KVG98' and 'Decay' regions could potentially shift towards the 'Juggling' region, which is largely insensitive to V^{so} .

5.4 Proposed direct phase measurement technique

We now explicitly describe the proposed technique to directly measure the differences of scattering phase shifts. In the atomic fountain we launch the first ball in the lower clock state $|1\rangle$, e.g. $|f, m_f = 3, 0\rangle$ for Cs. The microwave cavity drives a $\frac{\pi}{2}$ pulse producing the superposition $(|1\rangle + |2\rangle)/\sqrt{2}$, where $|2\rangle$ is the other clock state $(|4, 0\rangle$ for Cs). These atoms then collide with atoms in the second ball that are prepared in an energy eigenstate $|j\rangle$. The relative velocity $v = \hbar k/\mu$ for the scattering, with μ the reduced mass, is determined by the time delay between the launches. Considering only s-wave elastic scattering, the wavefunction of an atom in the first ball after the collision has the asymptotic form $(\Psi_1|1\rangle + \Psi_2|2\rangle)/\sqrt{2}$ with

$$\Psi_i(\vec{r}) = v^{-\frac{1}{2}} [e^{i\vec{k}\cdot\vec{r}} + e^{i\delta_i} \sin \delta_i \frac{e^{ikr}}{kr}], \quad (5.1)$$

where δ_i is the s-wave phase shift for an $i + j$ collision. After the second $\frac{\pi}{2}$ pulse the population in state $|2\rangle$ is measured. The detected population depends on the phase difference between the microwave field in the cavity on the return passage and the phase of the hyperfine precession of the two-state system. In the absence of collisions, the precession frequency has the unperturbed value ω_0 . The phase difference $\eta = (\omega - \omega_0)T$,

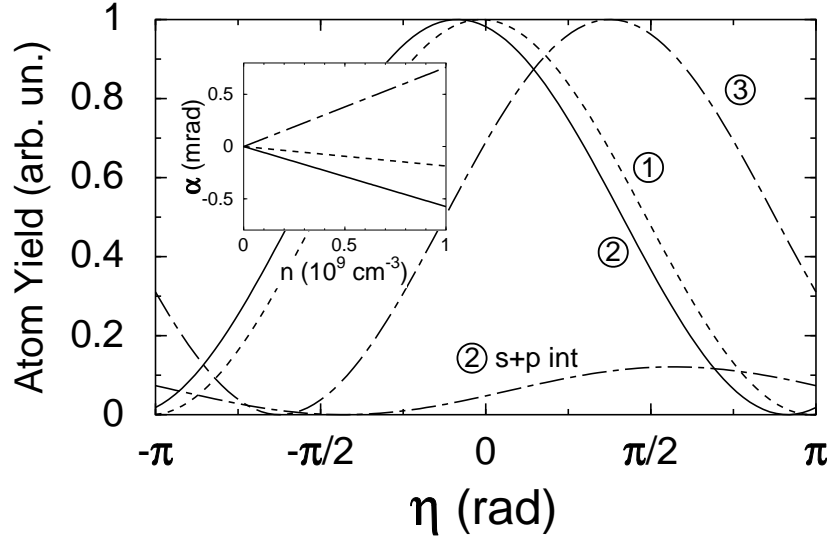


Figure 5.2 Calculated Ramsey fringes for a ^{133}Cs clock atom scattering off of $|3,0\rangle$ for the 3 regions of Fig. 5.1, $v = 10$ cm/s and detection centered at $\theta = 90^\circ$. Also shown is the small s-p interference contribution for $\theta = 80^\circ$ and, in the inset, the corresponding density-dependent clock phase shifts.

where T is the time between the microwave interactions and ω the cavity frequency, produces a Ramsey fringe $\cos^2 \eta/2$.

In the presence of collisions, the phase evolution of the two states is perturbed, and the projection of the wave function on state $|2\rangle$ after the second cavity passage is given by $\frac{1}{2}(e^{-i\eta/2}\Psi_1 + e^{i\eta/2}\Psi_2)$ [20]. The corresponding probability current can be separated into an unscattered part \vec{j}_{uns} , a scattered part \vec{j}_{sc} , and an interference term \vec{j}_{int} . The first two parts are given by

$$\vec{j}_{uns} = \hat{k} \cos^2(\eta/2), \quad (5.2)$$

$$\vec{j}_{sc} = \hat{r} \frac{1}{4k^2 r^2} [\sin^2 \delta_1 + \sin^2 \delta_2 + 2 \sin \delta_1 \sin \delta_2 \cos(\eta - (\delta_1 - \delta_2))], \quad (5.3)$$

while for large r , \vec{j}_{int} behaves as a δ -function [21]:

$$\vec{j}_{int} = \hat{k} \delta(\hat{r} - \hat{k}) \frac{\pi}{k^2 r^2} [-(1 + \cos \eta)(\sin^2 \delta_1 + \sin^2 \delta_2) + \frac{1}{2} \sin \eta (\sin 2\delta_1 - \sin 2\delta_2)]. \quad (5.4)$$

The above expressions \vec{j}_{sc} and \vec{j}_{int} describe the scattering of a clock atom off of an atom in state $|j\rangle$. For a collection of such scatterers with density n_j and a duration τ of the intercloud collision, the total population is proportional to $\cos^2 \frac{1}{2}(\eta - \alpha)$, apart from an additive contribution independent of η . The phase shift α contains all the information about the scattering:

$$\alpha = n_j v \tau \frac{\pi}{k^2} \sin 2(\delta_1 - \delta_2). \quad (5.5)$$

In this expression we recognize the frequency shift cross section $\lambda_j = \frac{\pi}{k^2} \sin 2(\delta_1 - \delta_2)$ due to collisions with atoms in state $|j\rangle$. We note that the phase shift α is proportional to the atomic density n_j .

By excluding the atoms in the forward direction, we detect only the scattered probability current \vec{j}_{sc} . From Eq. 5.3, it is clear that the Ramsey fringes from these components of the scattered atoms are shifted by $\delta_1 - \delta_2$. This phase shift is independent of the atomic density. In Fig. 5.2 we show the expected Ramsey fringes for $|j\rangle = |3, 0\rangle$ and regions (1)-(3). For a relative velocity of 10 cm/s these phase shifts are generally large, of order $\pi/2$, compared to the milliradian phase shifts measured in atomic clocks (see inset) [3].

This type of measurement is well suited to a juggling fountain. In a thermal sample, there is a wide range of relative velocities leading to a potentially large broadening and uncertainty in $\delta_1 - \delta_2$, especially for small relative velocities v as shown in Fig. 5.3. In the juggling fountain, the relative velocity is controlled by the launch delay and, since each ball has a low temperature, there is a narrow spread of relative velocities. To perform the measurement with Cs, one could detect \vec{j}_{sc} using a two-photon Raman pulse to velocity select the scattered part of the atoms in the $|4, 0\rangle$ state after the two balls collide and return through the cavity and transfer them to another state, such as $|3, -1\rangle$ [2]. The unselected atoms in $|4, 0\rangle$ are then cleared from the fountain with a laser beam. The atoms in $|3, -1\rangle$ are transferred to $f = 4$ where the population is detected using laser-induced fluorescence (LIF) [22].

5.5 Effect of p-wave scattering

The description above considers only s-wave collisions. However, the scattering will also contain p-waves, since the energy ranges from $E = 30$ to $100 \mu\text{K}$; effects from d-waves remain negligible [23]. We can suppress the p-wave effects by selecting a velocity midway between the velocities of the two balls. This corresponds to a center-of-mass scattering angle $\theta = 90^\circ$ where there is no p-wave contribution. Considering the small bandwidth around $\theta = 90^\circ$, the interference term between the scattered s and p waves does not contribute since the relative phase reverses on either side of $\theta = 90^\circ$.

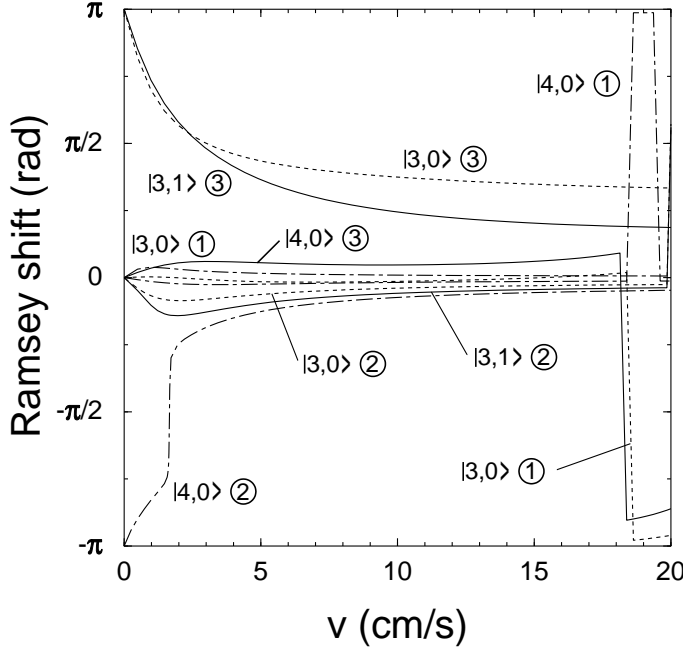


Figure 5.3 Phase shifts of the scattered atom Ramsey fringes as a function of relative velocity for $|j\rangle = |3,0\rangle$, $|3,1\rangle$, and $|4,0\rangle$ and for the parameter regions (1) - (3) in Fig. 5.1.

Therefore, there is only a small p-wave fringe with a phase shift $\delta_1^p - \delta_2^p$. Further, when we choose $|j\rangle = |3,0\rangle$ or $|4,0\rangle$, the pure p-wave Ramsey fringe vanishes due to Bose-symmetry. Specifically, for $|j\rangle = |3,0\rangle$, the scattered current has two terms: a pure s-wave term with phase shift $\delta_{30,30}^s - \delta_{30,40}^s$ and a single s-p interference term with phase shift $\delta_{30,30}^s - \delta_{30,40}^p$ (see Fig. 5.2). By detecting the Ramsey fringe as a function of scattering angle (velocity), these two terms can be isolated. For an arbitrary $|j\rangle$, the energy as well as the angular dependence can be exploited to extract the phase shifts. A clear way to use the energy dependence is to tune to the energy of a Ramsauer-Townsend s-wave minimum for one of the clock states colliding with $|j\rangle$. Again a single s-p interference Ramsey fringe remains, which is presumably small, as well as the pure p-wave Ramsey fringe which gives the difference of the p-wave scattering phase shifts.

5.6 Prospects

Figure 5.3 shows the phase shifts of the Ramsey fringes for scattered atoms as a function of relative velocity for the three parameter regions of Fig. 5.1. For each region these states $|j\rangle$ produce easily distinguishable phase shifts near $v = 10$ cm/s. In Fig. 5.4 we show contour plots of the phase shifts as a function of v_{DS} and v_{DT} . There is generally

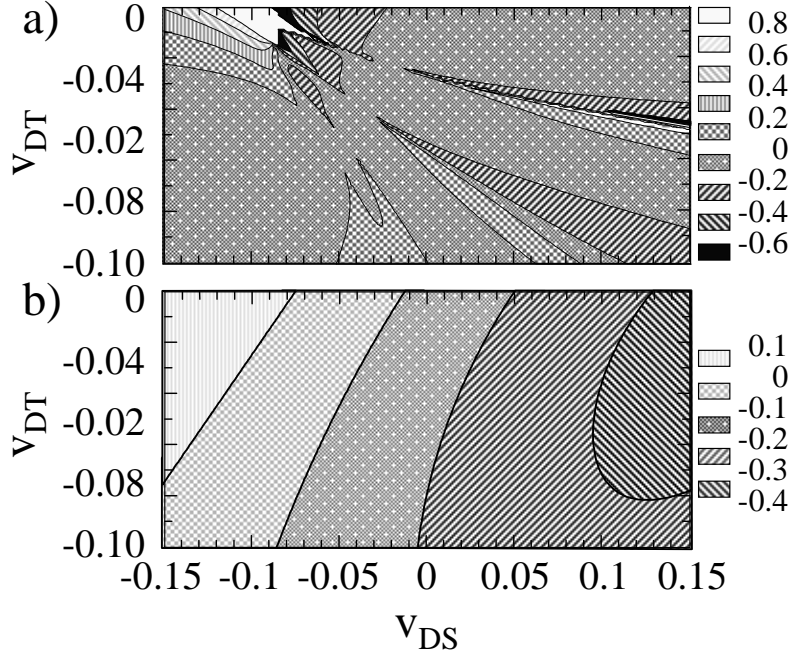


Figure 5.4 Contour plots of Ramsey fringe phase shifts as a function of v_{DS} and v_{DT} , for $C_6 = 6630$ a.u., $v = 10$ cm/s, and $|j\rangle =$ (a) $|3,0\rangle$ and (b) $|4,0\rangle$. The contours for $|3,1\rangle$ are similar to those for $|3,0\rangle$.

a large dependence of these shifts on the potential parameters. An elucidating case is hydrogen where the hyperfine interaction can be neglected to lowest order [24]. In that approximation, the phase shift differences are $+(-)\frac{1}{2}k[a_S - a_T]$ for $|j\rangle = |0,0\rangle$ ($|1,0\rangle$), with a_S and a_T the singlet and triplet scattering lengths. Fig. 5.4 shows that a combination of phase shift measurements clearly distinguish the three parameter regions. In addition, some of the phase shift differences have a large dependence on V^{so} while others are minimally affected. By comparing measured phase shifts with theory, we can isolate the effects of interactions such as V^{so} on the scattering.

In other areas of physics, density independent scattering phase shifts are also directly measured. These include correlation measurements [25], ratios of cross sections, and generally any measurement of the angular dependence of low energy scattering. Here, cold atom clock techniques allow us to perform a phase measurement as a frequency measurement; this essentially enables the high accuracy. Taking the signal-to-noise of Ref [2], 1 hour of integration will yield 10 mrad accuracy. For $|j\rangle = |4,0\rangle$, this corresponds to an atomic scattering length accuracy of 3%. Anticipating potentially as much as a 100 fold improvement in the experimental accuracy, and taking advantages

of resonances such as in Fig. 5.4(a), the measurements could be sensitive to C_6 and the scattering lengths with an unprecedented precision of 1 - 100 ppm.

Acknowledgement

RL and KG acknowledge support from the NSF.

References

- [1] K. Gibble and S. Chu, *Metrologia* **29**, 201 (1992); S.N. Lea *et al.*, *Phys. Script.* **51**, 78 (1994).
- [2] R. Legere and K. Gibble, *Phys. Rev. Lett.* **81**, 5780 (1998).
- [3] K. Gibble and S. Chu, *Phys. Rev. Lett.* **70**, 1771 (1993).
- [4] C. Raman *et al.*, *Phys. Rev. Lett.* **83**, 2502 (1999).
- [5] M. R. Matthews *et al.*, *Phys. Rev. Lett.* **83**, 2498 (1999).
- [6] B. deMarco and D. Jin, *Science* **285**, 1703 (1999).
- [7] F. Dalfovo *et al.*, *Rev. Mod. Phys.* **71**, 463 (1999).
- [8] B.J. Verhaar, in *Atomic Physics 14*, edited by C.E. Wieman, D.J. Wineland, and S.J. Smith (AIP, New York, 1995), pp. 351-368.
- [9] J. Weiner *et al.*, *Rev. Mod. Phys.* **71**, 1 (1999).
- [10] M.E. Hayden *et al.*, *Phys. Rev. A* **53**, 1589 (1996); M.E. Hayden *et al.*, *Phys. Rev. Lett.* **76**, 2041 (1996).
- [11] S.J.J.M.F. Kokkelmans and B.J. Verhaar, *Phys. Rev. A* **56**, 4038 (1997).
- [12] S.J.J.M.F. Kokkelmans, B.J. Verhaar, and K. Gibble, *Phys. Rev. Lett.* **81**, 951 (1998); see footnote 17.
- [13] P.J. Leo *et al.*, *Phys. Rev. Lett.* **81**, 1389 (1998).
- [14] F.H. Mies *et al.*, *J. Res. Natl. Inst. Stand. Technol.* **101**, 521 (1996).
- [15] J. Söding *et al.*, *Phys. Rev. Lett.* **80**, 1869 (1998).
- [16] D. Guéry-Odelin *et al.*, *Europhys. Lett.* **44**, 25 (1998).
- [17] V. Vuletić *et al.*, *Phys. Rev. Lett.* **83**, 943 (1999).
- [18] S.J.J.M.F. Kokkelmans, R.J. Legere, K. Gibble, and B.J. Verhaar, to be published.
- [19] The Feshbach resonances constrain C_6 to the range 6500 - 6700 a.u., to be compared with 6331 a.u. from M. Marinescu *et al.*, *Phys. Rev. A* **49**, 982 (1994) and the more recent value 6851 a.u. from A. Derevianko *et al.*, *Phys. Rev. Lett.* **82**, 3589 (1999).
- [20] N. F. Ramsey, *Molecular Beams*, Oxford (1956) p 127.
- [21] K. Gottfried, *Quantum Mechanics* (W.A. Benjamin Inc., New York, 1966), p. 107.
- [22] The atoms in $|3, 0\rangle$ can also be velocity selectively transferred to $|4, 0\rangle$ and detected.

- [23] Intra-ball and juggling collisions will produce small phase shifts (proportional to the density) as in a clock. There may also be some velocity redistribution on the scale of the thermal velocity of each ball.
- [24] J.M.V.A. Koelman *et al.*, Phys. Rev. A **38** 3535 (1988).
- [25] D.K.McDaniels *et al.*, Phys. Lett. **1** 295 (1962).

Formation of ultracold molecules via stimulated Raman scattering

S.J.J.M.F. Kokkelmans, H.M.J. Vissers, and B.J. Verhaar

Submitted to Phys. Rev. Lett.

We analyze the dynamics of a dilute trapped Bose-Einstein condensate coupled to a diatomic molecular Bose gas by coherent Raman transitions. The coupling is enhanced via a time-dependent magnetic field that sweeps over a Feshbach resonance. A calculation shows that a condensate of Na_2 molecules in a low rovibrational state is efficiently formed starting from an atomic condensate, depending on the laser intensities and detunings and the choice of the Feshbach resonance. We also propose the same Raman stimulated process as a tool to observe an indirect spin-spin interaction between two ground state Rb atoms, i.e., the second order spin-orbit interaction. Together with the magnetic dipole interaction this interaction is responsible for a substructure of weakly bound rovibrational levels with rotational orbital angular momentum $l > 0$. With the extreme resolution demonstrated in recent photoassociation experiments on a ^{87}Rb Bose-Einstein condensate it should be possible to resolve this subsplitting and determine for the first time the strength of the indirect spin-spin interaction. The Raman transition amplitude for each sublevel depends strongly on the choice of the laser polarizations. This makes the splitting look different with changes in polarization.

6.1 Introduction

Bose-Einstein condensation (BEC) has long been known to be a key element of macroscopic quantum phenomena such as superconductivity and superfluidity. BEC as such, however, eluded direct and unquestioned observation until 1995, when experimental groups produced condensates in dilute atomic alkali gases [1]. This development has stimulated an explosive growth of activities in the field of quantum fluids. The formation of a Bose-Einstein condensate of molecules is generally expected as a future further breakthrough, with the development of coherent beams of molecules (molecular lasers) as a possible application. With such goals in mind a considerable activity is going on in attempts to produce translationally and vibrationally cold molecules as a first step

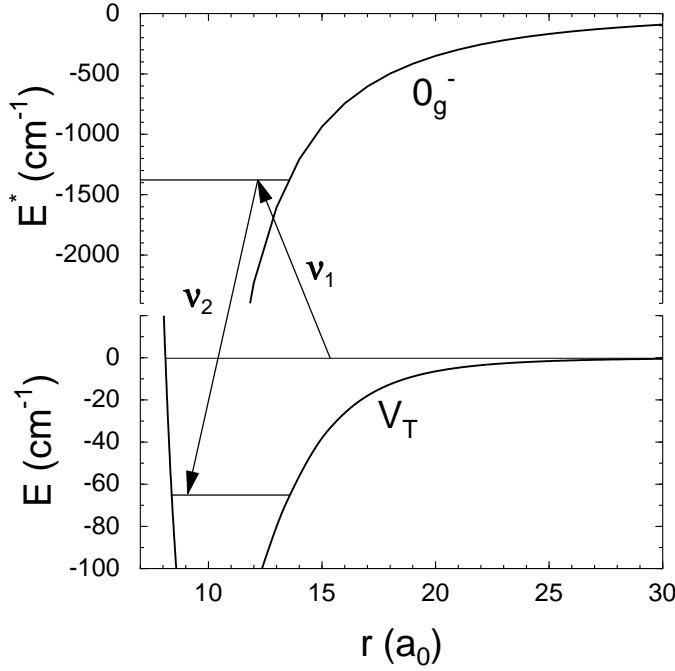


Figure 6.1 Raman photoassociation for Na. The first laser (frequency ν_1) transfers a pair of colliding atoms to an electronically excited state, while a second laser (frequency ν_2) transfers them to a molecular ground state.

towards BEC [2]. In this Letter we propose a more direct line of approach: the partial conversion of an atomic into a diatomic molecular condensate via a stimulated Raman transition, enhanced by a time-dependent magnetic field that sweeps over a Feshbach resonance.

6.2 Condensate of molecules formed in time-dependent field

A stimulated Raman transition of a freely moving pair of condensate atoms to a low-energy diatomic state induced by a pair of laser beams [3] has been proposed, but is not a very efficient process due to poor Franck-Condon overlap of the relatively short distances of atoms in the molecule and the more or less diffuse interatomic distances of a pair of interacting trapped atoms. The transition is further obstructed by a quantum reflection region [4] in the interatomic distance range that atom pairs have to cross to reach short distances. For atoms moving at the 1 nK kinetic energies typical for a condensate, this region is almost untransparent. A dramatic increase of the transition probability by over seven orders of magnitude can be achieved, however, by subjecting the condensate to a magnetic field for field strengths in the vicinity of a Feshbach

resonance. The resonant formation of a quasibound two-atom state increases the penetration of the colliding atoms to the short distance range, thus greatly increasing the overlap with the molecular state [5]. A recent experiment by Ketterle's group [6] showed other dramatic effects in a Na condensate induced by the same mechanism [7, 8].

The experiment we propose combines the transient generation of a condensate of quasibound di-atoms by the field sweep method of Ref. [6] in an optical trap with a coherent stimulated Raman transition [9], inducing the further conversion to a 'permanent' condensate of deeply bound ground state dimers during the brief existence of the quasibound state. The irreversibility introduced by the time dependent field is an essential element of our scheme, which helps to prevent back-dissociation via the reverse bound-bound-free path. In Fig. 6.1 the Raman transition is schematically shown.

6.3 Four-state model

We estimate the efficiency of this two-step approach by considering the atom pairs in their quasibound state as a molecular Bose-Einstein condensate, described by a coherent field $\phi_2(\vec{x}, t)$ in addition to the field $\phi_1(\vec{x}, t)$ describing the atomic condensate. Two further condensate components are considered: the molecules in the intermediate electronically excited state of the coherent Raman transition and the molecules in the final state, described by $\phi_3(\vec{x}, t)$ and $\phi_4(\vec{x}, t)$, respectively. The evolution of the mixed condensate system is described by a four-state model, governed by coupled Gross-Pitaevskii equations [10]:

$$\begin{aligned} i\hbar\dot{\phi}_1 &= U_0|\phi_1|^2\phi_1 + 2\alpha\phi_1^*\phi_2, \\ i\hbar\dot{\phi}_2 &= (\varepsilon_2 - \frac{i}{2}\gamma_0 - \frac{i}{2}\hbar G_{ma}|\phi_1|^2)\phi_2 + \alpha\phi_1^2 + \frac{1}{2}\hbar\Omega_{L_1}\phi_3, \\ i\hbar\dot{\phi}_3 &= (\varepsilon_3 - \frac{i}{2}\gamma_{sp} - \hbar\omega_{L_1})\phi_3 + \frac{1}{2}\hbar\Omega_{L_1}\phi_2 + \frac{1}{2}\hbar\Omega_{L_2}\phi_4, \\ i\hbar\dot{\phi}_4 &= (\varepsilon_4 - \hbar\omega_{L_1} + \hbar\omega_{L_2})\phi_4 + \frac{1}{2}\hbar\Omega_{L_2}\phi_3, \end{aligned} \quad (6.1)$$

with uniform amplitudes $\phi_j = \sqrt{n_j}\exp(i\theta)$ over the volume of the condensate. Here $U_0 = 4\pi\hbar^2 a_{bg}/m$ is the off-resonant strength of the atomic self-energy, the α terms describe the process that converts atoms into quasibound molecules [7], and $\varepsilon_2 - \frac{i}{2}\gamma_0 = (B(t) - B_0)\Delta\mu - \frac{i}{2}\gamma_0$ is the complex energy of the quasibound state relative to the continuum threshold including its (local) decay width γ_0 [7]. Similarly, $\varepsilon_3 - \frac{i}{2}\gamma_{sp}$ is the complex excited state energy with γ_{sp} the spontaneous decay width, and ε_4 is the energy of the final bound molecular state. The coupling between the ϕ_2 and ϕ_3 condensates is induced by laser 1 (frequency ω_{L_1} , Rabi frequency Ω_{L_1}), that between ϕ_3 and ϕ_4 by laser 2 (frequency ω_{L_2} , Rabi frequency Ω_{L_2}). We assume that the rovibrational relaxation of molecular states due to atom-molecule and molecule-molecule collisions

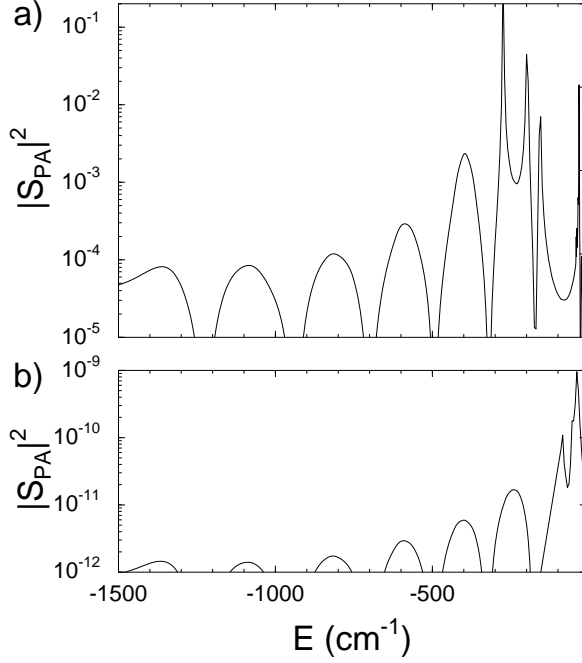


Figure 6.2 Photoassociation transition from an atomic Na BEC prepared in the $|1, +1\rangle$ state. (a) Almost resonant curve close to the 853 G resonance, calculated for a 0.0004 G detuning. Note that the resonant position shifts slightly as a function of energy E due to the ground-state - excited-state coupling. This is responsible for the apparently more resonant PA signal around $E = 350 \text{ cm}^{-1}$. (b) Off-resonant curve for $B = 800 \text{ G}$.

is negligible. We have verified that for the collisions between atoms and quasibound molecules by adding a term $\hbar G_{ma} |\phi_1|^2$ to γ_0 , with G_{ma} the rate coefficient. To very good approximation G_{ma} is equal to the value $4 \times 10^{-14} \text{ cm}^3 \text{ s}^{-1}$ for the 907 G resonance, extracted from experiment [6] in Ref. [7]. Note that the molecular states 3 and 4 are expected to be much less susceptible to relaxation and that molecule-molecule collisions are less frequent due to a much lower density of molecules. The α and Ω terms describe coherent intercondensate exchanges of atom pairs and play a role analogous to the coupling terms in the Gross-Pitaevskii equations for a coexisting mixed-condensate system of atomic ^{87}Rb hyperfine components [11].

The values of the α and Ω parameters are obtained by a full quantum coupled channels calculation (here referred to as Raman coupled channels) for static B and static laser frequencies and intensities, taking into account the relevant subspaces of free ground state collision channels, bound excited state channels and bound ground state channels. All laser couplings between these subspaces are taken into account to arbitrary order for the experimental polarizations and intensities, as well as a spon-

taneous emission decay width for the excited state. Within the subspaces the usual interatomic interactions are taken into account. For the ground-state subspaces we make use of a boundary condition at an interatomic distance $r_0 = 19 \text{ a}_0$ that accounts for inaccuracies in the singlet and triplet potentials for $r < r_0$. The boundary condition is given by accumulated singlet and triplet phases $\phi_S(E, l)$ and $\phi_T(E, l)$ [12] of the radial wave functions for energy E and angular momentum l , which summarize the history of the atomic motion for $r < r_0$, for both continuum and bound states. The phases $\phi_S(0, 0)$ and $\phi_T(0, 0)$ correspond to the fractional s-wave vibrational quantum numbers at dissociation v_{DS} and v_{DT} . The E and l dependences are extracted from the best available *ab initio* singlet and triplet potentials. For the excited-state subspace a similar accumulated phase is determined from experimentally observed bound rovibrational states. For concreteness we consider a Na condensate and focus on the Feshbach resonances at 853 G and 907 G in the lowest hyperfine state $|f, m_f\rangle = |1, +1\rangle$ for which the above mentioned superstrong decay was observed in Ref. [6] and explained in Ref. [7, 8]. Also, we consider a Raman transition via the excited electronic pair state of 0_g^- symmetry that connects asymptotically to the $3^2S_{1/2} + 3^2P_{1/2}$ dissociation limit. Of the above-mentioned two Feshbach resonances the one at 853 G is by far the most favorable, since its local decay rate γ_0/\hbar is roughly a factor 100 smaller than the other resonance [7]. We therefore continue with this choice.

We first determine the Rabi frequency Ω_{L_1} of laser 1 by setting the second laser intensity to zero, performing effectively a one-color photoassociation experiment. In Figure 6.2 we show the static photoassociation signal as a function of the excitation energy, given relative to the excited state threshold. The calculation is done for two cases: one for a field value very close to resonance and the other for an off-resonant field value. The maxima and minima correspond to the maxima and minima of the ground-state radial wave function squared. It is very clear that the Feshbach resonance enhances the loss signal dramatically. Especially the deeper 0_g^- states perform very well since in a non-resonant case they usually have a poor Franck-Condon overlap. The PA loss is described in a straightforward way by an analytical two-state model following from Feshbach's resonance theory [13] for the quasibound state and the excited state. The inelastic transition probability is given by

$$|S_{PA}|^2 = \frac{\frac{1}{4}\gamma_{sp}\gamma_{qb}\hbar^2\Omega_{L_1}^2}{\left[(E - \varepsilon_3 + \hbar\omega_{L_1})(E - \varepsilon_2) - \frac{1}{4}\hbar^2\Omega_{L_1}^2\right]^2 + \frac{1}{4}\hbar^2\gamma_{sp}^2(E - \varepsilon_2)^2}, \quad (6.2)$$

with γ_{qb} the width of the quasibound state depending on collision energy. As can be seen from Fig. 6.2 the PA signal and thus Ω_{L_1} decreases with increasing excited state binding energy. We want to have Ω_{L_1} as large as possible to counter-act the loss term γ_0 in the time-dependent case of Eq. (6.1). On the other hand we want to make the final ground-state molecules as stable as possible by choosing a low vibrational level.

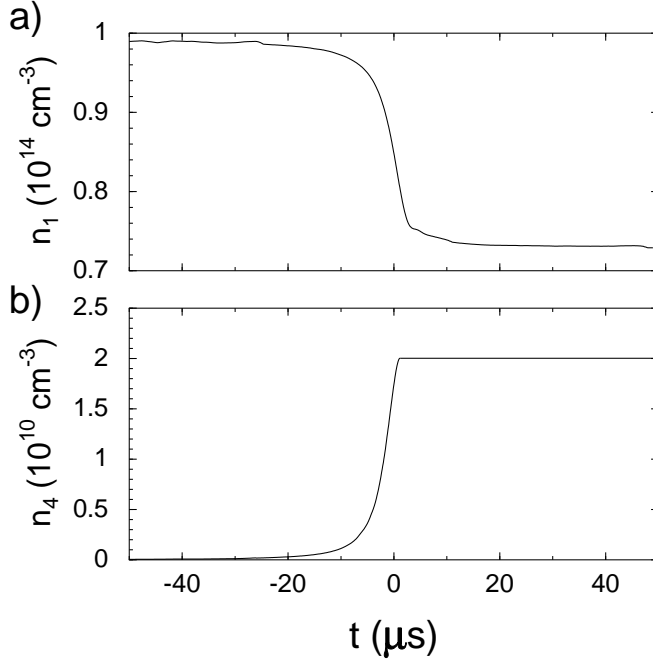


Figure 6.3 (a) Time-dependent solution of n_1 , the density of the atomic condensate. The magnetic field sweeps through the Feshbach resonance at $t = 0$. About 30% of the atoms are lost. (b) Time-dependent solution of n_4 , the density of the molecular condensate. The second laser is switched off shortly after $t = 0$.

Also the excitation energy has to be chosen such that the one-color PA signal is in a local maximum, i.e. the Franck-Condon radius matches a ground-state wave function maximum. This led us to select an excited bound state energy equal to -1380 cm^{-1} with an associated outer turning point $r = 13.7 a_0$. According to the Franck-Condon principle this excited state can be coupled efficiently to a molecular ground state with about the same outer turning point, i.e. the $\nu = 6, J = 0$ triplet level at -65.3 cm^{-1} from the $(1+1)+(1+1)$ collision threshold. From the static coupled channels calculation we find a Rabi frequency $\Omega_{L_1} = 0.76 \times 10^5 \text{ s}^{-1} \sqrt{I_{L_1} (\text{W}/\text{cm}^2)}$. This is a very satisfactory result taking into account the loss rate $\gamma_0/\hbar = 6.9 \times 10^5 \text{ s}^{-1}$. It is of considerable interest that the $|S_{PA}|^2$ maxima in Fig. 6.2 tend to level off at the larger binding energies $|E|$ after an initial decrease over several orders of magnitude.

The second Rabi frequency Ω_{L_2} is determined by considering the bound-bound transition by setting the first laser intensity and γ_{sp} to zero. In a dressed state picture the two levels involved repel each other with increasing laser coupling. For zero detuning the splitting is equal to $\hbar\Omega_{L_2}$ [14], allowing us to obtain Ω_{L_2} . For the above-mentioned states we find $\Omega_{L_2} = 1.0 \times 10^8 \text{ s}^{-1} \sqrt{I_{L_2} (\text{W}/\text{cm}^2)}$. Considering the spontaneous emis-

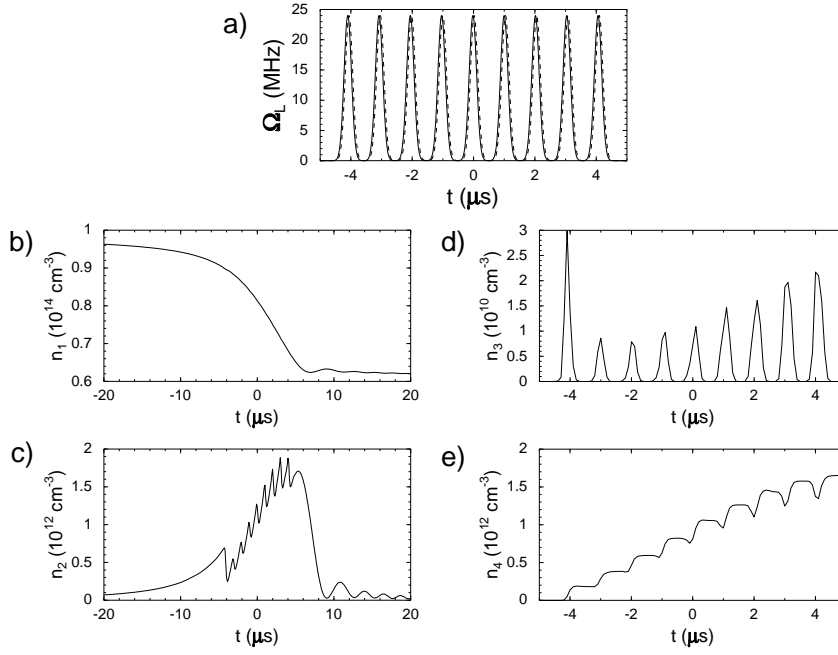


Figure 6.4 Solution of coupled Gross-Pitaevskii equations for sequence of nine Raman pulses separated by $1\mu\text{s}$ positioned symmetrically around time instant $t = 0$. This is shown in Fig. (a) by time-dependent Rabi frequencies of transition 2 (solid) and transition 1 (dashed). In each pulse the laser intensities have a Gaussian time dependence (FWHM= $0.28\mu\text{s}$) with the laser 2 and 1 signals separated by $0.04\mu\text{s}$. Maximum laser intensities: $I_{L_1} = 1000\text{ W/cm}^2$, $I_{L_2} = 0.056\text{ W/cm}^2$. Initial atomic density 10^{14} cm^{-3} . The figures (b) to (e) show the time-dependent solutions of n_1 , the density of the atomic condensate, and n_2 , n_3 , n_4 , the densities of the molecular condensates.

sion rate $\gamma_{sp}/\hbar = 6.0 \times 10^7\text{ s}^{-1}$ it should be possible to transfer very efficiently the electronically excited state condensate into a ground-state molecular condensate.

6.4 Efficient formation of molecules

Let us consider an experiment with static laser intensities of a few hundred W/cm^2 , small detunings, and a magnetic field ramp speed $\dot{B} = 1.4 \times 10^4\text{ G/s}$, for which an 30% transfer of atoms to a quasibound state occurs in the MIT experiment [6–8]. Fig. 6.3 shows the time-dependent build-up of the molecular condensate, starting from an atomic condensate with a density of 10^{14} cm^{-3} . With initially 10^7 atoms we end up with a condensate of roughly 2000 molecules, corresponding to a 4×10^{-4} efficiency. With a tailored time-dependence of the laser intensities and a more optimal choice of

detunings, it should be possible to improve this efficiency by a few orders of magnitude.

An approach with a sequence of Raman laser pulses using a "counter-intuitive" time ordering of lasers 1 and 2 according to the scheme of Bergman and coworkers [15] is an example of a more efficient method with a sequence of nine stimulated Raman pulses for instance a yield of a few percent can be obtained (see Fig. 6.4).

We conclude that an efficient conversion to a condensate of strongly bound Na_2 molecules is possible starting from an atomic condensate making use of huge Feshbach resonance enhancement. The low energy molecular state is expected to be much less susceptible to collision relaxation than the initially formed quasibound molecules [16].

One of the first priorities after a successful experiment of the above type would be a determination of the complex intermolecular scattering length. Its imaginary part, characterizing the rovibrational relaxation and recombination rate (formation of Na_3 molecules) due to molecule-molecule collisions, is of great importance for the lifetime of the condensate. It should be feasible experimentally to largely avoid the relaxation due to atom-molecule collisions by separating the atomic and molecular fractions by a selective laser manipulation of atoms. The remaining decay rate due to molecule-molecule collisions can be reduced by an expansion of the trap potential.

6.5 Determination of spin-dependent interaction for Rb

Spin flips in two-body collisions are an important mechanism limiting the lifetime of ultracold gas samples in magnetic traps. While for atomic hydrogen and all alkali species such spin flips arise from the direct magnetic dipole interaction V^{dip} between the valence electron spins, it is well-known [17] that an additional spin-spin interaction, here referred to as V^{so} , occurring indirectly via the electronic orbital degrees of freedom plays an important role. Despite its more complicated origin as a two-step process in the spin-orbit couplings of the two valence electrons going via a set of electronically excited states, its effective form in terms of the two spin directions and their relative angular position in space is the same as that of V^{dip} . Since each of the two atomic spin-orbit interactions is proportional to Z , its strength is expected to increase strongly with Z . An *ab initio* calculation [18] indeed showed that it is relatively unimportant for the properties of ultracold atoms lighter than Rb. On the other hand it was shown to be responsible for the fast decay of a doubly-polarized cesium gas sample, thus preventing Bose-Einstein condensation in experiments about two years ago [19, 20]. Theoretical calculations soon showed that the strength of V^{so} had to be a factor 4 larger than predicted by Ref. [18] in order to account for the strong decay, see chapter 4 [21, 22].

6.6 Subsplitting of rovibrational levels

It has been pointed out [23] that a rather weak magnetic field is already sufficient to reach the Paschen-Back regime of both the direct and indirect spin-spin couplings. In that regime the electron spin directions are strongly coupled to the field direction and two atoms with non-vanishing relative orbital angular momentum l in a diatomic molecule will experience a potential proportional to $Y_{20}(\hat{r})$ with the magnetic field direction as a symmetry axis. As a consequence, the two spin-spin interactions are expected to induce a subsplitting of the orbital level l into substates with well-defined m_l values, proportional $3m_l^2 - l(l+1)$ in first order. Since the two interactions have opposite sign, V^{so} will decrease the splitting caused by the dipole interaction solely. Here we propose the Raman photoassociation technique to observe this substructure and thus to determine the strength of V^{so} . Wynar *et al.* demonstrated an extremely high resolution on the kHz level in a Raman photoassociation experiment on a Bose-Einstein condensed atomic ^{87}Rb gas sample in a time-averaged, orbiting potential (TOP) magnetic trap [9]. They observed two Rb_2 molecular states just below dissociation. We will focus on this experimental set-up and show that it is possible to observe a subsplitting.

6.7 Raman photoassociation on ^{87}Rb

In the experiment one starts with a ^{87}Rb Bose condensate prepared in the $|f, m_f = 1, -1\rangle$ state and applies two laser fields with frequencies ν_1 and ν_2 . The first laser is polarized perpendicular to the plane of the rotating TOP magnetic field, the second laser's polarization is either in this plane or perpendicular. The first laser is tuned between the continuum ground-state collision channel and a bound level of the electronically excited 0_g^- state and this transition is responsible for trap loss. Resonances are observed by means of a decrease of this loss when the frequency difference $\nu_1 - \nu_2$ corresponds to a ground-state bound level. The Raman photoassociation spectrum of Wynar *et al.* contains two main levels at -637 MHz and -530 MHz. We are able to assign the spectrum as follows. No shift of the $\nu_1 - \nu_2$ dependence with magnetic field was observed for either of the two levels, indicating that these states have the same Zeeman dependence as the $(f_1, m_{f_1}) + (f_2, m_{f_2}) = (1, -1) + (1, -1)$ collision threshold. This is consistent with theoretical expectations. A calculation based on previously obtained interaction parameters for the rubidium isotopes [24, 25] indeed suggests that $l = 0$ and $l = 2$ levels with a spin structure closely resembling that of the incident channel should be expected for $\nu_1 - \nu_2$ near -637 MHz and -530 MHz, respectively [26].

Theoretical calculations predict more than two levels in the $\nu_1 - \nu_2$ range accessible in our experiment. However, Wynar *et al.* did not observe other lines. In order to understand this, we simulated the experiment with our Raman coupled channels

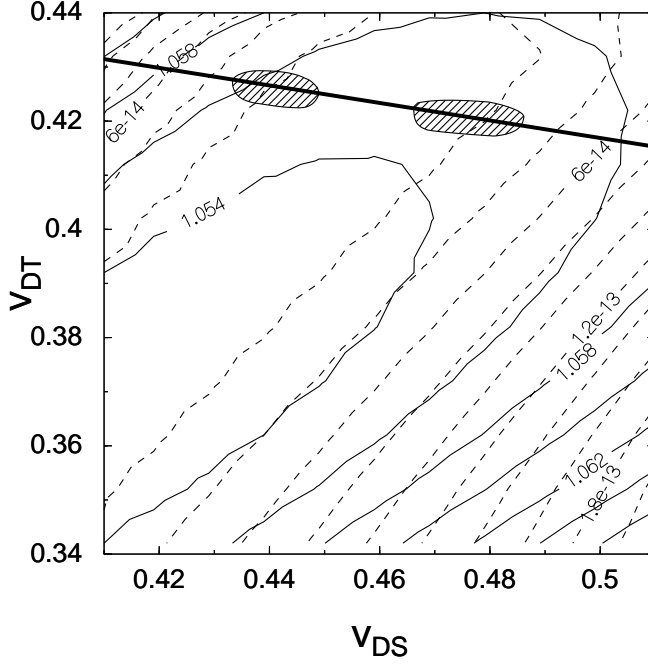


Figure 6.5 v_{DS}, v_{DT} plane for ^{87}Rb . The solid contours correspond to specific values of the scattering length ratio a_{1-1}/a_{22} (experimental value 1.062 ± 0.012) and the dashed lines to specific values of G (experimental value $(2.2 \pm 0.9) \times 10^{-14} \text{ cm}^3 \text{ s}^{-1}$). The bold solid line is determined by the new bound state energies for the central C_6 value. The shaded areas result from a combined χ^2 analysis of these three experiments.

program. In that way we confirmed that the signals for the remaining bound levels should be strongly suppressed in the experiment. Interestingly, however, the $l = 2$ level shows a substructure due to the spin-spin interactions to which we come back later.

For a reanalysis of the ^{87}Rb interaction parameters we first combine the information that comes from the absolute energy positions of the bound states reported in [9] with earlier experimental results: the suppressed decay rate coefficient G of two overlapping Bose condensates [11] and the ratio a_{1-1}/a_{22} of the scattering lengths for the hyperfine channels $(1, -1) + (1, -1)$ and $(2, 2) + (2, 2)$ [28]. In Fig. 6.5 we show the v_{DS}, v_{DT} plane with a χ^2 minimum due to the results of the three mentioned ^{87}Rb experiments for $C_6 = 4700 \pm 50 \text{ a.u.}$ [25, 29]. In the figure we also show contour lines for selected values of G and similarly for a_{1-1}/a_{22} values. The new bound state energies set a very narrow constraint along a straight line intersecting with the strip determined by G .

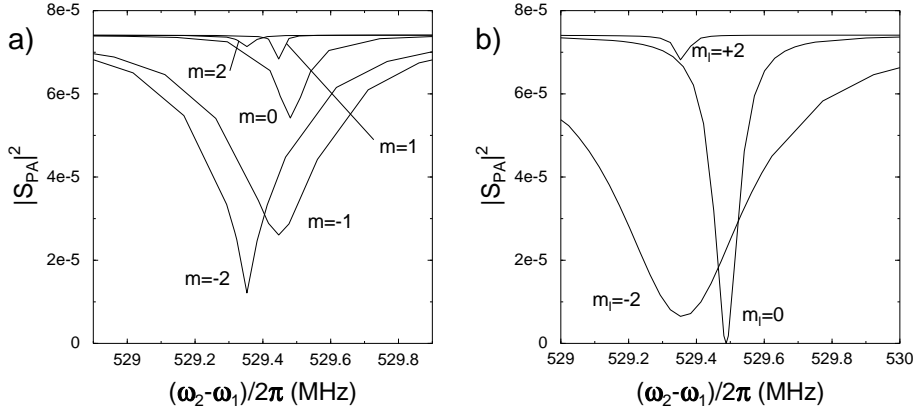


Figure 6.6 Two-color photoassociation spectrum for ^{87}Rb showing the subsplitting. (a) Second laser polarized in the plane of the rotating magnetic field. (b) Similar splitting for second laser polarization perpendicular to the plane.

6.8 Determination of interaction strength

The splitting of the $l = 2$ level can be explained as a combined effect due to the magnetic dipole interaction and the indirect spin-spin interaction. In Fig. 6.6 the calculated results are shown for two types of experiments. Figure 6.6(a) shows a spectrum with the second laser polarized in the plane of the rotating magnetic field. Figure 6.6(b) shows a similar splitting with that polarization perpendicular to the plane. It appears that the polarization largely determines which of the splitted levels are visible in the experiment. Figure 6.7 shows the expected Zeeman splitting of the $l = 2$ level without inclusion of $V^{dip} + V^{so}$. According to the Raman program all the magnetic sub-levels are strongly suppressed except for $m_F = -2$. When we include V^{dip} in our calculations a new structure appears with the dipolar interaction coupling the angular momentum vectors \vec{f}_1 , \vec{f}_2 , and \vec{l} [23]. For weak fields ($B < O(0.3 \text{ G})$) the resulting states are characterized by the quantum numbers $f_1, f_2, l, \mathcal{F}, m_{\mathcal{F}}$ with $\vec{\mathcal{F}} = \vec{F} + \vec{l}$. As mentioned above, the experimental field strength of 5 G is already strong enough to break this coupling so that F, m_F, l, m_l are the good quantum numbers. According to the Raman program a strong subsplitting emerges only for two values of m_l . All other m_l levels are largely suppressed. However, this splitting is far too large to be in agreement with preliminary observations. We repeat that the indirect spin-spin term V^{so} has the opposite sign with respect to V^{dip} and its inclusion will decrease the splitting. A calculation based on a model potential shows that V^{so} in the range $r < r_0$ can in very good approximation be accounted for within the accumulated phase method by a local S -matrix at r_0 that describes the influence on the triplet wave functions. It turns out that only one integral over the radial form factor of V^{so} weighed by the unperturbed

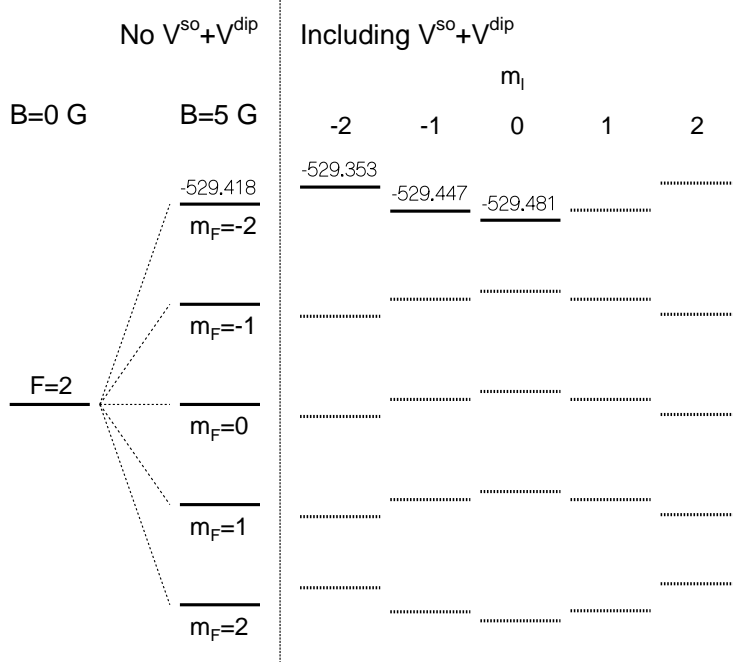


Figure 6.7 Diagram showing the expected bound $^{87}\text{Rb}_2$ levels. For $B = 0$ and no $V^{dip} + V^{so}$ the $F = 2$ level is degenerate. For a field of $B = 5$ G this level is splitted into five m_F states. Including $V^{dip} + V^{so}$ in our calculations these levels are splitted according to m_l .

triplet s-wave probability distribution characterizes the influence of V^{so} effectively, so that its detailed radial form is irrelevant. In the following, we characterize the value of this integral by modifying the coefficient C of the *ab initio* calculation by Mies *et al.*. In Fig. 6.7 we show the calculated subsplitting due to $V^{so} + V^{dip}$. The two levels for the first choice of polarization are an $m_l = -2$ and $m_l = -1$ level, both for $m_F = -2$. The other m_l levels are largely suppressed and are indicated by dashed lines. For the second polarization the measured levels are assigned to have $m_l = -2$ and $m_l = 0$ values, both for $m_F = -2$. The $m_l = -1$ and $m_l = +1$ transitions are forbidden because the two-photon transition should involve an even change of m_l when both lasers are polarized perpendicularly. The $m_l = 2$ level is again largely suppressed.

From this experiment we will be able to determine the strength parameter C , since the calculated splittings are much larger than the expected 1kHz resolution. Note that we expect C to be larger than the result of the *ab initio* calculation. In Fig. 6.7 we have chosen C equal to 0.004 a.u., a factor 4 larger than predicted by Mies *et al.*, equal to the enhancement factor in the case of cesium. If a Raman photoassociation experiment of a type as in Ref. [9] confirms our theoretical picture, we thus expect that it will be

possible for the first time to extract a value of the strength of V^{so} .

References

- [1] M.H. Anderson, J.R. Ensher, M.R. Matthews, C.E. Wieman, and E.A. Cornell, *Science* **269**, 198 (1995); K.B. Davis, M.-O. Mewes, M.R. Andrews, N.J. van Druten, D.S. Durfee, D.M. Kurn, and W. Ketterle, *Phys. Rev. Lett.* **75**, 3969 (1995); C.C. Bradley, C.A. Sackett, J.J. Tollett, and R.G. Hulet, *Phys. Rev. Lett.* **75**, 1687 (1995); C.C. Bradley, C.A. Sackett, J.J. Tollett, and R.G. Hulet, *ibid.* **75**, 985 (1995); C.C. Bradley, C.A. Sackett, and R.G. Hulet, *ibid.* **78**, 985 (1997).
- [2] P.S. Julienne, K. Burnett, Y.B. Band, W.C. Stwalley, *Phys. Rev. A* **58**, R797 (1998); Workshop on Prospects of cold molecules, Heidelberg (8-10 Nov. 1999).
- [3] J.L. Bohn and P.S. Julienne, *Phys. Rev. A* **54**, 4637 (1996); D.J. Heinzen, R.H. Wynar, P.D. Drummond, and K.V. Kheruntsyan (unpublished notes).
- [4] P.S. Julienne and F.H. Mies, *J. Opt. Soc. Am. B* **6**, 2257 (1989).
- [5] F.A. van Abeelen, D.J. Heinzen, and B.J. Verhaar, *Phys. Rev. A* **57**, R4102 (1998).
- [6] J. Stenger, S. Inouye, D.M. Stamper-Kurn, H.-J. Miesner, A.P. Chikkatur, and W. Ketterle, *Nature* **396**, 345 (1998).
- [7] F.A. van Abeelen, and B.J. Verhaar, *Phys. Rev. Lett.* **83**, 1550 (1999).
- [8] F.H. Mies, E. Tiesinga, and P.S. Julienne, *Phys. Rev. A* **61**, 022721 (2000).
- [9] R.H. Wynar, R.S. Freeland, D.J. Han, C. Ryu, and D.J. Heinzen, *Science* **287**, 1016 (2000); see also C.J. Williams and P.S. Julienne, *ibid.* **287**, 986 (2000).
- [10] F. Dalfovo, S. Giorgini, L.P. Pitaevskii, and S. Stringari, *Rev. Mod. Phys.* **71**, 463 (1999).
- [11] C.J. Myatt, E.A. Burt, R.W. Ghrist, E.A. Cornell, and C.E. Wieman, *Phys. Rev. Lett.* **78**, 586 (1997).
- [12] B.J. Verhaar, K. Gibble, and S. Chu, *Phys. Rev. A* **48**, R3429 (1993).
- [13] H. Feshbach, *Ann. Phys.* **5**, 357 (1958), *ibid.* **19**, 287 (1962).
- [14] C. Cohen-Tannoudji, J. Dupond-Roc, and G. Grynberg, *Atom-photon interactions* (John Wiley & Sons, New York, 1992).
- [15] U. Gaubatz, P. Rudecki, S. Schiemann, and K. Bergmann, *J. Chem. Phys.* **92**, 5363 (1990).
- [16] Balakrishnan et al., *Phys. Rev. Lett.* **80**, 3224 (1998).
- [17] M. Mizushima, *The theory of rotating diatomic molecules* (Wiley, New York, 1975) p. 233; P.S. Julienne et al., priv. comm.
- [18] F.H. Mies, C.J. Williams, P.S. Julienne, and M. Krauss, *J. Res. Natl. Inst. Stand. Technol.* **101**, 521 (1996).
- [19] J. Söding, D. Guéry-Odelin, P. Desbiolles, G. Ferrari, and J. Dalibard, *Phys. Rev. Lett.* **80**, 1869 (1998).
- [20] D. Guéry-Odelin, J. Söding, P. Desbiolles, and J. Dalibard, *Europhys. Lett.* **44**, 25 (1998).

- [21] S.J.J.M.F. Kokkelmans, B.J. Verhaar, and K. Gibble, Phys. Rev. Lett. **81**, 951 (1998); see especially footnote 17.
- [22] P.J. Leo, E. Tiesinga, P.S. Julienne, D.K. Walter, S. Kadlecek, and T.G. Walker, Phys. Rev. Lett. **81**, 1389 (1998).
- [23] H.M.J.M. Boesten, C.C. Tsai, D.J. Heinzen and B.J. Verhaar, Phys. Rev. Lett. **77**, 5194 (1997).
- [24] J.M. Vogels, C.C. Tsai, R.S. Freeland, S.J.J.M.F. Kokkelmans, B.J. Verhaar, and D.J. Heinzen, Phys. Rev. A **56**, 2 (1997).
- [25] J.L. Roberts, N.R. Claussen, J.P. Burke, Jr., C.H. Greene, E.A. Cornell, and C.E. Wieman, Phys. Rev. Lett. **81**, 5109 (1998).
- [26] Due to the near equality of the singlet and triplet scattering lengths, see chapter 7 [11,27], the single atom $f_1, m_{f_1}, f_2, m_{f_2}$ values are approximately good quantum numbers for the Rb_2 states.
- [27] S.J.J.M.F. Kokkelmans, H.M.J.M. Boesten, and B.J. Verhaar, Phys. Rev. A **55**, R1589 (1997).
- [28] M.R. Matthews *et al.*, Phys. Rev. Lett. **81**, 243 (1998).
- [29] J.M. Vogels, R.S. Freeland, C.C. Tsai, B.J. Verhaar, and D.J. Heinzen, Phys. Rev. **61**, 043407 (2000).

Role of collisions in creation of overlapping Bose condensates

S.J.J.M.F. Kokkelmans, H.M.J.M. Boesten, and B.J. Verhaar

Published in Phys. Rev. A **55**, R1589 (1997)

We study the elastic scattering length and inelastic decay rate associated with collisions of ^{23}Na and ^{87}Rb atoms in different hyperfine states: one with atoms in the $|f = 2, m_f = 2\rangle$ and one with atoms in the $|f = 1, m_f = -1\rangle$ state. For Na the real part of the $a_{(22)+(1-1)}$ scattering length for $|22\rangle + |1-1\rangle$ collisions is predicted to be positive and equal to $+65 \pm 5$ Bohr length units a_0 for small B . The zero-temperature low-field decay rate is of the order of a typical exchange rate: $G_{(22)+(1-1)} = (1.5 \pm 0.7)10^{-11} \text{ cm}^3\text{s}^{-1}$, showing that a two-condensate experiment is not feasible for a Na gas sample in a static magnetic trap. For the case of Rb atoms the present knowledge of the singlet interaction does not allow a similar calculation. The extreme suppression of $G_{(22)+(1-1)}$ demonstrated by a recent experiment is shown to be very restrictive for the value of the singlet accumulated phase.

7.1 Introduction

The successful realization of a Bose condensate in dilute ultracold gas samples of ^{87}Rb [1], ^{23}Na [2], and ^7Li [3] atoms has opened a rapidly expanding field of studies of condensate properties, starting with the study of its collective modes [4, 5]. A very remarkable new result [6] is the creation of overlapping ^{87}Rb condensates in two different ground-state hyperfine levels $|f = 2, m_f = 2\rangle$ and $|f = 1, m_f = -1\rangle$, thus realizing a fascinating system that has been studied theoretically long ago in the case of spin-polarized atomic hydrogen [7] and very recently also for binary mixtures of alkali Bose condensates [8]. The most remarkable aspect of this experiment is the slow decay due to mixed collisions of pairs of atoms in the two different hyperfine states: due to the presence of decay channels with the same total $m_F = +1$ value one would expect the much faster decay for a typical exchange collision ($G_{exch} \approx 10^{-11} \text{ cm}^3\text{s}^{-1}$ [9]) instead of that experimentally observed: $G_{(22)+(1-1)} = 2.2(9) \times 10^{-14} \text{ cm}^3\text{s}^{-1}$.

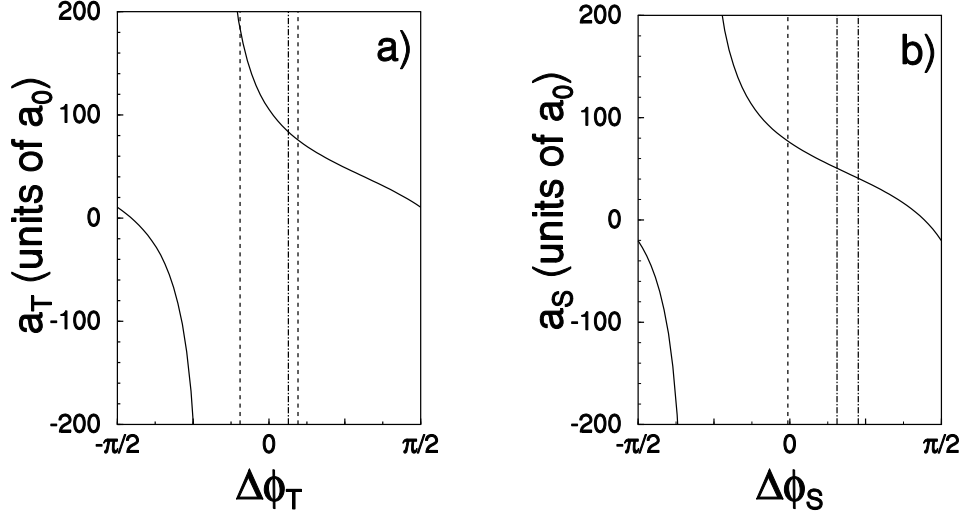


Figure 7.1 (a) Triplet scattering length, as a function of the triplet accumulated phase. (b) Singlet scattering length, as a function of the singlet accumulated phase. The phase ranges of Ref. [13] (dashed lines) and those derived from Ref. [14] (dash-dotted lines) are indicated. Small intervals are given by one single line.

In this paper we consider the question of whether this can be understood on the basis of the theory of cold collisions. We study the rates of decay due to mixed collisions to the three available exchange decay channels (21)+(10), (20)+(11), and (11)+(10), in the low-field range of experimental interest. Another mixed collision property of interest is the elastic (22)+(1-1) scattering length, its sign implying an effectively repulsive or attractive interaction of the condensates [10] and its magnitude determining the efficiency of the sympathetic cooling of the two interpenetrating gas samples. In view of the interest in similar experiments for a Na gas sample, an obvious second item to be considered is the analogous decay rate and elastic scattering length for Na. We start with this system, which has the advantage that the singlet and triplet interaction properties are rather well known, and find that for weak fields the mixed collisional decay rate has the full strength expected for exchange relaxation, while the scattering length is positive. Analogous results for lithium atoms are included in a separate paper [11] that is mainly devoted to a mixed system of a different kind: a combined boson-fermion system of ^7Li and ^6Li atoms. Note that the rates and scattering lengths that we calculate have implications for both condensate and noncondensate atoms. In the case of the inelastic rates, one needs to take into account the well-known reduction by a factor of 2 for processes inside a condensate [12]. This reduction is not yet included in the following rate equation 7.1.

7.2 Discussion of Na interactions

For the Na system the singlet and triplet interaction properties in cold collisions have been predicted rather accurately, both on the basis of the accumulated phases determined from interlevel spacings between highly excited rovibrational singlet and triplet Na₂ states [13] and from cold-atom photoassociation [14]. To compare the predicted singlet and triplet interaction properties obtained with these two methods, we present in Fig. 7.1 the triplet and singlet scattering lengths as a function of the accumulated phases of the decoupled triplet and singlet radial wave functions. The actual abscissa is the modification $\Delta\phi_T(\Delta\phi_S)$ relative to a reference value calculated for the IPA (inverse-perturbation-approach) singlet potential obtained by Moerdijk, Verhaar, and Axelsson [13] and the Rydberg-Klein-Rees triplet potential obtained by Zemke and Stwalley [15]. The dispersion coefficients characterizing the long-range interaction have been taken from Marinescu, Sadeghpour and Dalgarno [16]. The a_T and a_S intervals determined in Ref. [14] correspond to ranges $0.16 < \Delta\phi_T < 0.23$, $0.49 < \Delta\phi_S < 0.71$. While the range for $\Delta\phi_T$ is in agreement with that of Ref. [13] ($-0.3 < \Delta\phi_T < 0.3$), we find a considerable discrepancy in the case of $\Delta\phi_S$ ($-0.04 < \Delta\phi_S < 0.00$ from Ref. [13]). A strong point in favor of a $\Delta\phi_S$ interval close to 0 is its preference for the rather reliable IPA potential, analogous to the case of Li atoms [17, 18]. In the following we will present the predictions for the (22) + (1-1) collision properties for both choices of the $\Delta\phi_S$ interval.

7.3 Collisional decay in overlapping condensates

The decay rate due to (22)+(1-1) mixed atomic collisions is described by the equation

$$\frac{dn_{22}}{dt} = \frac{dn_{1-1}}{dt} = -G_{(22)+(1-1)}n_{22}n_{1-1}, \quad (7.1)$$

with n_{22} and n_{1-1} the respective number densities. The decay channels available for exchange relaxation are (21)+(10), (20)+(11), and (11)+(10). Since the former two channels become closed for $B \rightarrow 0$, one would expect the (11)+(10) decay channel to dominate at the very low B values of primary experimental interest. In this field range F is almost a good quantum number. For s-waves, only spin channels $\{f_1 f_2\} F m_F$ that are symmetric under exchange of the two atoms are allowed because of Bose symmetry. As a consequence, for $f_1 = f_2 = 1$ only $F = 0$ and 2 contribute. Since the $m_F = +1$ value in the initial channel is conserved, only $F = 2$ remains. If this part would be purely triplet or singlet for either the initial or final channel, an exchange transition would be forbidden. Some straightforward Clebsch-Gordan algebra shows that this is not the case: the initial channel spin state is 87.5% triplet and 12.5% singlet, and the final channel spin state is 81.25% triplet and 18.75% singlet. Of course, this does not exclude the fact that the exchange decay vanishes due to destructive interference of

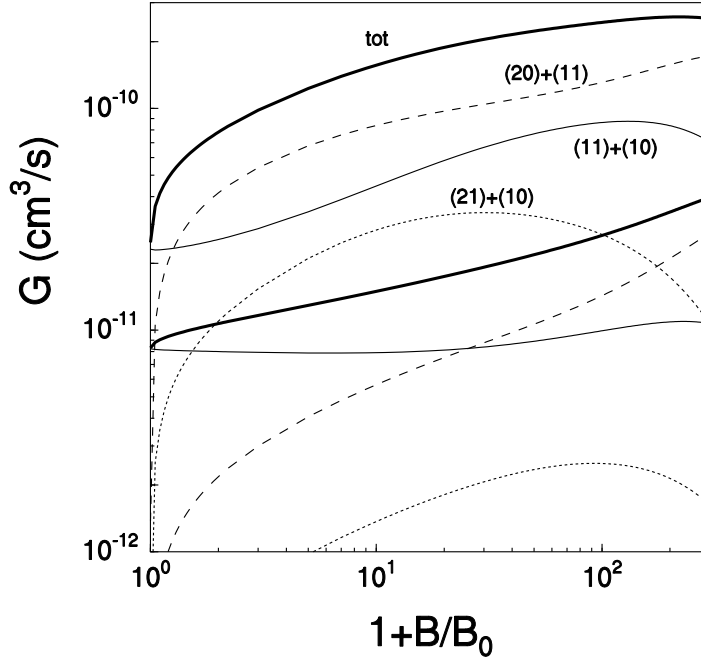


Figure 7.2 Zero-temperature partial and total decay rate constants G due to mixed collisions of Na atoms as a function of magnetic field for our choice of singlet and triplet accumulated phases. To combine the advantages of a linear field scale for small B and a logarithmic scale for large B we plot $1+B/B_0$ logarithmically with $B_0 = 1$ G. Pairs of lines of the same line type indicate results for two extreme choices of the phases corresponding to our error bars.

triplet and singlet amplitudes. The measured slow decay in the case of ^{87}Rb suggests that we are close to this accidental situation for this atom.

In Fig. 7.2 we present the zero-temperature value of $G_{(22)+(1-1)}$, as well as its contributions from the three separate decay channels for our choice of singlet and triplet accumulated phases, as a function of B . Results are given for two extreme choices of the phases corresponding to our error bars. The partial decay rates to the $(21)+(10)$ and $(20)+(11)$ channels increase proportional to $\sqrt{k_f} \sim \sqrt{B}$ in the ratio $1 : 3\sqrt{2}$ (k_f denotes the final wave number), as one should expect from the Clebsch-Gordan coefficients involved and from the ratio of final wave numbers: The decay rate to the $(11)+(10)$ channel starts from a nonvanishing value. At small B the total rate constant is of the order of $10^{-11} \text{ cm}^3\text{s}^{-1}$, showing that a two-condensate experiment is not feasible for a Na gas sample in a static magnetic trap. Figure 7.3 shows similar results for the above-mentioned phase intervals derived from Ref. [14]. Clearly, the low- B range of predicted G values is almost one order of magnitude larger than our

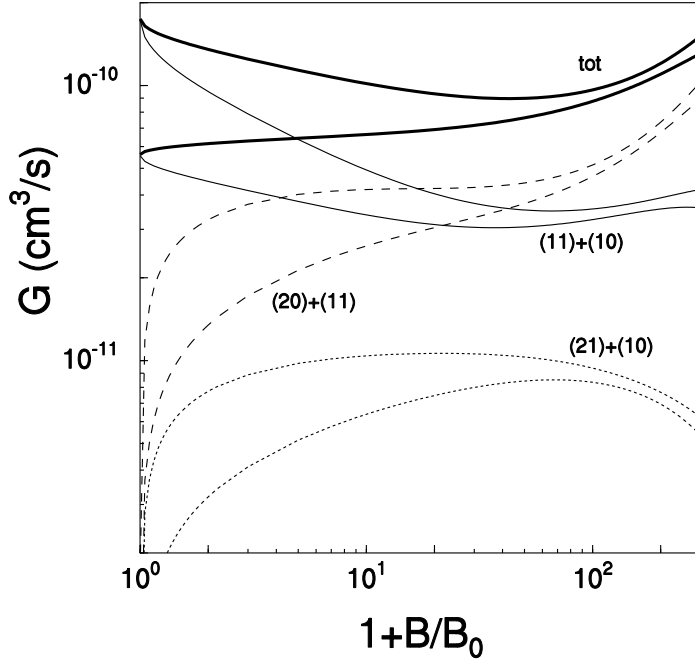


Figure 7.3 Same as Fig. 7.2 for the phase parameters derived from Ref. [14].

prediction, so that the two predictions may be distinguishable experimentally at the lower fields. Figure 7.4 shows the corresponding real parts of the complex scattering lengths $a_{(22)+(1-1)}$ (solid line, results for our phase values; dashed line, results for phase values derived from Ref. [14]). Clearly, the predicted mixed scattering length is large and positive, indicating an effectively repulsive interaction.

We note that the present results do not exclude a suppression of the two-condensate decay rate for fields in the vicinity of a Feshbach resonance in the $(22)+(1-1)$ channel. This would open the possibility of a two condensate experiment by appropriate tuning of the magnetic field. A detailed theoretical search, however, did not lead to such resonances in the field range in which both condensates can be magnetically trapped.

7.4 Equality of singlet and triplet scattering lengths for ^{87}Rb

In the case of ^{87}Rb the long-range triplet interaction is known rather accurately from photoassociation work [20,21]. The situation with respect to the singlet interaction is much less certain. In the following we discuss qualitatively what behavior of the mixed scattering length and decay rate can be expected, by applying the DIS (degenerate internal states) approximation [19]. This approximation neglects the atomic hyperfine splitting, i.e., classically speaking the hyperfine precession, during the collision. It

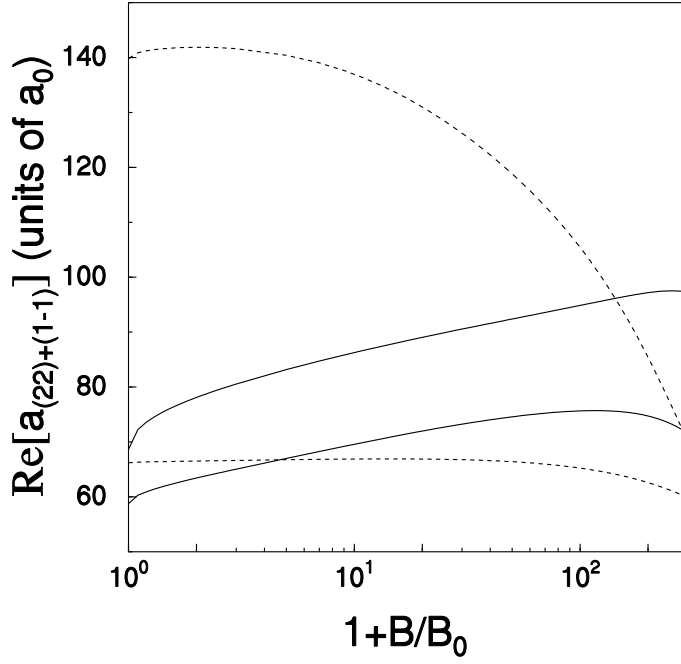


Figure 7.4 Elastic scattering length for mixed collisions of Na atoms for two extreme values of the phase parameters. Solid line, our phase values; dashed line, phase values derived from Ref. [14].

reduces the multichannel collision problem to a potential scattering problem of separate singlet and triplet waves in which the initial and final channel spin states can be expressed. The resulting expressions are

$$a_{(22)+(1-1)} = (\sin^2 \theta_{-1} + \frac{1}{2} \cos^2 \theta_{-1})a_T + \frac{1}{2}(\cos^2 \theta_{-1})a_S, \quad (7.2)$$

$$G_{(22)+(1-1) \rightarrow (21)+(10)} = \frac{2\pi\hbar k_f}{m} (\sin \theta_1 \sin \theta_0 \cos \theta_{-1})^2 (a_T - a_S)^2, \quad (7.3)$$

$$G_{(22)+(1-1) \rightarrow (20)+(11)} = \frac{2\pi\hbar k_f}{m} (\cos \theta_1 \cos \theta_0 \cos \theta_{-1})^2 (a_T - a_S)^2, \quad (7.4)$$

$$G_{(22)+(1-1) \rightarrow (11)+(10)} = \frac{2\pi\hbar k_f}{m} (\cos \theta_1 \sin \theta_0 \cos \theta_{-1})^2 (a_T - a_S)^2. \quad (7.5)$$

The parameters $\theta_1, \theta_0, \theta_{-1}$ are functions of the magnetic field B defined by

$$\tan 2\theta_{(\pm 1)} = \frac{a_{\text{hf}}\sqrt{3}}{\pm a_{\text{hf}} + \hbar B(\gamma_e + \gamma_N)}, \quad \tan 2\theta_0 = \frac{2a_{\text{hf}}}{\hbar B(\gamma_e + \gamma_N)}, \quad (7.6)$$

where a_{hf} is the hyperfine constant, and γ_e and γ_N are the electronic and nuclear gyromagnetic ratios.

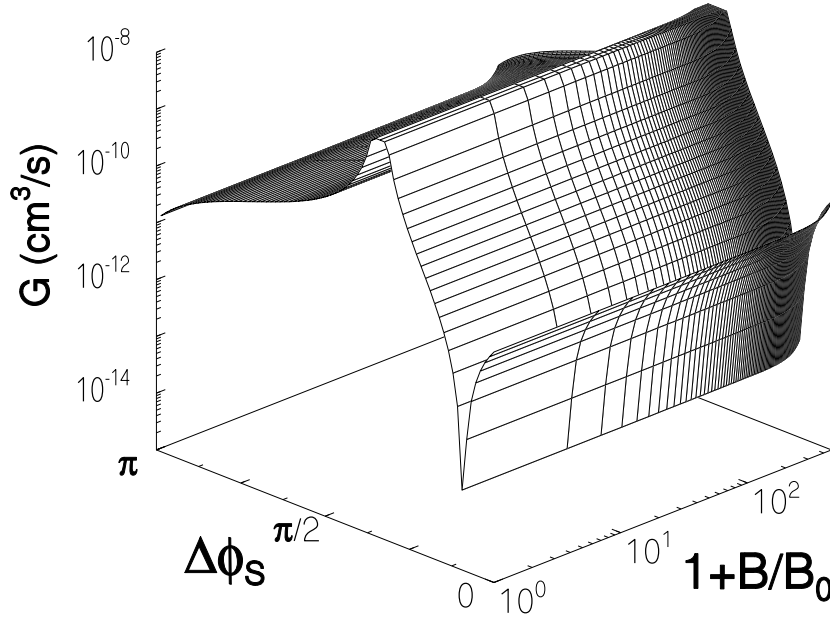


Figure 7.5 Zero-temperature total decay rate constant $G_{(22)+(1-1)}$ for ^{87}Rb in the DIS approximation, as a function of B and $\Delta\phi_S$. We plot $1 + B/B_0$ logarithmically with $B_0 = 1$ G.

The triplet scattering length is taken from Ref. [20]. We treat the singlet accumulated phase as a variable parameter. The singlet scattering length can be expressed in this phase and in C_6 . The value of the latter is taken from Ref. [21].

Figure 7.5 shows a three-dimensional diagram for the total decay rate constant $G_{(22)+(1-1)}$ as a function of both B and $\Delta\phi_S(\text{mod } \pi)$. Unlike the case of Na, the zero of the latter scale does not have a special significance. We indeed see a strong suppression of the total decay rate in a rather narrow phase interval. We therefore expect that the above-mentioned extremely small experimental value of the decay rate, $G_{(22)+(1-1)} = 2.2(9) \times 10^{-14} \text{ cm}^3\text{s}^{-1}$, almost three orders of magnitude smaller than for Na, will impose a strong constraint on the value of the singlet accumulated phase in a future more complete analysis [22]: Fig. 7.5 suggests that it will be possible to derive for the singlet phase a value with an error bar $\pm 0.003\pi$. Also, one would expect that the near equality of a_S and a_T following from the above DIS picture, would continue to hold in a more rigorous coupled-channels treatment.

Figure 7.6 shows the real part of the mixed $a_{(22)+(1-1)}$ scattering length at $B = 0$ as a function of $\Delta\phi_S(\text{mod } \pi)$, again in the DIS approximation. The excursion through $\pm\infty$ is due to the same feature in the $\Delta\phi_S$ dependence of a_S . It will probably be smoothed to a wiggle with a much reduced amplitude when deviations from the DIS

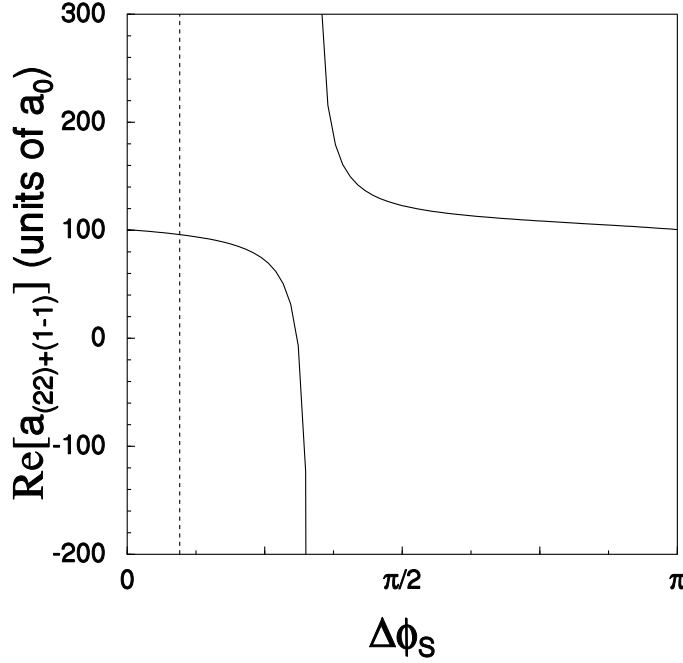


Figure 7.6 The $B = 0$ $a_{(22)+(1-1)}$ scattering length (DIS) for ^{87}Rb , as a function of $\Delta\phi_S$. The dashed line indicates the $\Delta\phi_S$ value corresponding to the experimental decay rate constant $G_{(22)+(1-1)}$ (see Fig. 7.5).

approximation are taken into account. In any case one would expect $\text{Re}[a_{(22)+(1-1)}]$ to be positive in the narrow interval of phase values corresponding to the experimental $G_{(22)+(1-1)}$ decay rate constant, in accordance with experiment [6] (see dashed line).

7.5 Conclusions

We conclude that the suppression of the ^{87}Rb decay due to mixed atomic collisions can be understood on the basis of the theory of cold atomic collisions: Destructive interference between triplet and singlet transition amplitudes between the $(22)+(1-1)$ and $(11)+(10)$ channels leads to a strong suppression relative to typical rates for exchange collisions by almost three orders of magnitude. For Na the decay rate is not suppressed, and a similar two-condensate experiment does not seem possible. In the case of ^{87}Rb the suppression can be used as a strong constraint in the determination of the boundary condition on the s-wave radial wave function at the boundary of the inner range of interatomic distances where the WKB approximation is valid.

References

- [1] M.H. Anderson, J.R. Ensher, M.R. Matthews, C.E. Wieman, and E.A. Cornell, *Science* **269**, 198 (1995).
- [2] K.B. Davis, M.-O. Mewes, M.R. Anderson, N.J. van Druten, D.S. Durfee, D.M. Kurn, and W. Ketterle, *Phys. Rev. Lett.* **75**, 3969 (1995).
- [3] C.C. Bradley, C.A. Sackett, J.J. Tollet, and R.G. Hulet, *Phys. Rev. Lett.* **75**, 1687 (1995).
- [4] D.S. Jin, J.R. Ensher, M.R. Matthews, C.E. Wieman, and E.A. Cornell, *Phys. Rev. Lett.* **77**, 420 (1996).
- [5] M.-O. Mewes, M.R. Andrews, N.J. van Druten, D.M. Kurn, D.S. Durfee, C.G. Townsend, and W. Ketterle, *Phys. Rev. Lett.* **77**, 988 (1996).
- [6] C.J. Myatt, E.A. Burt, R.W. Ghrist, E.A. Cornell, and C.E. Wieman, *Phys. Rev. Lett.* **78**, 586 (1997).
- [7] E.D. Siggia and A.E. Ruckenstein, *Phys. Rev. Lett.* **44**, 1423 (1980); E.D. Siggia and A.E. Ruckenstein, *Phys. Rev. B* **23**, 3580 (1981).
- [8] T.-L. Ho and V.B. Shenoy, *Phys. Rev. Lett.* **77**, 3276 (1996).
- [9] E. Tiesinga, S.J.M. Kuppens, B.J. Verhaar, and H.T.C. Stoof, *Phys. Rev. A* **43**, 5188 (1991).
- [10] K. Huang, *Statistical Mechanics* (Wiley, New York, 1963).
- [11] F.A. van Abeelen and B.J. Verhaar, *Phys. Rev. A* **55**, 4377 (1997).
- [12] Yu. Kagan *et al.*, *Pis'ma Zh. Éksp. Teor. Fiz.* **42**, 169 (1985) [*JETP Lett.* **42**, 209 (1985)]; H.T.C. Stoof, A.M.L. Janssen, J.M.V.A. Koelman, and B.J. Verhaar, *Phys. Rev. A* **39**, 3157 (1989).
- [13] A.J. Moerdijk, B.J. Verhaar and A. Axelsson, *Phys. Rev. A* **51**, 4852 (1995).
- [14] Eite Tiesinga, Carl J. Williams, Paul S. Julienne, Kevin M. Jones, Paul D. Lett, and William D. Phillips, *J. Res. Natl. Inst. Stand. Technol.* **101**, 505 (1996).
- [15] W.T. Zemke and W.C. Stwalley, *J. Chem. Phys.* **97**, 2053 (1993).
- [16] M. Marinescu, H.R. Sadeghpour, and A. Dalgarno, *Phys. Rev. A* **49**, 982 (1994).
- [17] A.J. Moerdijk, W.C. Stwalley, R.G. Hulet, and B.J. Verhaar, *Phys. Rev. Lett.* **72**, 40 (1994).
- [18] A.J. Moerdijk and B.J. Verhaar, *Phys. Rev. Lett.* **73**, 518 (1994).
- [19] B.J. Verhaar, J.M.V.A. Koelman, H.T.C. Stoof, O.J. Luiten, and S.B. Crampton, *Phys. Rev. A* **35**, 3825 (1987); H.T.C. Stoof, J.M.V.A. Koelman, and B.J. Verhaar, *Phys. Rev. B* **38**, 4688 (1988).
- [20] H.M.J.M. Boesten, C.C. Tsai, B.J. Verhaar, and D.J. Heinzen, *Phys. Rev. Lett.* **79**, 1245 (1997).
- [21] H.M.J.M. Boesten, C.C. Tsai, J.R. Gardner, D.J. Heinzen, and B.J. Verhaar, *Phys. Rev. A* **55**, 982 (1994).
- [22] C.C. Tsai, R.S. Freeland, J.M. Vogels, H.M.J.M. Boesten, B.J. Verhaar, and D.J. Heinzen, *Phys. Rev. Lett.* **79**, 1245 (1997).

Discrepancies in experiments with cold hydrogen atoms

S.J.J.M.F. Kokkelmans and B.J. Verhaar

Published in Phys. Rev. A **56**, 4038 (1997)

Recent experiments with atomic clocks and hydrogen gas samples have shown discrepancies between theory and experiment. There are serious disagreements with respect to four different parameters: two different frequency shift parameters and a line broadening cross section relating to the H-maser, and a longitudinal relaxation rate observed in a hydrogen gas sample. We study the changes in the short-range singlet and triplet potentials that would be needed to eliminate the above discrepancies. We find that no such changes can remove all four discrepancies simultaneously. In addition we investigate a possible role of spin-dipole interactions, which have been neglected in previous calculations.

8.1 Introduction

The cesium frequency standard is the most accurate existing atomic clock and the hydrogen maser the most stable atomic clock over time periods of 1 to 10^5 seconds [1]. In the last ten years a substantial further improvement has been accomplished for both instruments by means of versions operating with cold atoms. Modern laser-cooling methods have made it possible to build a cesium atomic fountain clock with an unprecedented accuracy [2]. Using cryogenic cooling by means of superfluid ^4He a version of the H maser has been constructed operating with increased stability at about 0.5 K [3].

These cold atomic clocks have revealed new limits to accuracy and stability, that stand in the way to achieving the full benefits envisaged for the new low-temperature versions. The most important restriction turns out to come from collisions between atoms which shift the frequency of the atomic oscillators. It has been pointed out [4] that this shift has a finite $T = 0$ quantum limit, despite the reduction expected intuitively on the basis of the elastic collision rate, decreasing according to $T^{1/2}$. In view of this the collisional frequency shift is the only known frequency shift in the Cs fountain that cannot be reduced by further lowering of the temperature [5].

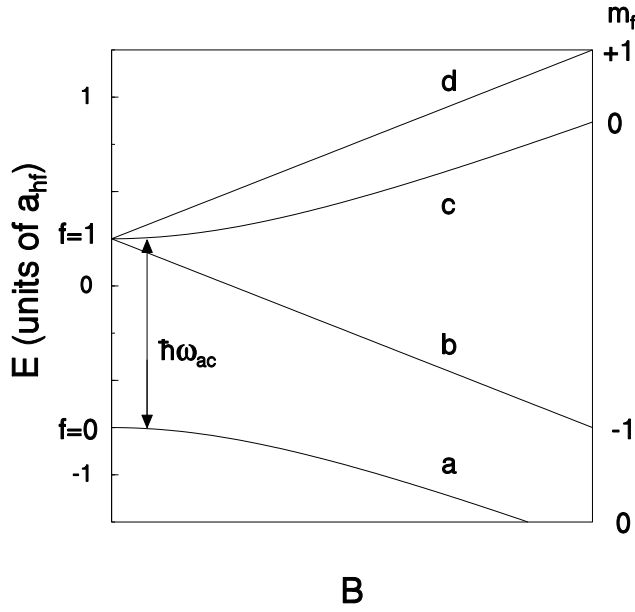


Figure 8.1 Four hyperfine states of the atomic hydrogen electronic ground state, labeled as $|a\rangle$, $|b\rangle$, $|c\rangle$, and $|d\rangle$ in order of increasing energy. The $a-c$ transition is field independent in first order, and is used for both the maser and relaxation experiments.

In the case of the conventional H maser it was already known that spin-exchange H+H collisions broaden and shift the atomic hyperfine transition, displayed in Fig. 8.1, thereby coupling fluctuations in the atomic density to the maser oscillation frequency ω_m . An essential element in the development of the present state-of-the-art H masers was the idea of spin-exchange tuning, by which ω_m is made insensitive to changes in the atomic density by choosing a particular detuning of the maser microwave cavity [6]. This method makes use of the fact that the spin-exchange induced frequency shift is proportional to the population inversion of the masing hyperfine states in the cavity (see Fig. 8.2), while the cavity-pulling shift shows the same proportionality, thus providing for the possibility to make these two shifts cancel.

About ten years ago, a study of the H atom spin-exchange process by our group [7] showed that with proper inclusion of hyperfine interactions, the frequency shifts actually depend in a more complicated way on the occupations of the various hyperfine states of the colliding atoms. As a consequence, the spin-exchange tuning procedure is not as efficient as it was once thought to be, in particular at low temperatures where atomic collision energies are comparable to the hyperfine interaction energy.

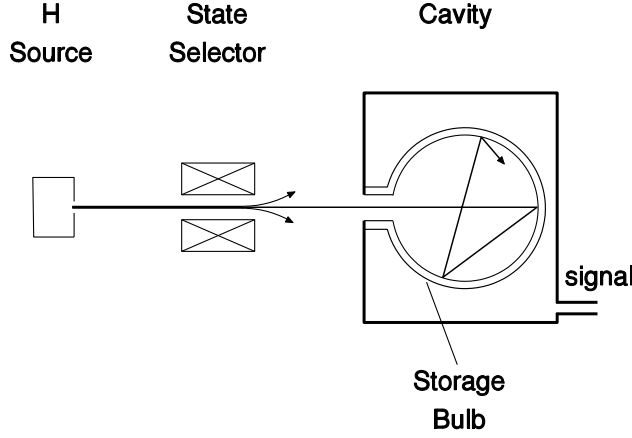


Figure 8.2 Schematic representation of the hydrogen maser. The high-field seeking states a and b are removed by the state selector, thus creating a $c - a$ population inversion

Two experiments have since then confirmed our theoretical prediction, one at room temperature in a conventional H maser [8], and the other at 0.5 K in a low temperature H maser [3]. In both cases a frequency shift beyond that predicted by the original theories of spin-exchange was observed and interpreted as being a direct consequence of hyperfine precessions during spin-exchange collisions (hyperfine-induced (HI) frequency shift).

There are growing indications, however, of serious disagreements between experiment and theory, not only with respect to the h-i shift but in total to three different quantities relating to the H maser [3, 8, 9]. Another recent experiment [10] shows that the disagreement is not restricted to the H maser: It also shows up in the longitudinal relaxation rate $(1/T_1)_{coll}$ due to collisions, observed in an electron spin resonance measurement on an atomic hydrogen gas sample at $T = 1.23$ K. An important reason to take these discrepancies seriously is the believed preciseness of the knowledge of the hydrogen atom interactions. The long-range singlet (S) and triplet (T) interaction potentials between two hydrogen atoms are accurately described by

$$V_{S,T}(r) = -C_6/r^6 - C_8/r^8 - C_{10}/r^{10} + V_{exch}, \quad (8.1)$$

with the dispersion coefficients taken from Yan et al. [11] and the exchange part from Smirnov and Chibisov [12]. The short range interactions (see Fig. 8.3) are believed to be precisely described by calculations in the literature, including adiabatic, radiative and relativistic corrections [13]. In addition to the above interactions the effective two-atom Hamiltonian contains a sum of atomic hyperfine interactions:

$$\begin{aligned}
V_{hf} &= \frac{a_{hf}}{\hbar^2} (\vec{s}_1 \cdot \vec{r}_1 + \vec{s}_2 \cdot \vec{r}_2) \\
&= \frac{1}{2} \frac{a_{hf}}{\hbar^2} (\vec{s}_1 + \vec{s}_2) \cdot (\vec{r}_1 + \vec{r}_2) + \frac{1}{2} \frac{a_{hf}}{\hbar^2} (\vec{s}_1 - \vec{s}_2) \cdot (\vec{r}_1 - \vec{r}_2) \\
&\equiv V_{hf}^+ + V_{hf}^-,
\end{aligned} \tag{8.2}$$

of which the part V_{hf}^- , antisymmetric in the electronic spin operators, couples the singlet and triplet subspaces. Here a_{hf} denotes the hyperfine constant.

In principle the discrepancies might point to effects not yet included in the present description of the maser and the electron spin resonance experiment, with possible fundamental consequences. In the case of the Cs fountain clock there is less strong evidence for a disagreement: It is surprising that an analysis [14] some years ago on the basis of the best interaction potentials available at that time could only explain the experimental frequency shifts by assuming the existence of resonances both in the singlet and triplet subspaces very close to threshold. It may well be that this strong requirement is also a signature of a new process that is not yet accounted for in the present theoretical description.

We have investigated whether a suitable modification of the singlet and triplet H+H interaction potentials makes it possible to eliminate all discrepancies at the same time. The strategy is to focus first on the disagreement in the atomic hydrogen experiments, in which case any interaction already included and any interaction not yet included can be calculated from first principles. It seems likely that a change in the description of the hydrogen system will have implications also for the Cs atomic clock. We also discuss a possible role of the magnetic dipole interaction between the electron spins of the colliding atoms.

In sections 8.2 and 8.3 we give a brief description of the measured quantities as well as the discrepancies. In section 8.4 we explore a possibility to remove the $1/T_1$ discrepancy by relaxing some of the assumptions in Ref. [10]. In section 8.5 this is followed by a description of our main approach and its results. Finally, in section 8.6 we discuss the relevance of the magnetic spin-dipole interaction in relation to the discrepancies. Some conclusions are given in section 8.7.

8.2 Description of frequency shifts and discrepancies

The four hyperfine states of the atomic hydrogen electronic ground state are in order of increasing energy labeled as $|a\rangle$, $|b\rangle$, $|c\rangle$ and $|d\rangle$ (see Fig. 8.1). The hydrogen maser, schematically represented in Fig. 8.2, operates on the $a - c$ transition which is field-independent in first order.

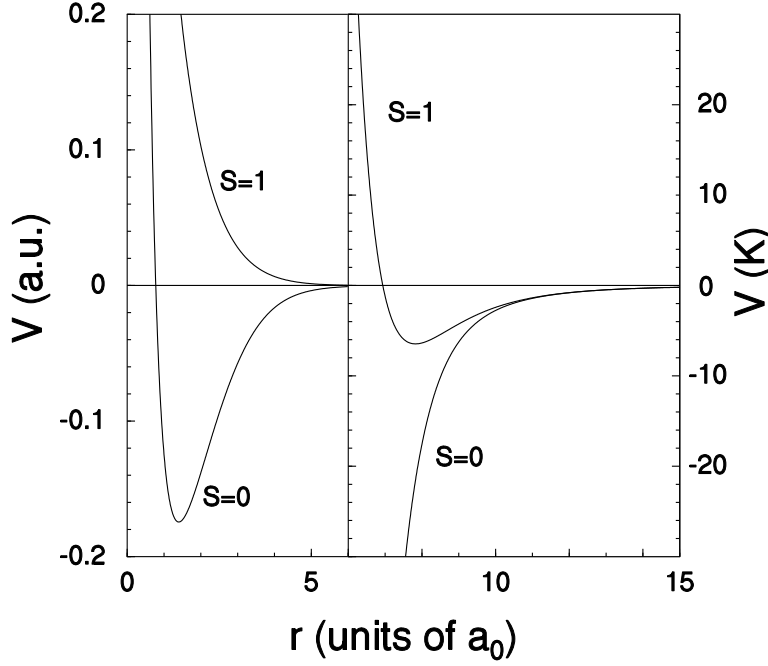


Figure 8.3 Singlet ($S=0$) and triplet ($S=1$) potentials of groundstate hydrogen.

Using the quantum Boltzmann equation, the frequency shift $\delta\omega$ and line broadening Γ due to spin-exchange collisions can be shown [7] to have the form

$$i\delta\omega - \Gamma = n \sum_j \rho_{jj} \langle v(i\lambda_j - \sigma_j) \rangle \equiv n \sum_j \rho_{jj} \langle v \rangle (i\bar{\lambda}_j - \bar{\sigma}_j). \quad (8.3)$$

The hydrogen atom density is denoted by n , the relative collision velocity by v and the single-atom spin-density matrix by ρ . The $\langle \rangle$ brackets denote thermal averaging over a Maxwell-Boltzmann distribution. The cross-sections λ_j and σ_j ($j = a, b, c, d$), characterizing the partial frequency shift and broadening due to collisions of a coherent $a+c$ state with atoms in state j (partial density $n\rho_{jj}$), are expressed in elastic S-matrix elements by

$$i\lambda_j - \sigma_j = (1 + \delta_{aj})(1 + \delta_{cj}) \frac{\pi}{k^2} \sum_l (2l+1) \left[S_{\{aj\},\{aj\}}^l S_{\{cj\},\{cj\}}^{l*} - 1 \right]. \quad (8.4)$$

The brackets $\{ \}$ denote symmetrization (antisymmetrization) of the spin states for relative orbital angular momentum l even (odd). The coefficients $\bar{\lambda}_j$ and $\bar{\sigma}_j$ describe explicitly how $\delta\omega$ and Γ depend on the partial occupancies ρ_{jj} of the four single-atom

hyperfine states. They can be calculated by thermally averaging the quantities $v\lambda_j$ and $v\sigma_j$, which in turn are given by the quadratic expressions (8.4) in terms of collisional S-matrix elements. All of these elastic S-matrix elements are to be calculated for a common value of the relative wave number k in the entrance channel, which varies over the above-mentioned Maxwell-Boltzmann distribution.

Rewriting the frequency shift and line broadening as

$$\delta\omega = n\langle v \rangle [(\rho_{cc} - \rho_{aa})\bar{\lambda}_0 + (\rho_{cc} + \rho_{aa})\bar{\lambda}_1 + \bar{\lambda}_2], \quad (8.5)$$

$$\Gamma = n\langle v \rangle [(\rho_{cc} - \rho_{aa})\bar{\sigma}_0 + (\rho_{cc} + \rho_{aa})\bar{\sigma}_1 + \bar{\sigma}_2], \quad (8.6)$$

we note that the $\bar{\lambda}_1$ and $\bar{\lambda}_2$ contributions vanish according to theoretical treatments of spin-exchange collisions [6, 15, 16] that ignore hyperfine interactions during collisions (the Degenerate-Internal-States approximation). Crampton [17] showed that for a certain detuning of the cavity the remaining $(\rho_{cc} - \rho_{aa})$ -dependent frequency shift, described by the parameter λ_0 , can be cancelled by cavity pulling, which has been a major factor in stabilizing conventional room temperature H masers. In 1975 Crampton and Wang [18] took into account the atomic hyperfine precession during collisions in a semi-classical straight-path approximation and found an additional ρ -independent $\bar{\lambda}_2$ term. They confirmed the presence of such a term experimentally in a room-temperature hydrogen maser. Its smallness makes it relatively unimportant for the stability of conventional hydrogen masers.

In the case of the sub-Kelvin hydrogen maser, however, the role of the hyperfine-induced $\bar{\lambda}_1$ and $\bar{\lambda}_2$ terms is of much greater importance. Hayden, Hürlimann and Hardy reviewed the situation in their recent paper [9]. In the same paper they confirmed the existence of a HI frequency shift in their experiment, proportional to $(\rho_{aa} + \rho_{cc})\bar{\lambda}_1 + \bar{\lambda}_2 = \frac{1}{2}\bar{\lambda}_1 + \bar{\lambda}_2$. They found its sign to be different from the theoretical prediction, however. In addition the value of $\bar{\lambda}_0$ was almost twice the theoretical value.

Finally, in the same experiment an ingenious method to measure the linear combination $(\rho_{aa} + \rho_{cc})\bar{\sigma}_1 + \bar{\sigma}_2 = \frac{1}{2}\bar{\sigma}_1 + \bar{\sigma}_2$ of broadening cross sections was applied. This result too showed a discrepancy with the theoretical value calculated by our group. Table 8.1 summarizes the experimental and theoretical values for the three above quantities. It also shows a result from an experiment by Walsworth *et al.* [8] for the room-temperature maser, which also appears to show a discrepancy with theory. We should note, however, that the theoretical calculation of the $\bar{\lambda}$ and $\bar{\sigma}$ cross-sections at room temperature involves a thermal average over a range of collision energies containing a huge number of resonances. Due to the complications involved in such a calculation we consider the evidence for a discrepancy between theory and experiment to be less direct than in the cryogenic case. Therefore, in the following we will focus on the cryogenic data.

Table 8.1 Parameters showing discrepancies.

Quantity	Theory (cm ²)	Experiment (cm ²)	Ref.
$\bar{\lambda}_0$	-1.19×10^{-15}	$(-2.17 \pm 0.28) \times 10^{-15}$	[9]
$\frac{1}{2}\bar{\lambda}_1 + \bar{\lambda}_2$	-2.04×10^{-18}	$(2.2_{-1.0}^{+0.5}) \times 10^{-18}$	[9]
$\frac{1}{2}\bar{\sigma}_1 + \bar{\sigma}_2$	26.3×10^{-18}	$(38.5 \pm 3) \times 10^{-18}$	[9]
$\bar{\lambda}_1$	3.0×10^{-19}	-1.8×10^{-18}	[8]
$\bar{\sigma}_{T_1}$	37×10^{-18}	$(51 \pm 2) \times 10^{-18}$	[10]

8.3 Description of longitudinal relaxation time and discrepancies

In a recent paper [10] the evidence for a discrepancy with theory was considerably extended by means of experimental data that do not involve the complications of a (re-circulating) cryogenic hydrogen maser. Applying pulsed hyperfine magnetic resonance techniques to a gas of hydrogen atoms at a temperature of 1.23 K in a magnetic field of 60 G, it was possible to determine the longitudinal relaxation time T_1 for the $a - c$ transition. Essentially, starting with equilibrium populations of the a, b, c, d levels, an initial π pulse inverted the a and c populations. The return to equilibrium was monitored by means of a $\pi/2$ pulse with a variable delay time and an observation of the subsequent free induction decay.

For the analysis the authors used rate equations, which we reformulate here in a more rigorous form to exclude already a few of the possibilities for an explanation of the T_1 discrepancy. Our starting point is again the quantum Boltzmann equation. The time evolution of a partial density is then found to be given by [7, 19]

$$\frac{d}{dt}n_\alpha = \sum_{\beta} \sum_{\{\alpha'\beta'\}} (1 + \delta_{\alpha\beta})(G_{\alpha'\beta' \rightarrow \alpha\beta} n_{\alpha'} n_{\beta'} - G_{\alpha\beta \rightarrow \alpha'\beta'} n_\alpha n_\beta), \quad (8.7)$$

with rate constants

$$G_{\alpha\beta \rightarrow \alpha'\beta'} = \left\langle \frac{2\pi\hbar}{mk} \sum_l (2l+1) |S_{\{\alpha'\beta'\}, \{\alpha\beta\}}^l - \delta_{\{\alpha'\beta'\}, \{\alpha\beta\}}|^2 \right\rangle, \quad (8.8)$$

where the slow relaxation due to the dipolar spin-spin interaction is neglected.

For an analysis of their experiment Hayden and Hardy introduce the approximate equalities $G_{aa \rightarrow bd} \approx G_{cc \rightarrow bd}$, $G_{\alpha\beta \rightarrow \gamma\delta} \approx G_{\gamma\delta \rightarrow \alpha\beta}$ and $n_a + n_c \approx n/2$, referring to the large value of $k_B T$ compared to the internal energy intervals. Equation (8.7) then reduces to the simple form

$$\frac{d}{dt}(n_a - n_c) = -(2G_{cc \rightarrow aa} + G_{bd \rightarrow aa})n(n_a - n_c). \quad (8.9)$$

This equation leads to the expression

$$\frac{1}{T_1} = (2G_{cc \rightarrow aa} + G_{bd \rightarrow aa})n \equiv n\langle v \rangle \bar{\sigma}_{T_1} \quad (8.10)$$

for the longitudinal relaxation time.

The experimental result $\bar{\sigma}_{T_1} = (51 \pm 2) \times 10^{-18} \text{ cm}^2$ is in disagreement with the theoretical value $37 \times 10^{-18} \text{ cm}^2$ following from calculated rate constants $G_{\alpha\beta \rightarrow \gamma\delta}$ [19]. Both values are included in Table 8.1. A recalculation using the most recent potentials [13] in the framework of the present paper, confirmed all theoretical values in this table, changes relative to the old values being at most of order 1%.

8.4 Comparison with more rigorous expression for longitudinal relaxation time

In a first attempt to eliminate discrepancies we consider separately the longitudinal relaxation time. The objective is to compare the experimental $\bar{\sigma}_{T_1}$ also with a more rigorous theoretical expression, relaxing the above-mentioned simplifying assumptions of Ref. [10] and using the rigorous rate equations (8.7) as a starting point. One of the effects included in such an approach is that the non-equilibrium populations of the a and c levels induced by the π pulse may affect subsequently the b and d populations via the collision processes included in (8.7), which in turn might influence the relaxation of $n_a - n_c$.

Linearizing the set of equations (8.7) around equilibrium ($n_\alpha = n_\alpha^0$), it reduces to the form

$$\frac{d(n_\alpha - n_\alpha^0)}{dt} = -n\langle v \rangle \sum_{\beta} M_{\alpha\beta}(n_\beta - n_\beta^0), \quad (8.11)$$

with the hyperfine states arranged in the order $\alpha = a, b, c, d$. The coefficients $M_{\alpha\beta}$ stand for linear combinations of Gn^0 products with an overall factor $n\langle v \rangle$ splitted off. Each of the $M_{\alpha\beta}$ elements is a function of temperature T and magnetic field B .

We calculate the eigenvectors and eigenvalues of the 4×4 matrix M . Two of the eigenvalues turn out to be 0, corresponding to the linear relations

$$\sum_{\alpha} M_{\alpha\beta} = 0, \quad (8.12)$$

$$M_{b\beta} - M_{d\beta} = 0, \quad (8.13)$$

among the rows of M . The relation (8.12) is connected with conservation of the total density $n_a + n_b + n_c + n_d$ and relation (8.13) with conservation of $n_b - n_d$, i.e. of the total spin magnetic quantum number m_F . Note that in exchange collisions the spin and orbital magnetic quantum numbers are separately conserved. As a consequence, we end up with two non-trivial rate equations associated with the two remaining eigenvalues describing the combined decay of $n_a - n_c$ and $(n_a + n_c) - (n_b + n_d)$ to their equilibrium values. The initial condition at $t = 0$ right after the π pulse, is a superposition of the two eigenvectors with $(n_a + n_c) - (n_b + n_d)$ equal to its equilibrium value. In principle, at times $t > 0$ we thus obtain two decaying exponentials combining to a time-dependent solution with both $n_a - n_c$ and $(n_a + n_c) - (n_b + n_d)$ different from their equilibrium values. The time dependence of the quantities

$$\Delta n_{a-c} \equiv (n_a - n_c) - (n_a - n_c)^0, \quad (8.14)$$

$$\Delta n_{a+c} \equiv [(n_a + n_c) - (n_b + n_d)] - [(n_a + n_c) - (n_b + n_d)]^0, \quad (8.15)$$

calculated for the experimental values of n , T and B , is presented in Fig. 8.4. It turns out, however, that the difference of the eigenvalues is only about 2%. In addition, their average is equal to the theoretical value $37 \times 10^{-18} \text{ cm}^2$ for $\bar{\sigma}_{T_1}$ quoted above as following from the simplifying assumptions of Ref. [10].

Consistent with these results we find that n_b and n_d as well as $n_a + n_c$ to good approximation retain their equilibrium values, the deviations reaching a maximum of order 1% after a time of about 13 s, whereas $n_a - n_c$ behaves approximately according to the simplified equation (8.10), the deviations again being of order 1%. We therefore continue our investigation of the T_1 discrepancy on the basis of Eq. (8.10).

8.5 Modification of potentials

In this section we explore the possibility to resolve the discrepancies by modifying the interaction potentials, in particular in the range of interatomic distances up to about $7a_0$ where the atomic electron clouds overlap leading to a strongly attractive singlet and a strongly repulsive triplet potential (see Fig. 8.2). As we will show, the effect of changes in a potential in this radial range can be studied in a model-independent way, i.e. irrespective of the precise nature of the modification, following an approach in the spirit of the accumulated-phase method [20, 21]. This method has been highly successful in analyzing cold collisions among ground-state alkali atoms. The idea is to account for a possible change of an interaction potential by modifying the boundary

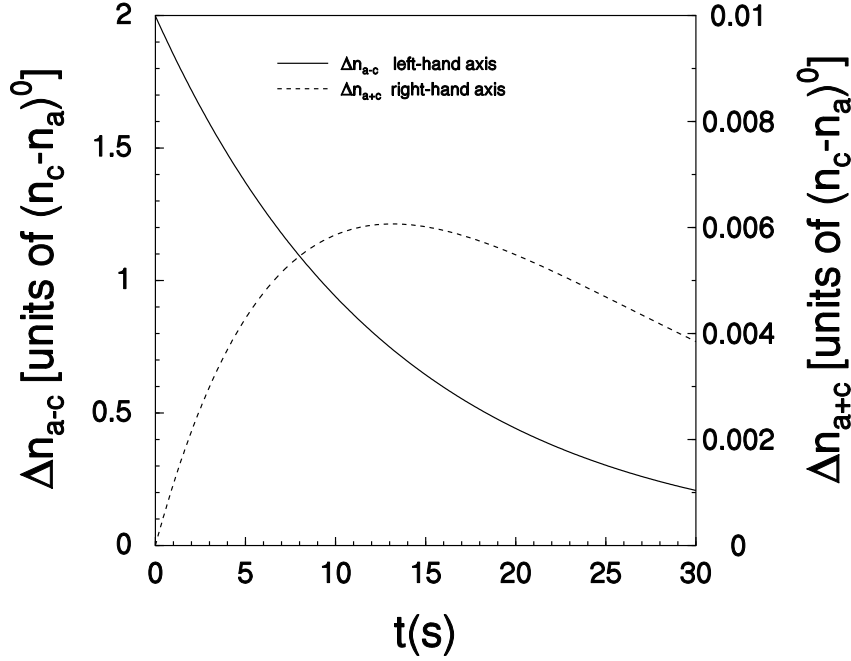


Figure 8.4 Time-dependent relaxation of $n_a - n_c$ and $n_a + n_c - (n_b + n_d)$ to their equilibrium values, due to two slightly different relaxation eigenvalues. Experimental circumstances: Temperature $T = 1.23$ K, $B = 60$ G and hydrogen density $n = 8.9 \times 10^{10} \text{ cm}^{-3}$.

condition for the radial wave function at the boundary r_0 of the radial range considered. In this range the singlet and triplet electronic states are so far apart in energy compared with the hyperfine coupling V_{hf} that the $S=0$ and $S=1$ channels are still uncoupled. The new boundary condition then determines the solution of Schrödinger's equation in the further radial range $r > r_0$ and especially the interference of the singlet and triplet channels under the influence of V_{hf} . The change of the boundary condition simply summarizes the effect of the change of the potentials, wherever it occurs inside r_0 . The actual modification of the boundary condition can be effected by an adjustment of the local phase ϕ of the radial wave function $F(r)$ as in Ref. [20, 21] or by a change of the logarithmic derivative F'/F . We prefer the latter possibility so that we can deal with a real-valued quantity only: The phase ϕ would be imaginary inside the classical turning point for the triplet potential near $7 a_0$.

Note that the actual position of r_0 is unimportant, as long it is not too far out: A modified F'/F at r_0 not only simulates a changed interaction inside r_0 , but also one outside r_0 where the $S=0$ and $S=1$ subspaces are still sufficiently decoupled. As a matter of fact, by a modification of F'/F at r_0 , one can also effect an arbitrary change

at larger r . The actual value used for r_0 is $4 a_0$.

Note also that F'/F , like ϕ , is in principle a function of energy E and relative angular momentum l in the collision. In the small E and l range involved in cold collisions, however, this variation is negligible since r_0 is sufficiently far from the turning points both in the classically inaccessible range for the triplet channel and the classically accessible range for the singlet potential.

The problem we thus face is to determine the theoretical dependence of the quantities $\bar{\lambda}_0$, $\frac{1}{2}\bar{\lambda}_1 + \bar{\lambda}_2$, $\frac{1}{2}\bar{\sigma}_1 + \bar{\sigma}_2$ and $\bar{\sigma}_{T_1}$ on the singlet and triplet increments

$$\Delta_S = \Delta (F'_S/F_S)_{r_0}, \quad \Delta_T = \Delta (F'_T/F_T)_{r_0}, \quad (8.16)$$

to see if there exist reasonable Δ_S , Δ_T values for which all four discrepancies can be eliminated simultaneously.

Figure 8.5 shows the changes Δ_S , Δ_T of logarithmic derivatives needed to bring the theoretical values of the observables to within twice the standard deviations from the experimental values. To compress the ranges of large Δ values where the actual differences of the radial wave functions is small, we have chosen to plot Δ_S and Δ_T in a nonlinear way: We calculate the corresponding phase changes $\Delta\phi_S$ and $\Delta\phi_T$ at the deepest points of the two potentials and vary these quantities linearly along the axis. Note that $\Delta\phi_S$ will have to be small relative to π to avoid disagreement with experimental data for the singlet H_2 rovibrational states. The total $\Delta\phi_S$ range included in the figure is certainly larger than that allowed by these experimental data. The total $\Delta\phi_T$ range studied is also larger than it can conceivably be: It runs from a very small negative value -2.2×10^{-4} , hardly distinguishable from the abscissa, where $\Delta_T = +\infty$, to the value $= 1.34$, indicated by a horizontal dashed line, where the triplet potential is so deep that a triplet state becomes bound. Positive values for $\Delta\phi_T$ exceeding 1.34 are excluded because none of the many experiments on spin-polarized atomic hydrogen has indicated the existence of a triplet bound state. Negative values extending beyond -2.2×10^{-4} are not allowed because the corresponding value for Δ_T is the maximum possible value $+\infty$ for this correction of the logarithmic derivative of the radial wavefunction. To give an impression of the degree to which the quantities $\Delta\phi_S$ and $\Delta\phi_T$ have converged, we note that the changes of these phase differences in going from the old to the new H+H potentials [13] are at most of order 0.001 radians.

Even between these unrealistically wide limits no overlap region for all observables simultaneously is found. The only overlap that occurs is between the pair of $\bar{\lambda}$ quantities and between the pair of $\bar{\sigma}$ quantities. We conclude that the option of better singlet and triplet potentials for internuclear distances where the electron clouds overlap strongly is not a viable solution for the existing discrepancies.

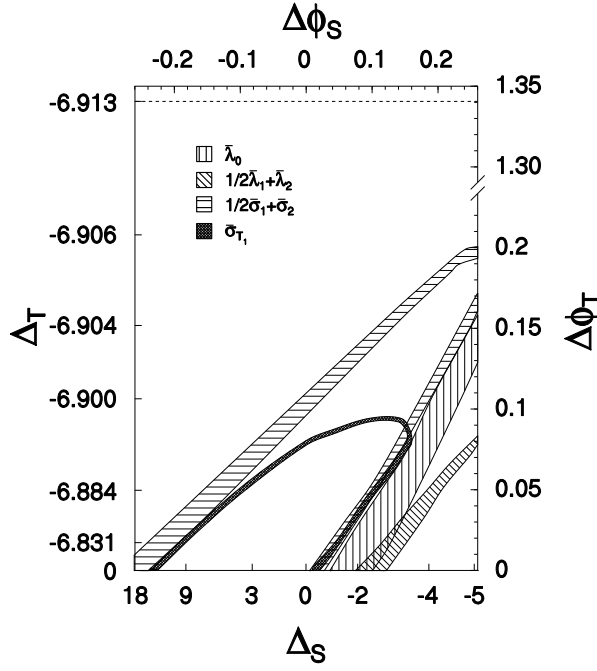


Figure 8.5 Parameter regions in the Δ_S, Δ_T (or equivalently $\Delta\phi_S, \Delta\phi_T$) plane, where discrepancies in observables $\bar{\lambda}_0$, $\frac{1}{2}\bar{\lambda}_1 + \bar{\lambda}_2$, $\frac{1}{2}\bar{\sigma}_1 + \bar{\sigma}_2$, and $\bar{\sigma}_{T_1}$ are eliminated.

8.6 Influence of magnetic dipole interaction

In our previous calculations [7] we have neglected the magnetic dipole interaction between the spin magnetic moments (electron and proton) of the two atoms, in view of the general dominance of electric vs magnetic interactions. This dominance is illustrated, e.g., by the fact that dipolar relaxation rates are typically three orders of magnitude smaller than spin-exchange rates [19]. We point out, however, that interference between the two kinds of amplitude, which are absent in these rates, could give rise to more important contributions. Moreover, the hyperfine-induced $\frac{1}{2}\bar{\lambda}_1 + \bar{\lambda}_2$ cross section is by itself a small effect relative to $\bar{\lambda}_0$, so that the dipole interaction might in principle resolve the discrepancy in the measured hyperfine-induced frequency shift. This is what we are going to investigate in this section. We restrict ourselves to the electron-electron part of the interatomic dipole interaction, the electron-proton and proton-proton parts being much weaker.

On the basis of the structure of the $|a\rangle$ and $|c\rangle$ states the $\langle a|\vec{s}_i|a\rangle$ and $\langle c|\vec{s}_i|c\rangle$ matrix elements are zero for $B = 0$, and negligible for the weak experimental field. We conclude that no direct dipolar transitions are possible in collisions where only $|a\rangle$ or $|c\rangle$ states are involved.

For small values of the collisional quantum number l the central interaction is also involved. The combination of these two interactions can result in a 'two-step' process, where the dipolar interaction is involved in a transition from $|a\rangle$ to $|a\rangle$ or $|c\rangle$ to $|c\rangle$, via a central interaction step between $|a\rangle$ and $|c\rangle$. Considering the quantum Boltzmann equation including the dipole interaction, the frequency shift and broadening cross sections are given by

$$\begin{aligned} i\lambda_a - \sigma_a &= \frac{2\pi}{k^2} \sum_{l'm'} \sum_{lm} \left[S_{\{aa\},\{aa\}}^{l'm',lm} S_{\{ac\},\{ac\}}^{l'm',lm*} - 1 \right], \\ i\lambda_c - \sigma_c &= \frac{2\pi}{k^2} \sum_{l'm'} \sum_{lm} \left[S_{\{ac\},\{ac\}}^{l'm',lm} S_{\{cc\},\{cc\}}^{l'm',lm*} - 1 \right], \\ i\lambda_b - \sigma_b = i\lambda_d - \sigma_d &= \frac{\pi}{k^2} \sum_{l'm'} \sum_{lm} 2S_{\{ab\},\{ad\}}^{l'm',lm} S_{\{cb\},\{cd\}}^{l'm',lm*} + \left[S_{\{ad\},\{ad\}}^{l'm',lm} S_{\{cd\},\{cd\}}^{l'm',lm*} - 1 \right]. \end{aligned} \quad (8.17)$$

In comparison with expressions (8.4) there are some differences. First, in this case also inelastic S -matrix elements contribute. Second, the angular momentum quantum numbers l' and l are not necessarily identical due to the selection rules of the dipole interaction we have $l' = l - 2$, $l' = l$ or $l' = l + 2$, with the exception of $l' = l = 0$. In view of the experimental temperatures of order 1 K, we restrict ourselves to s and d partial waves. For the cross sections in (8.17) with subscripts b or d p→p transitions are not forbidden by Bose symmetry. They are not included in the following, but are expected to contribute with similar orders of magnitude.

To begin with we note that $S_{\{aa\},\{aa\}}^{20,00} = S_{\{aa\},\{aa\}}^{00,20} = 0$, because of angular momentum conservation: the total two-atom spin is zero in both the initial and final state, so that l has to be conserved. We divide the λ contributions additional to the expressions (8.4) in three categories. First, the 'dipolar' transitions taking place only if the dipole interaction takes part, i.e. contributions to λ_d from $\{ad\} \rightarrow \{ab\}$ and $\{cd\} \rightarrow \{cb\}$ transitions. Second, interference contributions due to dipolar corrections to central elastic processes that could already take place via the central interaction, i.e. $\{ad\} \rightarrow \{ad\}$ and $\{cd\} \rightarrow \{cd\}$ contributions to λ_d . Third, contributions to λ_c with the same character, i.e. involving $\{ca\} \rightarrow \{ca\}$ and $\{cc\} \rightarrow \{cc\}$ processes. The first two will give a frequency shift proportional to n_b or n_d , the last one proportional to n_c (a contribution proportional to n_a is absent in view of the above argument).

In Table 8.2 we give results for these additional contributions, calculated for a collision energy of 0.5 K. Clearly, comparing with the discrepancies in Table 8.1 we see that these values are far too small to be of any significance. They are even smaller than could be expected on the basis of the dipolar decay rates. The reason is essentially, as on analysis of the S -matrix elements shows, that the matrix elements $S_{\{c\alpha\},\{c\beta\}}^{20,00}$ and $S_{\{a\alpha\},\{a\beta\}}^{20,00}$ are nearly equal, so that the corresponding contribution to the frequency

Table 8.2 Contributions to frequency shift cross sections from magnetic dipole interaction, subdivided into three categories.

λ_c elastic	λ_d elastic	λ_d inelastic
$-1.03 \times 10^{-23} \text{ cm}^2$	$-1.19 \times 10^{-25} \text{ cm}^2$	$-1.03 \times 10^{-24} \text{ cm}^2$

shifts vanishes. We conclude that the inclusion of the magnetic dipole interaction does not resolve the $\frac{1}{2}\bar{\lambda}_1 + \bar{\lambda}_2$ discrepancy.

8.7 Conclusions

We have reviewed four types of discrepancies between experiment and existing theory, connected with cold atomic hydrogen gas samples. Three are associated with the sub-Kelvin hydrogen maser, one with a pulsed hyperfine magnetic resonance experiment. The discovery of the latter discrepancy in recent work has been of great importance since it thereby becomes more probable that the resolution of the inconsistencies has to be found in the theoretical description of the cold H+H collisions. This contrasts with the earlier discrepancies, all three relating to the hydrogen maser, which could have been ascribed to an incomplete description of this setup. We have investigated two issues in connection with the inconsistencies.

First, we have studied the possibility that an additional term in the collisional Hamiltonian, operating at small internuclear distances in the region of strongly overlapping electron clouds, is overlooked in present descriptions of cold atomic collisions. We have shown that no such additional terms can eliminate all four discrepancies at the same time, without leading to other inconsistencies, such as the introduction of triplet H_2 bound states.

Secondly, we have investigated the possibility that the magnetic dipole forces operating between the electron spins, left out in existing theoretical descriptions of the above experiments, might lead to significant changes of the predictions. We have found that the additional contributions from this source fall short by orders of magnitude.

The growing importance of cold collisions in a number of present basic developments (Bose-Einstein condensation, atom lasers, atomic fountain clocks) underlines the need to spend further effort to finding a solution for the discrepancies. Also in this connection atomic hydrogen can play a role as a model system, its relative simplicity offering the possibility to reveal aspects in which the existing cold collision theory is incomplete. Recent progress in describing cold collisions of Rb atoms [22,23] makes it possible to turn to this atom species as a possible second example where discrepancies might be detected in precision experiments. In this connection envisaged experiments with a Rb

atomic fountain clock [24] would be especially interesting.

References

- [1] J. Vanier and C. Audoin, *The quantum physics of atomic frequency standards*, Adam Hilger, Philadelphia (1989).
- [2] M. Kasevich, E. Riis, S. Chu, R. DeVoe, Phys. Rev. Lett. **63**, 612 (1989); A. Clairon, C. Salomon, S. Guellati, and W.D. Phillips, Europhys. Lett. **16**, 165 (1991).
- [3] M.E. Hayden, Ph.D. Dissertation, University of British Columbia, 1991 (unpublished); M.E. Hayden, M.D. Hürlimann, and W.N. Hardy, IEEE Trans. on Instr. and Measurement **42**, 314 (1993).
- [4] E. Tiesinga, B.J. Verhaar, H.T.C. Stoof, and D. van Bragt, Phys. Rev. A **45**, 2671 (1992).
- [5] K. Gibble and S. Chu, Metrologia **29**, 201 (1992).
- [6] S.B. Crampton, Ph.D. dissertation, Harvard University, 1964 (unpublished) and Phys. Rev. **158**, 57 (1967).
- [7] B.J. Verhaar, J.M.V.A. Koelman, H.T.C. Stoof, O.J. Luiten, and S.B. Crampton, Phys. Rev. A **35**, 3825 (1987); J.M.V.A. Koelman, S.B. Crampton, H.T.C. Stoof, O.J. Luiten, and B.J. Verhaar, *ibid.* **38**, 3535 (1988).
- [8] R.L. Walsworth, Ph.D. dissertation, Harvard University, 1991 (unpublished); R.L. Walsworth, I.F. Silvera, E.M. Mattison, and R.C. Vessot, Phys. Rev. A **46**, 2495 (1992).
- [9] M.E. Hayden, M.D. Hürlimann, and W.N. Hardy, Phys. Rev. A **53**, 1589 (1996).
- [10] M.E. Hayden and W.N. Hardy, Phys. Rev. Lett. **76**, 2041 (1996).
- [11] Z.-C. Yan, J.F. Babb, A. Dalgarno, and G.W.F. Drake, Phys. Rev. A **54**, 2824 (1996).
- [12] B.M. Smirnov and M.I. Chibisov, Zh. Eksp. Teor. Fiz. **48**, 939 (1965) [JETP **21**, 624 (1965)].
- [13] L. Wolniewicz, J. Chem. Phys. **103**, 1792 (1995) and references therein.
- [14] Boudewijn Verhaar, Kurt Gibble and Steven Chu, Phys. Rev. A **48**, R3429 (1993).
- [15] P.L. Bender, Phys. Rev. **132**, 2154 (1963).
- [16] L.C. Balling, R.J. Hanson, and F.M. Pipkin, Phys. Rev. **133**, A607 (1964).
- [17] S.B. Crampton, Phys. Rev. **158**, 57 (1967).
- [18] S.B. Crampton and H.T.M. Wang, Phys. Rev. A **12**, 1305 (1975).
- [19] H.T.C. Stoof, J.M.V.A. Koelman, and B.J. Verhaar, Phys. Rev. B. **38**, 4688 (1988).
- [20] A.J. Moerdijk and B.J. Verhaar, Phys. Rev. Lett. **73**, 518 (1994).
- [21] A.J. Moerdijk, B.J. Verhaar and A. Axelsson, Phys. Rev. A **51**, 4852 (1995).
- [22] J.M. Vogels, R.S. Freeland, C.C. Tsai, S.J.J.M.F. Kokkelmans, B.J. Verhaar, and D.J. Heinzen, Phys. Rev. A **56**, R1067 (1997).
- [23] C.C. Tsai, R.S. Freeland, J.M. Vogels, H.M.J.M. Boesten, D.J. Heinzen, and B.J. Verhaar, Phys. Rev. Lett. **79**, 1245 (1997).
- [24] K. Gibble (private communication).

Summary

In recent years new possibilities have become available to manipulate atomic gasses with laser light and magnetic fields. This led to the observation of a variety of remarkable phenomena and achievements, such as Bose-Einstein condensation (BEC) and atomic clocks with a dramatically improved accuracy. Interatomic interactions play a crucial role in these dilute systems. In creating a condensate large elastic cross sections are required for efficient evaporative cooling, while inelastic rates should be small. In addition, the sign of the scattering length is important for the stability of the condensate. In cold atomic clocks the collisional frequency shift is *the* limiting factor to accuracy. To be able to make predictions we need detailed information about the interactions. We have shown that part of the interaction parameters can be reliably extracted from experiments.

A very intriguing experiment was done in 1996 at JILA (Boulder, Colorado). Two overlapping condensates in different hyperfine states appeared to be coexisting, something completely unforeseen. Usually inelastic processes would cause a rapid decay of both condensates. The fact that almost no other hyperfine states are produced by collisions requires that the singlet and triplet scattering lengths are almost the same. Along with this information we were able to deduce interaction parameters for rubidium that allowed us to make a prediction of the collisional frequency shift for a cold ^{87}Rb clock. The near equality of singlet and triplet scattering lengths for this species makes all scattering lengths approximately equal, yielding a small frequency shift, more than an order of magnitude smaller than for the cold cesium atomic clock. This prediction has meanwhile been experimentally confirmed at Yale University. Also a clock based on ^{85}Rb would have great advantages since the partial shifts have opposite signs and can be made to cancel with a special technique.

In contrast to the weak inelastic decay for ^{87}Rb the inelastic losses for Cs are large, thus obstructing an easy realization of a cesium BEC. Via a second order spin-orbit interaction (often indicated as indirect spin-spin interaction), that only plays a role of importance for heavier alkali atoms, we could explain these large losses and determine the strength of this interaction. A whole scala of experimental results pointed to almost resonant potentials, and allowed us to predict Feshbach resonances in an easily accessible magnetic field range. These resonances offer the opportunity to vary the strength of the effective interatomic interactions and even change the sign of the scattering length by tuning a magnetic field. A negative scattering length implies attractive interactions and should cause the collapse of a condensate, if sufficiently

strong. Since the prediction in this thesis work the resonances have experimentally been found at Stanford. In the meantime, however, two experiments have been performed with results inconsistent with earlier predictions but also mutually inconsistent: a measurement of the decay rates measured at ENS (Paris) and a juggling experiment carried out at Yale University. In the latter case we were closely involved both in the experiment and the analysis. To resolve these discrepancies, we propose a new method that will allow for very accurate measurements of the scattering phases for a wide range of internal states and collision energies. The new method is based on a combination of atomic clock techniques and a juggling fountain and is expected to have wider applicability in the field of cold atom physics.

The indirect spin-spin interaction plays an important role in collisions between cold cesium atoms. For rubidium this interaction is much weaker, but still of comparable size as the magnetic dipole interaction. We predict a subsplitting of rubidium bound ground-state levels caused by both interactions, where the indirect spin-spin interaction diminishes the effect of the dipole interaction. With the extreme resolution demonstrated in a recent Raman photoassociation experiment on a Bose-Einstein condensate it should be possible to resolve this subsplitting, allowing us to extract for the first time the strength of the indirect spin-spin interaction for rubidium. In this Raman experiment a laser excites two colliding ground-state atoms to an electronically excited molecular state. Without the presence of a second laser this state would decay back to free ground-state atoms with increased kinetic energy large enough to leave the trap. Turning on a second laser tuned to a ground-state bound level will decrease the trap loss. In this thesis we present an analytical model for both one-photon and two-photon processes.

In the same experiment, the coherent Raman transition partially converts an atomic Bose condensate into a molecular condensate. We show that this process is drastically enhanced by a magnetic field sweep over a Feshbach resonance. The resulting resonant formation of a quasibound state increases the presence of the colliding atoms at short distances. This greatly increases the Raman overlap with deeply-bound molecular states yielding an efficient production of highly stable condensed molecules.

The ground-state interactions between hydrogen atoms are believed to be reliably determined from *ab initio* calculations. Still, some experiments have pointed to discrepancies with theory: three experiments dealing with the cryogenic hydrogen maser and a measurement of the longitudinal relaxation time in a cold hydrogen gas sample. The most uncertain part in the interaction occurs at small interatomic distances. We show that changes in the short range singlet and triplet potentials are not able to remove all discrepancies simultaneously.

Samenvatting

De laatste jaren zijn nieuwe mogelijkheden ter beschikking gekomen om atomaire gasen te manipuleren met lasers en magnetische velden. Dit heeft geleid tot de waarneming van talrijke opzienbarende verschijnselen en tot nieuwe toepassingen, zoals Bose-Einstein condensatie (BEC) en atoomklokken met drastisch verbeterde nauwkeurigheid. Interatomaire interacties spelen een cruciale rol in deze ijle systemen. Bij de vorming van een condensaat zijn grote elastische werkzame doorsneden vereist voor efficiënte afdampkoeling terwijl inelastische verliezen klein moeten zijn. Bovendien is het teken van de verstrooiingslengte belangrijk voor de stabiliteit van het condensaat. In koude atoomklokken is de botsingsgeïnduceerde frequentieverschuiving *de* limiterende factor voor de nauwkeurigheid. Om voorspellingen te kunnen doen hebben we gedetailleerde informatie over de interacties nodig. We hebben aangetoond dat een gedeelte van de interactie parameters betrouwbaar bepaald kan worden uit experimentele gegevens.

Een zeer intrigerend experiment werd in 1996 uitgevoerd op JILA (Boulder, Colorado). Twee overlappende condensaten in verschillende hyperfijn toestanden bleken tegelijkertijd te kunnen bestaan, iets dat voor onmogelijk werd gehouden. Normaal gesproken zouden inelastische processen voor een snel verlies van beide condensaten zorgen. Het feit dat bijna geen andere hyperfijn toestanden door botsingen geproduceerd worden vereist dat de singlet en triplet verstrooiingslengten bijna gelijk zijn. Onder andere met deze informatie waren we in staat om interactie parameters voor rubidium te bepalen waarmee wij de frequentie verschuiving voor een koude ^{87}Rb klok konden voorspellen. De bijna identieke singlet en triplet verstrooiingslengten voor dit isotoop zijn er verantwoordelijk voor dat alle verstrooiingslengten ongeveer gelijk zijn. Daarom is de frequentie verschuiving ook klein, meer dan een grootte orde kleiner dan voor de koude cesium atoomklok. Ondertussen is deze voorspelling experimenteel bevestigd op Yale University. Ook een klok gebaseerd op ^{85}Rb zal grote voordelen bieden omdat de partiële frequentie verschuivingen tegengestelde tekens hebben. Met een speciale techniek kan zo de totale verschuiving geëlimineerd worden.

In tegenstelling tot het zwakke inelastische verval bij ^{87}Rb zijn de inelastische verliezen bij Cs groot, hetgeen een makkelijke realisatie van een cesium BEC in de weg staat. Door middel van een tweede orde spin-baan interactie (vaak aangeduid als indirecte spin-spin interactie), die alleen een belangrijke rol speelt bij de zwaardere alkali atomen, konden we deze grote verliezen verklaren en tevens de sterkte van de interactie bepalen. Een heel scala aan experimentele gegevens leek te wijzen op bijna resonante

potentialen, waarmee we Feshbach resonanties konden voorspellen in een gemakkelijk toegankelijk bereik van het magnetisch veld. Deze resonanties bieden de mogelijkheid om de sterkte van de effectieve interatomaire interactie te variëren door een magnetisch veld te verstemmen. Zelfs het teken van de verstrooiingslengte kan zo veranderd worden. Een negatieve verstrooiingslengte impliceert dat de interacties attractief zijn en veroorzaakt, indien voldoende sterk, het ineenstorten van een condensaat. Deze resonanties zijn experimenteel gevonden op Stanford na de voorspellingen in dit proefschrift. Sindsdien zijn er twee experimenten uitgevoerd waarvan de resultaten inconsistent zijn met eerdere voorspellingen maar ook onderling inconsistent: een meting van verliesnelheden op ENS (Parijs) en een 'juggling' (jongleren) experiment op Yale University. Bij het laatste experiment waren we nauw betrokken in zowel het experiment als de analyse. Om deze discrepanties op te lossen hebben we een nieuwe methode voorgesteld waarmee zeer nauwkeurige metingen van de verstrooiingsfasen gerealiseerd kunnen worden door de technieken van een atoomklok en een juggling fontein te combineren. Het ligt in de verwachting dat deze methode breder toepasbaar zal zijn op het gebied van de koude atoomfysica.

De indirecte spin-spin interactie speelt een belangrijke rol in botsingen tussen koude cesium atomen. Voor rubidium is deze interactie veel zwakker, maar qua grootte nog steeds vergelijkbaar met de magnetische dipool interactie. We voorspellen een substructuur van de gebonden grondtoestand niveaus van rubidium veroorzaakt door beide interacties, waarbij de indirecte spin-spin interactie het effect van de dipool interactie verkleint. Het moet mogelijk zijn deze substructuur te onderscheiden, getuige de extreme resolutie die behaald werd in een recent Raman fotoassociatie experiment met een Bose-Einstein condensaat. Daarmee kunnen we voor het eerst de sterkte van de indirecte spin-spin interactie voor rubidium bepalen. In dit Raman experiment exciteert een laser twee botsende grondtoestands atomen naar een elektronisch aangeslagen moleculaire toestand. Zonder de aanwezigheid van een tweede laser zou deze toestand terug vervallen naar vrije grondtoestands atomen waarbij ze voldoende kinetische energie vergaard hebben om de valkuil te verlaten. Een tweede laser die afgestemd is op een grondtoestands gebonden niveau zal het verlies uit de valkuil verkleinen. In dit proefschrift presenteren we een analytisch model voor beide één-foton en twee-foton processen.

In hetzelfde experiment zet de coherente Raman overgang gedeeltelijk een atomair Bose condensaat om in een moleculair condensaat. We laten zien dat dit proces drastisch versterkt wordt door met een tijdafhankelijk magnetisch veld de Feshbach resonantie te passeren. De hierbij resulterende resonante vorming van een quasi gebonden toestand verhoogt de aanwezigheid van de botsende atomen op korte afstand. Dit zorgt voor een grote toename van de Raman overlap met diep-gelegen moleculaire toestanden, resulterend in een efficiënte productie van zeer stabiele gecondenseerde

moleculen.

Van de grondtoestands interacties tussen waterstof atomen wordt algemeen aangenomen dat deze nauwkeurig bepaald zijn uit *ab initio* berekeningen. Echter, enkele experimenten hebben gewezen op discrepanties met de theorie: drie experimenten aangaande de cryogene waterstof maser en een meting van de longitudinale relaxatie tijd in een koud waterstof gas. Het meest onzekere deel van de interactie heeft betrekking op kleine afstanden. We laten zien dat het met veranderingen in de korte dracht singlet en triplet potentialen niet mogelijk is alle discrepanties tegelijkertijd op te heffen.

Dankwoord

Hier wil ik enkele mensen in het bijzonder bedanken voor hun bijgedrage aan de totstandkoming van dit proefschrift en voor de plezierige tijd die ik met hen de afgelopen vier jaar heb gehad. Natuurlijk in de eerste plaats mijn promotor Boudewijn Verhaar, die met zijn plezierige en stimulerende begeleiding in staat is je over elk onderwerp enthousiast te maken, en die altijd zijn volledige inzet geeft bij het aanpakken van een probleem. Mijn tweede promotor Herman Beijerinck stond altijd klaar om persoonlijke adviezen te geven.

Ik heb me altijd kostelijk geamuseerd met Johnny Vogels en zijn vreemde ideeën, en de kookkunst van Frank van Abeelen zal me ook altijd bijblijven.

Hugo Boesten heeft me in het eerste jaar de beginselen van het 'multi-tasking' bijgebracht, en ik ben hem ook veel dank verschuldigd voor allerlei andere wijsheden.

De studenten Peter Prinsen en Harm Vissers hebben ook een belangrijke bijdrage aan mijn werk geleverd. Ik wil verder de A.I.O.'s, studenten en vaste medewerkers van het werkverband Theoretische Natuurkunde bedanken voor de gezellige koffie, lunch en thee bijeenkomsten.

I am also very thankful to Kurt Gible, Ron Legere and Chad Fertig for the great time during my visit to Yale University. Kurt is not only a devoted experimentalist but also an expert on cloggy jokes. I had a lot of fun with Ron while running the juggling experiment overnight. Our collaboration reached a dramatic climax during the production and wrapping of the 'King coil.

Mijn ouders hebben mij mijn hele leven altijd al ontzettend gestimuleerd en gesteund, en stonden zelfs op de meest ongunstige momenten altijd voor me klaar. Ik denk dat ik van jullie mijn doorzettingsvermogen gekregen heb.

En tenslotte Esther, onze vreugdevolle momenten, je totaal onverwachte verrassingen en je geweldige steun hebben de afgelopen vier jaar tot fantastische jaren gemaakt.

Curriculum Vitae

7 november 1973	Geboren te Heerlen
1986–1992	Atheneum, Scholengemeenschap Sophianum te Gulpen
1992–1996	Studie Technische Natuurkunde (cum laude), Technische Universiteit Eindhoven
1996–2000	Promotieonderzoek, groep Atoomfysica en Quantumelectronica, Faculteit Technische Natuurkunde, Technische Universiteit Eindhoven
1997	Onderwijsprijs post-propedeuse, Werkcollege Mathematisch Fysica en Theoretische Mechanica
feb 1998–juni 1998	Werkbezoek Yale University